Production of Multi-Purpose Bio-Solid Feedstock for Oxidation in Cement Calciner using Microalgae

By

Ahmed Naser M. Khafhafera

A thesis submitted to the Department of Chemical Engineering

in conformity with the requirements for the

Degree of Master of Applied Science

Queen's University

Kingston, Ontario, Canada

August, 2017

Abstract

The concentration of carbon dioxide (CO_2) in the atmosphere is rising and its impact (e.g. climate change) is established among the scientific community. Fuel switching in commercial sectors (e.g. cement plants) is one method to reduce fossil CO_2 emissions. Microalgae cultivation provides an opportunity to reduce CO_2 via photosynthesis and to produce biomass crop for fuel-switching. Industrial scale production of environmentally sound fuel using microalgae systems is still a challenge due to the small cell size and the low concentration in the growth culture. This study investigates a dewatering approach consisting of electrocoagulation, gravity sedimentation, sand filtration, briquetting and passive drying to harvest the algal bio-solids and to produce a multi-purpose feedstock for use in cement plants.

The microalgae suspension in solution is first destabilized via electrocoagulation by means of charge neutralization and micro-bubble flotation. The highest destabilization achieved at 15 Amp/m^2 using aluminum and iron anodes, with 60 min of operational time, were 90% and 48% respectively. The variation of solution pH and stirring speed had no noticeable effects on the overall performance. Further densification of algal bio-solids took place in a sedimentation vessel in which 92% of the process water was removed, allowing for recycling, and the water content was concomitantly reduced from 99.88% to 99.24%. The algal bio-solids obtained after a combined treatment of electrocoagulation and sedimentation were characterized using ICP-OES, TGA, and bomb calorimeter. The metal hydroxides (i.e. aluminum and iron) contribute in the reduction of raw materials used in cement making. Limestone micro-aggregates were employed as filter medium to reduce the water content of pre-concentrated algal solution from 99.24% to 93.45%, removing 84% of the entrained water. Multi-purpose briquettes were

prepared from algal cake, containing metal hydroxides, and a portion of the filter bed, where the water content further reduced to 65% due to the limestone blending. The water content of the briquettes was reduced to less than 15% within few days under ambient condition (i.e. passive drying). Full substitution of calciner fuel leads to 4% of CO_2 reduction compared to coal, and enhances biogenic carbon dioxide (bCO_2) generation which accounts for 18% of the total CO_2 emissions.

Acknowledgements

يقول الله تعالى في كتابه العزيز: (وسيجزي الله الشاكرين)، صدق الله العظيم

First and foremost, many thanks to Allah (Great Lord), the most gracious, the most merciful, for giving me the will and inspiration to achieve such accomplishment.

To my supervisor:

I would like to thank very much my supervisor, Dr. Frank Zeman, for giving me the opportunity to perform this research study. I also greatly appreciate his guidance, advice, and motivation throughout the entire research period. Working under his supervision was a great honor and privilege as I had the opportunity to be exposed to both environments at Queen's University and the Royal Military College of Canada.

To the technicians:

Much appreciation to Mr. Clarence McEwen, Mr. Dave Twigg, Dr. Pavel Samuleev, Dr. Mark Button, Dr. Jennifer Snelgrove and Ms. Agatha Dobosz for providing an exceptional technical support throughout the past two years journey.

To my family and friends:

I would like to express my warm gratitude to my entire beloved family for encouragement and support; they were and will always be there for me to achieve my goals. Undoubtedly, they are my source of love, happiness, strength, and success. Especial thanks to my uncle, Dr. Abdalla Mansur, who was the tactical planner of my entire educational journey, for his limitless guidance. Lastly, to my friends, I truly appreciate your honest advices and painful criticisms; which in a way helped me to be myself.

Table of Contents

List of Figures

List of Tables

List of Abbreviations

Acronyms	Definition
Al	Aluminum
Al_2O_3	Aluminum Oxide
$Al(OH)_3$	Aluminum Hydroxide
$Al_2(SO_4)_3$	Alum
BBMs	Bold's Basal Medium
bCO_2	Biogenic Carbon Dioxide
CO_2	Carbon Dioxide
$CaCO_3$	Calcium Carbonate/ Calcite
CCU	Carbon Capture and Utilization
CKD	Cement Kiln Dust
EC	Electrocoagulation
Fe	Iron
Fe_2O_3	Iron(III) Oxide/ Ferric Oxide
$Fe(OH)_3$	Iron Hydroxide
$FeCl_3$	Ferric Chloride
GHG	Greenhouse Gas
ICP-OES	Inductively Coupled Plasma-Optical Emission Spectrometry
$MgCO_3$	Magnesium Carbonate
MgO	Magnesium Oxide
NaCl	Sodium Chloride
OH^-	Hydroxide Ion
Sed.	Sedimentation
SiO_2	Silicon Dioxide/ Silica
TGA	Thermogravimetric Analysis

Symbols	Definition
Amp.	Ampere
CD	Current Density (Amp/m^2)
SS	Stirring Speed (rpm)
CN	Cells Number
cm	Centimeter
E	Power Consumption ($kWh/kg_{dry\ biomass}$)
ECT	Electrocoagulation time (min)
GtC	Gigatonne or Billion Tonnes of Carbon
hr	Hour
I	Current (Amp)
kJ	Kilo Joule
kg	Kilogram
kWh	Kilowatt Hour
L	Litre
m	Mass (kg)

mg	Milligram
mm	Millimeter
mV	Millivolt
Mt	Megatonne or Million Metric Tonnes
MJ	Mega Joule
μm	Micrometer
nm	Nanometer
OD	Optical Density
PMR	Process Medium Removed (%)
ppm	Part Per Million
rpm	Revolution Per Minute
U	Voltage (volt)
WC	Water Content (%)
wt%	Weight Percent
w/v %	Weight/Volume Percent
η	Recovery (Destabilization) Efficiency (%)
ρ	Density (kg/m^3)

Subscripts	**Definition**
CC	Cell Count
cli	Clinker
DM	Dry Mass
f	Final
i	Initial
OD	Optical Density

"Climate change is no longer a marginal issue. We live with its effects everyday. And we should prepare ourselves for its full impact in the years ahead. It is time to begin planning for climate change in the mainstream of business life"*

*: The Association of British Insurers report is A changing Climate for Insurance (June 2004). Available at http:// www.abi.org.uk/climatechange

Chapter 1 Introduction

1.1. Climate Change

Scientific consensus exists that long-term change in earth's climate is mainly driven by anthropogenic activities (e.g. carbon dioxide emissions). The annual low point concentration of atmospheric carbon dioxide (CO_2) exceeded 400 ppm in 2017 [1]. Globally, the annual CO_2 emission generated from anthropogenic sources is 13.5 billion tonnes of carbon (GtC). In the Copenhagen Accord (2009), the Canadian government made a commitment of 17% reduction of CO_2 emissions by 2020. The reduction is benchmarked against emissions from 2005 (i.e. 749 Mt CO_2) [2]. Canada re-emphasised its commitment to GHGs reduction in the Paris Accord (2015); moreover, it promised to achieve a target of 30% reduction of the total carbon emissions through the development of green technologies, energy efficiency improvements, and imposing more regulations and restrictions on major emitters [3]. One significant industrial source is the cement industry responsible for 5-7% of the global total emissions in 2014 [4]. Cement plants are the second largest industrial source after power plants and have lower CO_2 emission per source (0.79 Mt/source) [5], which may increase CO_2 transportation costs. As a response to climate change, the cement industry has focused on "alternative fuels", those containing biogenic carbon and therefore considered climate neutral, and "blending", which refers to reducing the clinker content of cement through the addition of wastes (e.g. fly ash) and naturally pozzolanic materials [6].

1.2. Carbon Dioxide in Cement Industry

Cement plants can be considered the backbone of modern society, since concrete is the dominant material in construction and therefore development. Cement is the binding agent in the concrete, usually 10% by mass. Clinker, the major constituent of cement, is produced at high temperature in two pyro-processes (i.e. calciner, 850 ^{o}C and kiln, 1450 ^{o}C) [7]. CO_2 is generated

primarily from two sources in a modern pre-calciner configuration; 60% is generated from raw material decomposition or limestone calcination and the remaining 40% from fuel combustion with two thirds of the fuel consumed in the calciner and the remainder in the kiln [8]. The heat of combustion provided by fossil fuels (typically coal or petcoke) in the calciner is 1905 kJ per kg of clinker produced [7]. The amount of CO_2 released per kg of clinker produced is approximately 0.53 kg from the calcination reaction and 0.35 kg from the fossil fuel combustion. Biogenic fuels have attracted the attention of the cement industry because they can be substituted into the plant and are considered carbon neutral [4]. For example, the substitution of alternative fuel in the Canadian cement kilns (e.g. St. Marys Cement Plant) ranges from 20-24% [9]. The European cement industry substituted approximately 39% of its fossil fuel use in 2015 with a target of 60% substitution by 2050 [10].

As 100% substitution of alternative fuels is unlikely, other options, such as CO_2 capture must be considered. Several CO_2 capture technologies are applicable to the cement industry including amine scrubbing, calcium looping, oxy-fuel combustion (full or partial), and microalgae bio-fixation [11, 12, 13]. Post combustion systems, such as amine scrubbing or algal cultures, do not directly affect the plant operations and are more amenable to slipstreaming. The major obstacle of amine scrubbers is the energy penalty; requiring 3000-4000 kJ/kgCO_2 captured [14]. Calcium looping technology is also considered for CO_2 capture, where calcium oxide acts as sorbent for carbon dioxide producing calcium carbonate in a carbonator reactor at high temperatures [15]. Barker et al. [16] have reported the technical issues associated with the implementation of oxy-combustion carbon dioxide capture in cement industry including providing oxygen-rich supply. Others have noted that oxygen combustion has inherent advantages [17] and creates fuel-switching opportunities [18]. All the aforementioned techniques

increase fossil fuel consumption and therefore require underground storage of CO_2 for centuries; however, biogenic solutions create a circular economy.

1.3. Microalgae as Alternative Fuel Feedstock

Microalgae systems provide the opportunity for CO_2 capture, fuel switching, and a mechanism for raw material addition. The challenges of algal systems are size and water content. Previous efforts focus on processing microalgae to produce bio-hydrogen, bio-ethanol, bio-diesel, bio-methane, and bio-oil [19]; however, these systems benefit from readily separable mixtures, i.e. gas/liquid and oil/water. Producing a solid biofuel is more challenging due to the high water content. From environmental standpoint, microalgae are suitable technology for capturing CO_2 from exhaust streams due to rapid growth [20], also they have high carbon fixation capabilities, capturing 1.38 g CO_2 per 1 g of algal biomass produced [21]. Microalgae cultivation is advantageous over other plant-based sequestration techniques in that CO_2 is the only carbon input, arable land is not required and growth can occur in saline or fresh water environments [22]. Additionally, the energy requirement to capture CO_2 via microalgae in a large scale raceway pond accounts for 900 kJ/kg of CO_2 (the energy can be consumed during solution mixing, pumping, and gas injection) [23].

Despite these advantages, utilization of microalgae as a potential method to bio-fix carbon dioxide emissions from cement plants is not well-established. A company called “Pond Biofuels” states that “it is running the first project of its kind in the world to capture carbon dioxide directly via microalgae from St. Marys cement industry”. The project launched in 2010 with scale-up yet to be demonstrated [24]. Cement flue gas has been shown to have no noticeable effects on the growth and chemical composition of multiple microalgae types, including

Chlorella vulgaris [25]. Talec et. al. also demonstrated that cement kiln dust (CKD) did not inhibit microalgae growth at concentrations up to 13.6 mg/L, toxicity was observed at 680 mg/L.

Despite the desirable energy content of dried microalgae biomass (15-25 MJ/kg), the challenge of microalgae systems lies in extracting the biomass from solution due to small cell size (2-50 µm) and low concentration in the growth culture, i.e. 99.99 wt% H_2O [26]. The necessary standards for alternative fuel are taken as 14 MJ/kg with a maximum of 15 wt% H_2O [27]. Microalgae de-watering processes (i.e. centrifuges and membrane separation) will consume energy, reducing the net energy available from the algae and potentially lead to fugitive CO_2 emissions associated with electricity generation. Algae fuel options can range from using minimally processed algae cultures as a low energy fuel source adding biogenic carbon dioxide (bCO_2) to the exhaust stream to 100% substitution after sufficient dewatering. The conceptual basis for this process is shown in Figure 1 below.

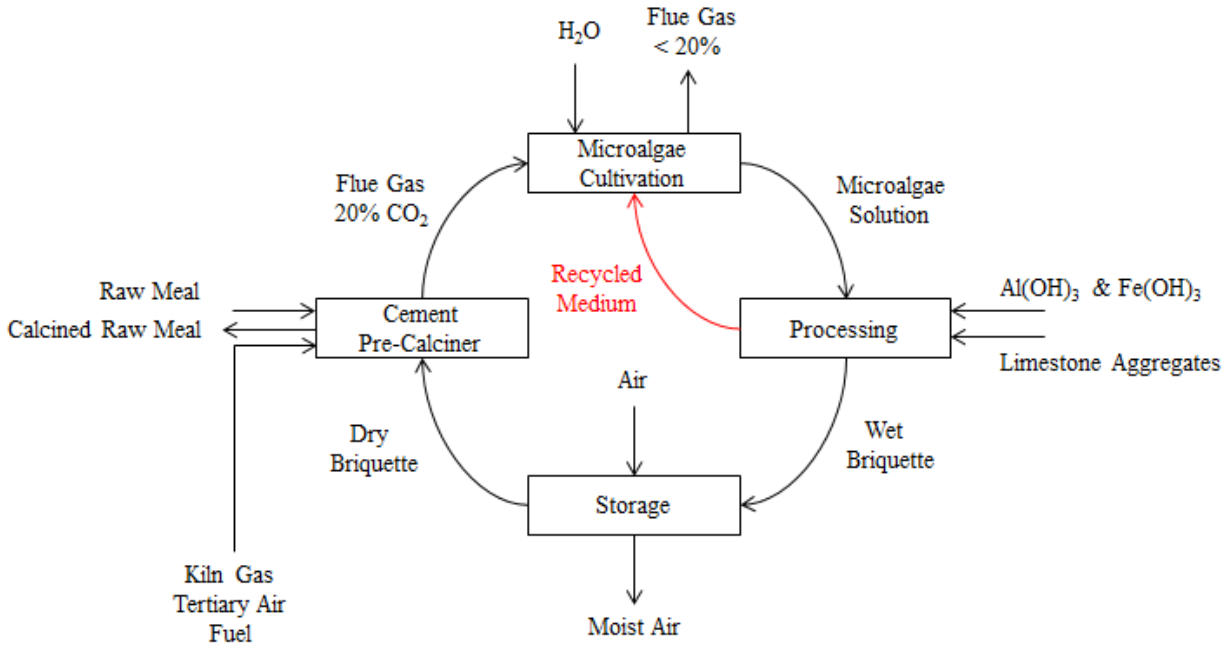

Figure 1: Schematic Diagram of Circular Economy Pathway in Cement Plant.

To make the microalgae dewatering technically and economically feasible, a novel dewatering process is proposed, consisting of five units, including electrocoagulation, sedimentation, limestone filtration, briquetting, and passive drying. The proposed design avoids direct thermal drying of algae as well as certain technical issues such as fouling of membrane filter. Additionally, the proposed approach, shown in Figure 2, integrates raw materials used in cement manufacturing, such as iron, aluminum and limestone. A slipstream is envisioned at this stage so that Carbon Capture and Utilization (CCU) can be implemented on the exhaust stream, which will now contain a fraction of the biogenic CO2 resulting from combustion of the algae. This process would result in net CO2 reduction as a stand-alone concept.

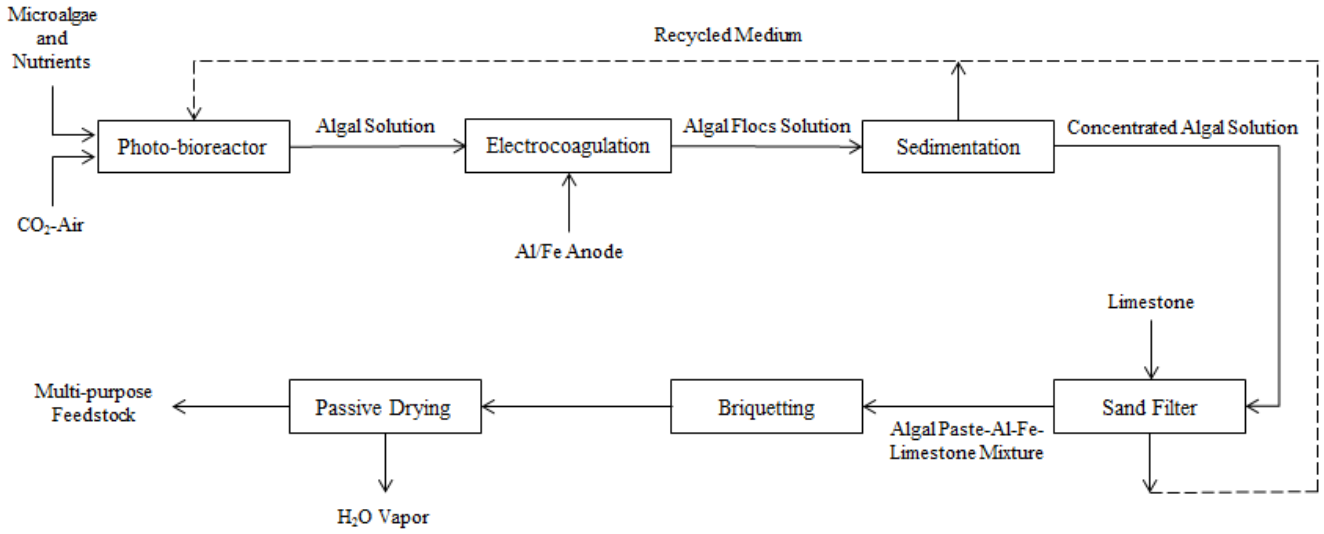

Figure 2: Schematic Diagram of Microalgae Dewatering Processes.

1.4. Expected Outcomes

A successful process will dewater microalgae biomass and produce an alternative fuel/feedstock for cement plants. Five processes have been investigated to bring the water

content of microalgae solution from 99.99 wt% to less than 15 wt% without the use of thermal drying. First, the microalgae suspension is destabilized by charge neutralization via electrocoagulation, where the algal biomass is loaded with aluminum and iron hydroxides. The coagulated solids are naturally settled to increase their concentration and the process water is recycled to be reused in cultivation. The water content of the concentrated algal broth is then further reduced in a sand filter. Limestone is selected as the filter bed media since it is the main constituent used raw meal. After filtration, the microalgae cake and a portion of the filter bed are mixed to form briquettes. An ideal mixing ratio between biomass and limestone is established to meet the minimum energy requirements. The water content of the wet briquette is further reduced below the target by passive drying under ambient conditions.

1.5. Thesis Organization

Chapter 1 introduces the research motivation to mitigate CO_2 emissions in cement plants using microalgae. A novel dewatering process is proposed to concentrate the algal solids without the aid of energy intensive technologies (e.g. thermal drying and centrifugation). Chapter 2 covers the background and fundamentals of cement making processes, alternative fuel switching via microalgae, and the existing dewatering technologies to layout the basis for establishing the methodology to remove the aqueous solution associated with microalgae cultivation system. Chapter 3 describes the apparatus design and detailed experimental procedure for each unit; all units were running on a batch mode to investigate the validity of the dewatering approach. Chapter 4-5 discuss the experimental findings, summarize the research contributions and provide future directions.

Chapter 2 Literature Review

In this chapter, a comprehensive review of clinker production including raw meal preparation, pyro-processes, CO_2 sources, and alternative fuel substitution are provided. To produce a viable biofuel with the intention of CO_2 reduction for cement plants, a positive energy balance of the overall process has to be maintained. Microalgae is a promising feedstock for CO_2 mitigation and biofuel production but the energy consumption remains relatively high due to costly dewatering pathways. The technical and energetic aspects of the most common dewatering technologies have been reviewed to assess the suitability and viability for microalgae concentration. The dewatering technologies include electrocoagulation, chemical coagulation, microbial bio-flocculation, sedimentation, granular media filtration, membrane filtration, centrifugation, magnetic separation, passive and active drying. Despite the diversity of algal biofuel conversion pathways, direct combustion is relatively advantageous and therefore few applications are discussed.

2.1. Cement Manufacturing

Cement is one of the most important materials for human development, due to its binding ability forming concrete, used to support the large structures necessary for industrialization. The modern cement mix was invented by a British engineer, J. Aspdin, in the early 19^{th} century [28]. The cement feed, termed raw meal, is processed at high temperatures in a kiln to form a product called “clinker”, which is then blended with gypsum to form cement [29]. Figure 3 is a schematic of clinker-making processes.

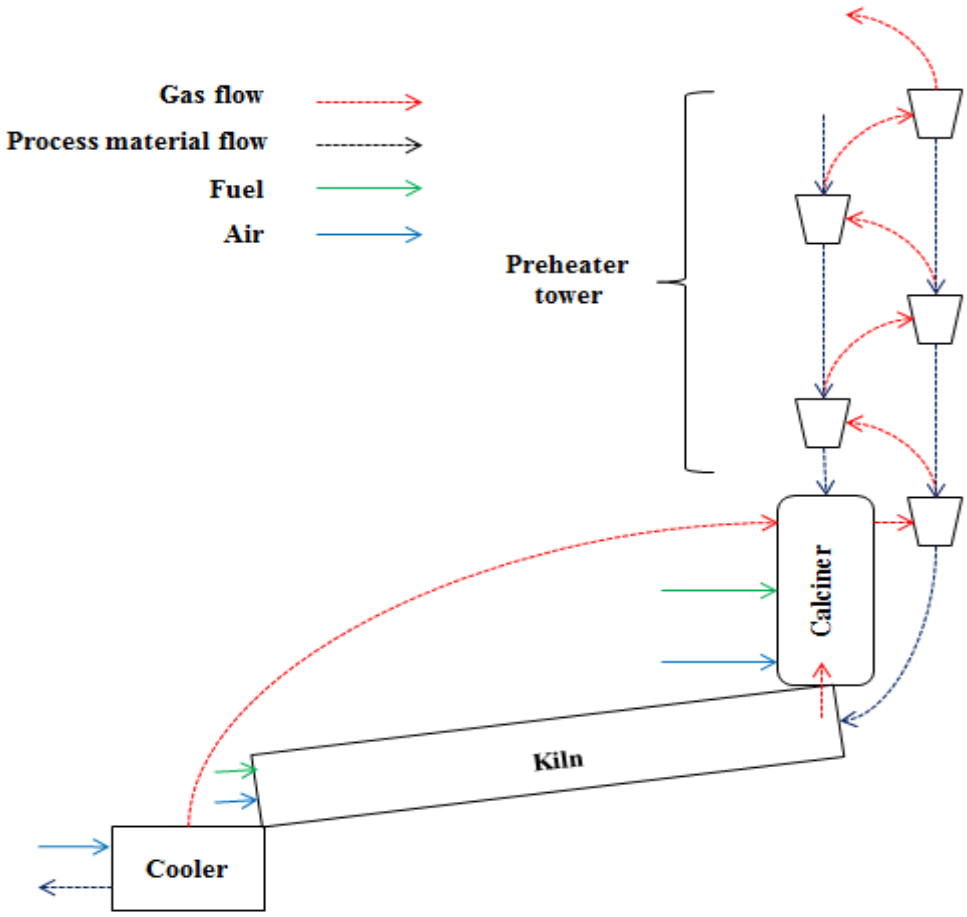

Figure 3: Schematic of Clinker-making Processes, adopted from [30].

2.1.1. Raw Meal Composition and Preparation

The raw materials used in cement manufacturing are first reduced in size by crushing and grinding. The fine materials are stockpiled in silos prior to feeding into the pre-heater tower. The composition of cement raw materials varies slightly from one plant to another, depending on the final product, which could be Ordinary Portland, Masonry or Mortar, Oil-well Cement, and Blended Cement. In other words, the higher the limestone in the raw meal is, the higher the CO_2 emission would be. For simplicity, the composition of Ordinary Portland raw meal consists predominantly of limestone, silica, aluminum oxide, and iron oxide (see Table 1). Cement plants

are almost always built near limestone quarries where the rest of constituents (i.e. silica and metal additives) are locally supplied in sufficient quantities [31].

Table 1: Composition of Cement Raw Meal, Adopted from [7].

Constituent	$CaCO_3$	SiO_2	Al_2O_3	Fe_2O_3
Proportion (wt%)	80.68	14.36	3.71	1.25

2.1.2. Clinker Production

As shown in Figure 3, there are two main pyro-processing stages for clinker production in the modern configuration of cement plants, the calciner and kiln. These combustion zones have heat transfer units at each end. The ground raw meal is fed to the top of pre-heater tower to be heated by the current flow of hot exhausted gases discharged from the calciner in a multi-stage cyclone system. The temperature in the pre-heater tower can reach up to 550 ^{o}C at which the feed material starts to decompose [32]. Often times, the lower cyclone in the pre-heater tower has lower separation efficiency, resulting in dust leaving the calciner outlet and continuously circulating. Cyclones are an effective tool for energy transfer between gas and solid streams [33].

Calciner is a flameless combustion zone located at the base of preheater tower whose is function to convert the limestone into lime before it enters the kiln. The majority of the fuel (60-65%) is consumed in this unit calcining 90-95% of the limestone. The operation temperature of most calciners is ~850 ^{o}C but it can be raised to 900 ^{o}C depending on the CO_2 partial pressure [18]. The typical chemical reactions occurring in the calciner are as follows [33]:

$$CaCO_3 \rightarrow CaO + CO_2 \qquad \Delta H_f^{o} = 179.2 \text{ kJ/mol} \qquad R(1)$$

$$MgCO_3 \rightarrow MgO + CO_2 \qquad \Delta H_f^{o} = 100.6 \text{ kJ/mol} \qquad R(2)$$

$$C + O_2 \rightarrow CO_2 \qquad \Delta H_f^{o} = -393.5 \text{ kJ/mol} \qquad R(3)$$

The kiln is the final thermal process in cement manufacturing used to produce clinker from calcined raw meal at 1450 ^{o}C [18]. Final decomposition of remaining limestone occurs at the inlet of the kiln. Clinkerization reactions of solid-solid and solid-liquid phases take place as the material moves down towards the kiln burner. As the raw material clinkerizes and melts, an internal coating of the clinkerized material is formed on the refractory of the kiln [34]. Fuel and air as a source of O_2 are injected to the rotating inclined cylinder to provide the high temperature lame to drive mineralization. The end-product, "clinker", is produced as a result of series of chemical reactions between calcium, silicon, iron and aluminum oxides [30]. The clinker exists as larger particles, which requires down-stream processing (i.e. grinding). In short, discharging any type of fuel to the calciner should not affect the calcination rate while the required heat is provided.

2.1.3. Alternative Fuels

Carbon dioxide emissions can be reduced using biogenic fuels in the cement plant. The utilization of alternative fuels in the calciner is less problematic than the kiln due to the flameless combustion behaviour, which simplifies the injection, and the fact that the clinker quality does not get affected. The substitution of alternative fuels in the kiln often requires dramatic design changes of burner channels to control the flame shape and combustion behaviour [33]. Also, sophisticated thermograph systems have to be in place to monitor the combustion behaviour [35]. Suitable alternative fuels can be potentially derived from different sources such as agricultural and non-agricultural biomass residues, petroleum based wastes, miscellaneous wastes, chemical and hazardous wastes [32].

Most alternative fuels have approximately 20-25% lower carbon intensity compared to conventional fossil fuels (i.e. coal and pet-coke). Lower carbon intensity results in lower CO_2

emissions from combustion, thus, the cement sector sets a target of 50% replacement by 2020 as a potential strategy for carbon dioxide mitigation. The Canadian cement industry has only 10% alternative fuel substitution as of 2011. Nationwide, cement plants in Quebec are experiencing the highest level of substitution, which has reached a level of 30%. The provincial government of Ontario has yet to set a specific framework for alternative fuel utilization; especially in cement plants. Waste tires, composite plastics, roofing shingles, and municipal solid waste are potential materials that considered to be used as alternative fuels in Ontario. The life cycle issues of burning some alternative fuels are concerning; for instance, the chlorine content in composite plastics can lead to HCl emissions [6].

2.2. Microalgae

Microalgae are eukaryotic organisms that are present in nature as both unicellular and multi-cellular lifeforms [36]. Microalgae convert solar energy to chemical energy thereby the atmospheric oxygen content is enhanced and CO_2 is diminished. Microalgae characteristics differ significantly from one family to another in terms of morphology, size, colour, and chemical composition. From a technical standpoint, the selection criteria of microalgae depend on the desired end-product and specific growth environment. Algal research started intensively during the Second-World-War by a German scientist to derive a biofuel. The goal at that time was to overcome the issue of conventional fuel shortages. The lineages of microalgae investigated during wartime were related to green and red microalgae families; for instance, *Chlorella, Spirulina, Dunaliella, Scenedesmus, Botryococcus, and Porphyridium* [37].

2.2.1. Morphology and Composition

Chlorella vulgaris is one of the most studied types of microalgae, fastest growing organism, and therefore it is a logical choice for this study. *Chlorella vulgaris* have a spherical

shape with a typical cell size of 2-10 μm in diameter [38]. Microalgae biomass consists of four components, which are protein, carbohydrate, lipids, and nucleic acid as illustrated in Table 2 [37]. To better understand the combustion characteristics of *Chlorella vulgaris*, shows the proximate and ultimate analysis. Proximate analysis determines the percentages of moisture, fixed carbon, volatile matter, and ash using a TGA while ultimate analysis determines the elemental compositions. As mentioned in section 1.2, the energy required to produce 1 kg of clinker is 1905 kJ. Taking the energy content of dried microalgae solids as 24,000 kJ/kg, the mass of calciner fuel is estimated as 0.079 kg/kg_{cil}. Energy penalty to drive the endothermic reaction of metal hydroxides associated with the fuel is not considered.

Table 2: Chemical Composition of *C. vulgaris*, adopted from [37].

Protein (%)	Carbohydrates (%)	Lipids (%)	Nucleic Acid (%)
51-58	12-17	14-22	4-5

Table 3: The Proximate and Ultimate Analysis of *C. vulgaris* Biomass [39].

Parameter		*C. vulgaris*
Proximate Analysis (wt%)	Volatiles	88.92
	Fixed Carbon	4.05
	Ash	7.03
Ultimate Analysis (wt%)	Carbon (C)	47.11
	Hydrogen (H)	7.47
	Oxygen (O)	37.16
	Nitrogen (N)	8.26

2.2.2. Growth Kinetics

Microalgae grow naturally in the aquatic environment by using sunlight, nutrients and CO_2. Recently, industrial microalgae production techniques have been studied that mimic the optimal growing conditions. The three growth methods that have been established are photoautotrophic, heterotrophic, and mixotrophic. Light is utilized as the only energy source to enhance the algal growth under photoautotrophic conditions; whereas, carbon and organic

compounds are used as the only energy source to promote the algal growth under heterotrophic conditions. The most common approach for artificial growth is mixotrophic which is a combination of the two aforementioned approaches where both light and carbon are provided to enhance the growth of algal biomass [12]. There are different phases of microalgae growth in batch operation including lag, exponential, linear, and stationary phases, shown below in Figure 4. The exponential phase starts on second day and ends after the fifth day of culturing at an approximate biomass density of 1.3 kg/m^3. The stationary phase of the culture is established on day 10, in which the biomass density levels off at about 4 kg/m^3, noting the experiment was conducted in an outdoor bubble column bioreactor with a working volume of 0.06 m^3 [40].

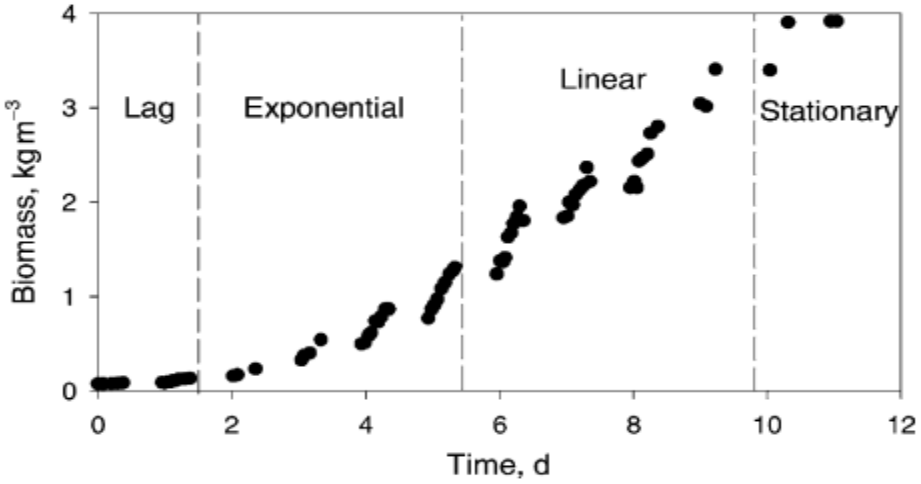

Figure 4: Microalgae Growth Phases in Bubble Column Photo-bioreactor [40].

2.2.3. Algae Cultivation Systems

Cultivation can occur in open ponds or closed photo-bioreactors, depending on the desired product and CO_2 source. Open pond or "racetrack" systems are the most abundant configuration for large-scale microalgae production due to their simplicity and low capital cost. The culturing medium employed in constructed ponds can be fresh water, seawater, brackish water, or even wastewater. The addition of nutrient can be minimized where brackish water and

wastewater are used due to their chemistry. Microalgae cultivation in open ponds is weather dependent and the growth rate cannot be regulated due temperature and light variations. The typical biomass density attained in an open pond cultivation system is 8.5 g/m^2.day within a growth cycle of 10-13 days [41].

The efficiency of an open pond system depends significantly on the whether thus the location. Cross-contamination is another obstacle for producing a desirable amount of microalgae biomass in open ponds. The depth of the pond should be ideally determined to allow light to reach the bottom of the culturing medium; the typical depth is 0.25-0.30 m [42]. The pond walls should be made of inexpensive materials that prevent biofouling, concrete is often a good choice, but capital cost can be an issue when constructing larger ponds. Often times, paddle wheels are used for homogenizing the microalgae culture to avoid temperature and oxygen stratification [43]. Figure 5 illustrates the design and dimensions of an open pond for commercial microalgae cultivation.

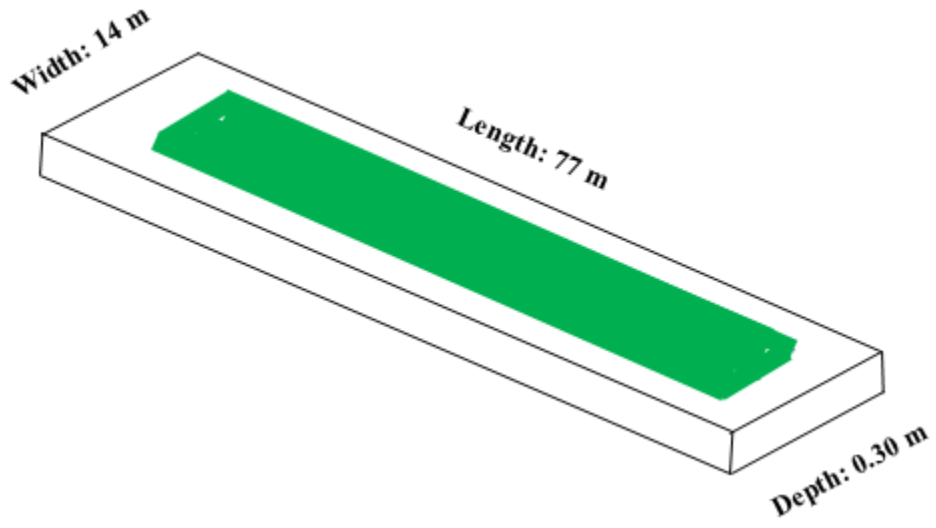

Figure 5: Schematic of an Open Pond for Microalgae Cultivation, adopted from [43].

In a closed photo-bioreactor system, the microalgae grow in a constrained space with a controlled supply of light, heat, and nutrients. There are different configurations used in cultivating microalgae biomass such as airlift photo-bioreactor, tubular photo-bioreactor, and vertical-column photo-bioreactor. Technically, photo-bioreactors are more efficient for biomass production, but specific design parameters have to be carefully considered such as choice of shell materials, which can differ slightly depending on the operating conditions (i.e. light, temperature, and volume). CO_2 and air are injected into the reactor in form of micro-bubbles and the light source can be the sun in case of outdoor culturing or electric bulbs in case of indoor culturing [43]. Cuellar-Bermudez et al. reported the biomass productivity of *Chlorella Sp*. cultivated in tubular photo-bioreactors as 0.70 g/L.day [12]. Further comparisons of cultivation systems are described in Appendix A-1.

Saline water and wastewater are better alternatives for culturing medium as they minimize use of freshwater. Freshwater is often the most accessible source because cultivation systems are typically built near the CO_2 source, which may not be located close to the sea or a wastewater treatment facility. Water recycling of microalgae culturing medium reduces water competition with other applications such as human consumption and agricultural irrigation [44].

The rate of microalgae growth depends on the amount of nutrients provided in the culturing medium. Nitrate $(NO_3)^-$ and phosphate $(PO_4)^{-3}$ are the major components required by the microalgae cell to produce proteins and nucleic acids. Photosynthesis rates are sufficient when CO_2 is injected into the culturing medium as gas and it transforms to ionic form e.g. bicarbonate ions. A trace amount of metals (i.e. zinc, iron, cobalt, copper, manganese, and nickel) also accelerates the photosynthesis of microalgae. Excessive concentration of metals in the culturing medium may inhibit the growth due to the toxicological effects. Metal ions are

digested by the cell through a membrane due to carboxylic, sulfhydryl, and phosphatic groups present on the cell surface [45].

2.3. Harvesting and Dewatering Technologies

Converting aqueous microalgae culture to a combustible fuel is a multi-stage process. Using an appropriate dewatering technology, including physical, chemical, and thermal methods, is critical in determining the feasibility of fuel production. Background, fundamentals, efficiency, and energy consumption of most common existing processes are reviewed.

2.3.1. Electrocoagulation

Electrocoagulation is an electrochemical process is used to destabilize particles of opposite charge (e.g. suspensions and colloids). The use of electrocoagulation was proposed in the late nineteenth century (1889) in England. The invention of an electrocoagulation process, using both iron and aluminum electrodes, was officially patented in 1909. The first industrial application of electrocoagulation was implemented to purify drinking water in the USA in 1946. Electrochemical treatment became an important field to study over the past few decades with the advent of regulations on the quality and standards of drinking water and wastewater discharge; especially, in North America [46]. Russian scientists were successfully able to separate oil from an oil-in-water emulsion using an electrocoagulation cell in 1980s [47]. Electrocoagulation has been marketed globally to remove a wide range of contaminates; e.g. suspended solids, heavy metals, dyes, etc. [48]. Vandamme et al. (2011) investigated the electrocoagulation effectiveness to remove fresh and marine microalgae; the recovery efficiency was found to be quite promising. Electrocoagulation is capable of concentrating microalgae up to 6 wt% solids (e.g. concentrating the biomass from 0.5 g/L to 60 g/L) with energy demand of 0.70 kWh per 1 m^3 of solution [49].

2.3.1.1. Fundamentals

Electrocoagulation involves both physical and chemical mechanisms where oxidation and reduction reactions take place as a result of electrical current passing through the solution being treated [50]. The following half reactions take place in the electrocoagulation unit.

$$M \rightarrow M^{n+} + ne^- \quad R(4)$$

$$M^{n+} + n\,OH^- \rightarrow M(OH)_n \quad R(5)$$

$$2H_2O + 2e^- \rightarrow 2OH^-_{(aq)} + H_{2(g)} \quad R(6)$$

In addition, oxygen and hydrogen are produced at the anode surface as a side reaction via water oxidation:

$$2H_2O \rightarrow O_2 + 4H^+ + 4e^- \quad R(7)$$

The electrocoagulation units consist of an anode and a cathode; with the configuration varying depending on the specific treatment. Metal hydroxides are formed in situ through ion dissolution from the sacrificial anode; which is usually made of iron and/or aluminum. Charge neutralization by counter ions is the key mechanism in electrocoagulation to destabilize collides and suspensions in order to form larger particles [51]. The delivery method of the counter ions (metallic cations) to the solution is the main difference between electrochemical and chemical coagulation [52].

The electrocoagulation phenomenon overs via three steps. The first step is formation of metallic complexes as a result of oxidation at the sacrificial anode. The second step is destabilization of the suspended particles by charge neutralization. The destabilization takes place due to shrinking and compressing the diffusion double layer, which is enhanced by interactions with counter metallic hydroxide complexes. The presence of counter complexes leads to a charge neutralization where the electrostatic repulsion force is reduced and van der

Waals attraction increases. The third step is agglomeration of destabilized particles to form larger particles. These are formed when positively charged metal ions and metal hydroxide bind to negatively charged particles that are moving toward the anode via electrophoretic motion. The coagulants can then be separated by electro-flotation, sedimentation, or conventional filtration. Electro-flotation takes place due to water electrolysis, where oxygen and hydrogen micro-bubbles are produced at the anode and the cathode respectively [53]. Figure 6 highlights the main components of electrocoagulation unit and the pathways of metal hydroxide formation.

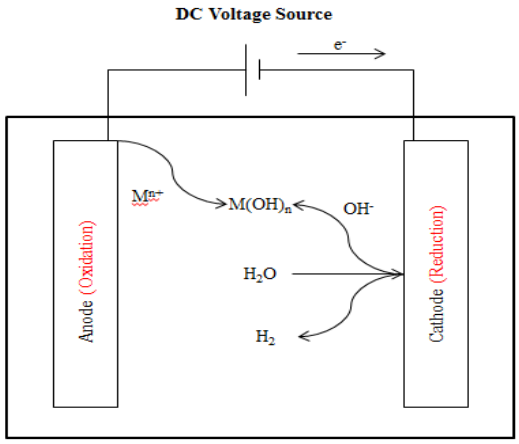

Figure 6: A Schematic Diagram of Electrocoagulation Process, adopted from [53].

2.3.1.2 Parameters Affecting Electrocoagulation Performance

There are many control parameters that can affect electrocoagulation performance such as current density, solution pH, stirring speed, electrolyte addition, electrode material, electrode configuration, and anode passivation [48]. Current density is the amount of applied current distributed over the active area of the electrodes. At low current density, the contaminants removal is enhanced by metal hydroxides binding and micro-bubbles flotation; whereas, at higher current density, the predominant removal mechanism is micro-bubbles flotation. The metal speciation and formation is strongly pH dependent; however, both acidic and neutral pH

levels are more desirable in removing contaminants from solution than an alkaline environment. Aluminum and iron ions tend to form positively charged polymeric and monomeric complexes in a pH range of 4-9; whereas, negatively charged complexes are promoted at pH higher than 9. The formation of aluminum hydroxide complexes is described in the following order depending on the solution pH; $Al \rightarrow Al(OH)_n^{3-n} \rightarrow Al_2(OH)^{2+} \rightarrow Al_{13}$ Complex $\rightarrow Al(OH)_3$ [54]. Zhang et. al (2015) showed that electrocoagulation processes consumes less electricity under acidic than alkaline conditions [55].

Mixing may provide a suitable environment to enhance the formation of particles. However, the performance at moderate stirring speed (i.e. 60-150 rpm) is better than at higher mixing speeds due to shearing effects. The selection of sacrificial anode material depends mainly on the chemistry of contaminants to be removed. For example, electrode materials to be used in purifying drinking water must not have hazardous effects on human health. Iron and aluminum are the most popular materials used due to their effectiveness and low cost. There are two possible electrode configurations, mono-polar and bipolar. The sacrificial anodes in mono-polar arrangement are connected with one another in series; whereas, the cathodes connections follow the same manner. In bipolar arrangement, only a single anode and cathode are directly connected to external power source and the remaining electrodes are placed in between.

The addition of electrolytes, e.g. NaCl, in the solution increases the electrical conductivity thus reducing the resistance and less power is consumed. Among the anions present in the solution, around 20% should be chlorine ions to enhance the electrical conductivity and prevent the formation of insulating agents. The addition of 1 g/L of NaCl reduced the voltage from 5.8 V to 2.4 V at applied current of 3 Amp. [56]. The passivation of the working electrode is a concern in determining its lifetime, simply because metal dissolution and electron transfer are limited as

the passivation layer develops. Passivation effects are reduced by replacing the electrodes periodically, by regular polarity reversal of the electrodes, by anions addition (i.e. Cl^-, Br^-,I^-, F^-, etc.), and by hydro-mechanical cleaning.

2.3.2. Chemical Coagulation

Chemical coagulation is a potential harvesting method used in industry to destabilize suspensions by the addition of salts such as alum ($Al_2(SO_4)_3$) and ferric chloride ($FeCl_3$) [57]. The zeta potential (i.e. the electrical charge of particular particle present in liquid) is minimized to a point below the van der Walls attraction by counter ions provided by coagulation agents. The double layer distance of negative particles is reduced by the high-valence cations added; which results in larger particles formation by charge neutralization. Generally, chemical coagulation takes place in four steps which are: the addition of salts to the targeted solution, followed by a rapid mixing to ensure homogenous distribution of counter ions, and then slow mixing to ensure a complete contact between particles of opposite charge leading to precipitation, followed by particles removal using conventional techniques such as sedimentation or filtration [52].

The typical obstacle of using chemical coagulants is the corrosive elements (e.g. chloride) embedded in the biomass-sludge, which may cause operational problems depending on downstream use. The dosage of coagulants depends on the targeted efficiency, meaning that adding more coagulants leads to higher the recovery efficiency and more sludge generated which affects the chemical composition of the solids extracted. For instance, a removal efficiency of 87.5% using 20 mg/L of aluminum-based compounds and 97.5% using 20 mg/L of iron-based compounds [58].

2.3.3. Microbial Bio-flocculation

The technique of microbial bio-flocculation to harvest microalgae is one of the newest research areas. The methodology of this technique is very simple wherein microbial colonies are added to microalgae suspension leading to a formation of algal-bacterial flocs. The fundamentals are not yet well understood, but theories suggest that flocs are formed due to biological and physicochemical interactions. Bio-flocculation can lead to complications; for instance, inconsistent floc productivity at different weather conditions [59].

2.3.4. Sedimentation

Sedimentation is a gravity-based separation technique operating on the density difference between the solids in suspension and the liquid medium. Gravity sedimentation to harvest microalgae biomass has been shown less promising than other techniques due to the small cell size (2-10 μm) [38] and negative surface charge of the suspension (-40 mV) [60] with the free settling velocity estimated at 0.1-2.6 cm/h [61]. The average solids content of microalgae biomass via gravity sedimentation was found to range from 0.5-1.5 wt% solids at a power consumption of 0.1 kWh/m^3 [62]. Sedimentation is often used in conjunction with coagulation and flocculation to improve the settling rates. In addition, sedimentation processes can effectively remove 80%-93% of the process water. Sedimentation is often used prior to any filtration step to treat large-scale volumes in order to effectively handle the solids loading under optimal conditions. The design selection of a clarifier depends on several factors such as installation size, site conditions, preference and experience of designer [63]. The performance of a sedimentation unit (i.e. settling velocity) is governed by two main parameters, density of suspended solids and the particle radius. However, Stokes' Law can be only applied for non-flocculated particles to determine the settling of individual particles [64].

2.3.5. Granular Media Filtration

The main function of a granular media filter is removal of suspended solids by physical interactions with the bed media. There are a variety of materials that are utilized as the filter bed, i.e. sand, glass beads, etc. Granular media filters have a high potential for recovering microorganisms (e.g. microalgae) with a recovery efficiency of ~85% at a filtration rate of 120 m/h [61]. A previous study showed that the performance of granular media filter dramatically improves as the bed particle size gets smaller; however, 96% of microalgae removal was achieved with 0.2 mm diameter sand and a depth of 3.175 mm at a filtration rate of 10.3 m/h [65]. The overall performance of granular filter is determined by several factors including fouling rate, head loss, and cleaning mechanisms.

2.3.5.1. Filter Elements

The design of granular filters consists of four main elements. The first is the supernatant solution reservoir, which is the space provided above the bed to be occupied by the solution being filtered. It is also called filter head because it offers a pressure gradient to push the solution through the bed material. The second element is the filter bed which can be made of different materials and sizes. The under-drainage system is the third element, which provides a physical support for the bed material. The particles size of the lower layer must be larger than the opening channels of the drainage system to prevent bed material loss. Control valves are the last element. Flow rates of solution being treated have to be regulated to maintain a steady operation before and after cleaning [66].

2.3.5.2. Extraction Mechanism

Despite the design simplicity of granular media filters, there are several complicated extraction mechanisms involved including transport, attachment and purification. Transport mechanisms include several separation sub-processes such as physical screening, inertial forces, and electrostatic attraction. Trapping of particles by screening is a process where the solution is passed through bed pores and solids are retained on the top surface of the bed forming a thick paste called a filter cake [66]. The pores size depends on the shape and uniformity of bed particles. Nevertheless, the passage of solids that is 1/7 the size of the bed particles is prevented when spherical and uniform particles are used as bed material. The smallest particles size that suggested to be used as filter bed material is 150 µm which provides approximately pores of 20 µm. The filter cake, known as Schmutzdecke or filter skin, enhances the overall performance due to solid accumulation that results in a higher resistance of solution passage. Inertial forces promote attachments of contaminants to the bed particles due to the difference in specific gravity between the targeted contaminants and the surrounding water. Electrostatic attraction is based on the charge difference between the filter bed particles and contaminants to be removed. For instance, fresh sand particles carry a negative charge and have a higher tendency to bind to positively charged particles [66].

2.3.5.3. Filter Cleaning and Bed Replacement

The resistance of the filter bed increases until the solution passage is stopped due to the accumulation of biomass. At that point in time, the filter is no longer functioning well and cleaning becomes necessary. The filter bed material is often dried for a period of time, (e.g. overnight) to ensure the rigidity of the filter cake. Having multiple filters in place rather than a

single filter avoids overloading and delays during the cleaning process. There are two common cleaning methods, manual cleaning (hand cleaning) and mechanical cleaning. Manual cleaning is carried out by workers who scrape the cake layer using equipment; such as shovels, baskets, buckets, handcarts, etc. Manual cleaning is not a sufficient method when dealing with large areas of filter beds. Mechanical cleaning involves skimming equipment that used to remove the upper layer (i.e. 1-3 cm) of the clogged filter bed, and the scraped materials are collected using belt and screw conveyors [66].

Granular media replacement takes place when the depth of filter bed is reduced to the permissible minimum after frequent cleaning (e.g. 20-30 scrapings). The remaining layer of the filter bed should also be scraped before adding the new granular material to avoid fouling and resistance risks that may occur due to the penetration of biochemical and biological products. This scraped layer is not discarded but is often replaced on the top of fresh material added. This technique is known as throwing over. Granular material of scrapes are sometimes washed and reused in areas where obtaining fresh materials is either unsustainable or economically unfeasible [66].

2.3.6. Membrane Filtration

Membrane filters recover microalgae biomass at high efficiencies by providing a physical barrier that is tuneable via pore size. No other extraction mechanisms (e.g. adsorption) are involved in membrane filtration. One associated drawback is filter clogging where the permeate flux is reduced due to accumulation of microalgae biomass on the surface of the membrane [67]. The pores size of the membrane has to be in micron size to capture the microalgae cells. Generally, smaller pore sizes results in a faster bioaccumulation. One of the techniques proposed to prevent the decline of permeate flux is increasing the temperature of the solution being

filtered, but results showed that the membrane material can be decomposed at elevated temperatures. To increase 1mol of water by 1 ^{o}C, the energy needed is 75.4 J. The energy input required to heat 1L of algal solution after sedimentation treatment at 1.5 wt% is 4185 J/^{o}C. the microalgae solids present in 1L of concentrated solution is 15 g which is equivalent to 0.36 MJ (assuming the microalgae solids has heating value of 24 MJ/kg). Based on the energy calculation, the concentrated algal solution after sedimentation can be heated up-to 86 ^{o}C and it is still energy-neutral. Surface modifications with functional coating materials and shear-rate enhancements are two possible ways to eliminate clogging risks and increase the membrane performance [57]. Chen et al. reported the energy demand of microfiltration membrane as 2.06 kWh per 1 m^3 of solution to concentrate microalgae biomass from 0.06 to 8.88 wt% solids (i.e. 88.8 g/L) [68].

2.3.7. Centrifugation

Centrifugation extracts solids based on the physical principle of Stokes' law, as in sedimentation, with the addition of centrifugal acceleration [69]. The energy requirement is 8 kWh per 1 m3 of solution [62] with maximum densification to 20 wt% solids (e.g. concentrating the microalgae biomass from 0.5 g/L to 200 g/L) [49]. The separation cost using centrifugation can be reduced if the algal solution is pre-concentrated by conventional techniques such as sedimentation, meaning that the amount of electricity consumed per unit volume will be reduced. Centrifugation is often used to extract high valued products (i.e. pharmaceutical products) in which the characteristic may be adversely affected if alternative separation processes are implemented [70].

2.3.8. Magnetic Separation

This type of separation occurs due to the attraction between materials with different magnetic moments and a magnetic field. Magnetic nano-materials (i.e. Fe_3O_4 and silica coated magnetic particles) and microalgae cells bind together due to electrostatic interactions. Even though, magnetic separation is considered to be advantageous based on several perspectives (i.e. energy efficient, simplicity, etc.) but it is not recommended to be used as a primary approach to harvest microalgae suspension. One of the major obstacles is the required amount of magnetic nano-materials and its associated cost, which makes the separation technique impractical to implement for treating large volumes of microalgae solution. Achieving higher recovery efficiency is a function of several sensitive control parameters, solution pH, dosage of magnetic material, strength of magnetic field, and stirring speed which are not yet optimized for large scale operations [71]. Table 4 summarizes the recovery efficiency and the power consumption of each existing dewatering technology, which are essential for the determination of the process viability.

Table 4: Summary of Microalgae Dewatering Technologies and their Suitability for this Study [49, 62, 68, 71, 65, 72, 73].

Process	Recovery Efficiency (%)	Power (kWh/m^3)	Suitability
Electrocoagulation	90-95	0.7	yes
Chemical Coagulation/Flocculation	79	Negligible	No
Microbial Bio-flocculation	99	Negligible	No
Sedimentation	72	0.1	yes
Granular Media Filtration	98.7	N/A	yes
Membrane Filtration	98	2.06	No
Centrifugation	95	8	No
Magnetic Separation	98	0.03	No

2.4. Passive vs. Active Drying

Passive drying is a conventional method used to bring down the water content of products by natural air movement and the passage of time. Passive drying is an operation where water evaporation is maintained under ambient conditions without applying an external energy input. The phenomenon is known as *Equilibrium Moisture Content*, where the product's water content evaporates to the environment until a balance or saturation point is reached. The difference in relative humidity between solid product and surrounding air provides the driving force for passive drying [74].

There are three different categories of passive drying, field or work place drying, exposed shallow layers drying, and ventilated structure drying. In the first type, no structure is needed and the product of interest is exposed directly to ambient air at the site. Field drying is considered as insufficient technique as the product to be dried is not protected from climate conditions; for instance, rain and snow. In the second type, the product is placed in shallow trays with transparent plastic covers that allow sun light and wind access. The only obstacle of shallow-layer drying is uneven distribution of heat and air leading to uneven quality among trays. A shed is needed for the last type where ambient air is allowed to flow through the structure via permanent openings. Ventilated structure drying is an efficient method due to protection of product but it is still dependent on the flow rate of free air [74].

Active drying, on the other hand, is a technique by which temperature and air movement are regulated by external sources. The principle of active drying for water removal is the same as in passive drying, only at a faster rate. Despite the high power consumption, active drying has been attempted on algal biomass [75]. Design and operational factors (i.e. feedstock characteristics, available space, waste heat sources, maintenance cost, etc.) play a role in

selection of suitable dryer. The thermal drier reduced the water content from 60% to 0% [76]. In order to evaporate 1 m^3 of water, a total of 679 kWh_{th} are required, based on an enthalpy of vaporization of water at 44 kJ/mol and 25 ^oC [77].

2.5. Direct combustion of Algal Biomass

Microalgae biomass can be processed to produce a wide range of bio-fuels [19]. Direct combustion of algal biomass is one energy recovery pathway well suited for use in a cement plants. Dry algal biomass has a heating value of 15-25 kJ/g; however, authors used Aspen Plus to simulate the cost of generating 1 kWh of electricity using algal biomass, which was found to be approximately $0.95. The cost of generating electricity using biomass-derived fuel estimated as approximately 4 times higher than using conventional diesel [78], and 9.5 times higher than the cost of electricity in Ontario (i.e. 0.10 $/kWh). A study investigated the combustion behaviour of algal/diesel mixture in a modern diesel engine. Xu et. al showed that the engine performance using algal/diesel mixture increased, which indicates an energy contribution released from algae. However, the heat release rate is found to peak when the mixture consists of 5% w/v dry biomass and diesel. Afterwards, the heat released starts to decline because of higher density that leads to poorer injection pressure [79]. The utilization of algae as solid biofuel is limited, therefore, it is worth of further investigation.

Chapter 3 Materials and Methods

In this chapter, the materials and procedures for culturing and dewatering microalgae are described in details. The parameters regulating the algal growth, i.e. nutrients concentration, light, and CO_2/air mixture, are established. The design and the associated measurements for each process are stated to reduce the water content of algal bio-solids to a burnable level.

3.1. Microalgae Type and Source

The microalga strain used in this study was *Chlorella vulgaris*. The initial microalgae solution was obtained from the civil engineering department (Dr. P. Champagne Lab) at Queen's University. No testing was done on the sample to determine any specific biological parameters.

3.2. Culturing Medium

The culturing medium used in growing microalgae was a version of Bold's Basal Medium (BBMs) [80]. The medium consists mainly of macro-nutrients and little portion of micro-nutrients to provide a suitable growth environment. Preparation of stock solution took place every two months, depending on the experimental demand. The chemical formulation (recipe) of the BBMs used is described in Table 5 with the addition of 10 mL of "trace metals" per 10 L of solution.

Table 5: Chemical Formulation of Bold's Basal Medium.

Chemical Component	Concentration (g/10L H_2O)	Chemical Component	Concentration (g/10L H_2O)
KH_2PO_4	1.75	NaCl	0.25
$CaCl_2.2H_2O$	0.25	$Na_2EDTA.2H_2O$	0.1
$MgSO_4$	0.37	$Fe_2SO_4.7H_2O$	0.0498
$NaNO_3$	2.5	H_3BO_3	0.0805
K_2HPO_4	0.75	-	-

3.3. Photo-bioreactor Apparatus

The experimental set-up consists of two tubular photo-bioreactors made of transparent PVC and one stock jar (19 L). The dimensions of the tubular reactors are 34 cm in height and 9.50 cm diameter. The tubular reactors were placed on stirring plates to provide homogenous mixing at 300 rpm. This limited the sedimentation of microalgae suspension during growth period. Air was supplied from a building compressor via laboratory valve at a pressure of 22-24 psi and "bone dry" CO_2 was supplied from an external cylinder at a pressure of 20 psi. The flow rates of pressurized air and CO_2 mixture were regulated using Mass Flow Controller (OMEGA, FMA-5520) and sparged to both reactors. The maximum capacity of the rotameters is 1 L/min, where microalgae were grown at 20-30% CO_2 and 70-80% air. Stone spargers were used to generate dispersed bubbles in which the supplied gas was distributed over the working volume of the reactors.

Four electrical tubular bulbs were used to provide a fixed light intensity required for microalgae photosynthesis. A fan was positioned towards the reactors to dissipate the heat radiated by the bulbs. The cultivation of microalgae in the stock jar ran in continuous mode to have enough algal stock solution, where BBMs solution was added as needed, depending on the experimental consumption. The microalgae in experimental reactors were grown in a batch mode to have a consistent production, usually over a time period of 5 days. A schematic of the photo-bioreactor set-up is shown in Figure 7.

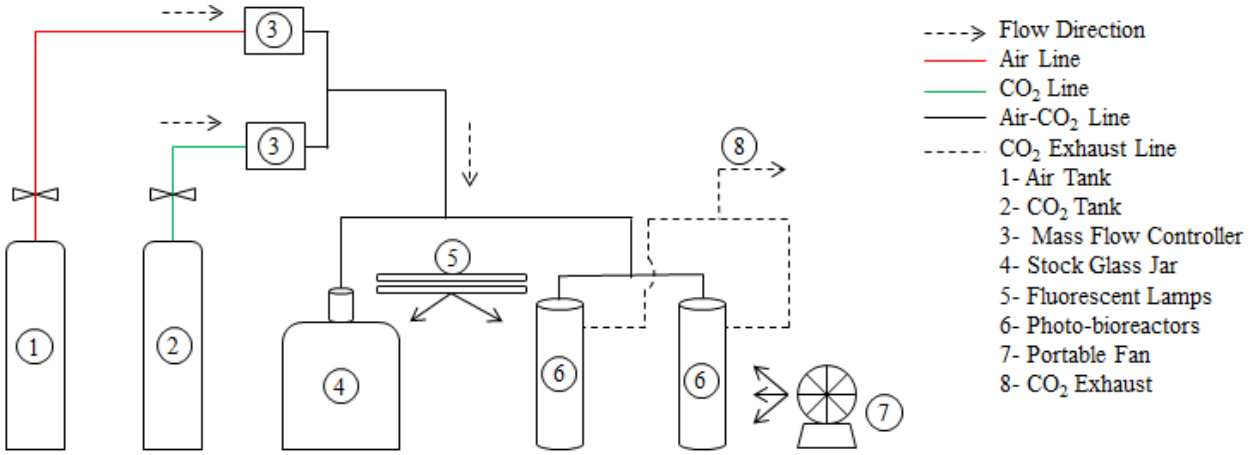

Figure 7: Microalgae Cultivation System.

3.4. Analytical Measurements for Microalgae Growth

3.4.1. Cell Count

A 1 mL sample was withdrawn by pipette from each reactor every 24 hours. The samples were diluted in de-ionized water to avoid the overcrowding of microalgae cells. 10 µL of the diluted samples was placed on the surface of hemacytometer and pictures of a counting grid were taken at 10X magnification using a digital camera on the light microscope (ZEISS, Primo Star). The pictures were analysed using ImageJ Software for automated cell counting (see Appendix C-1).

3.4.2. Optical Density

A spectrophotometer (Infinite, M1000Pro) was used to determine the optical density of each microalgae sample in solution. A 200 µL sample was withdrawn from each reactor by pipette every 24 hours and then transferred to a disposable plastic cuvette tray. De-ionized water passed through a Millipore filter (Synergy®UV, SYNSVHF00) was used as a blank for comparison. The optical density of microalgae samples were analysed at a wavelength of 680 nm, i.e. the absorption peak of chlorophyll detection (see Appendix C-2). The optical density measurement was repeated on a daily basis until a stationary phase was observed.

3.4.3. Dry Mass

Aluminum pans were used for determination of the microalgae dry biomass. The pans were weighed using a balance (DENVER INSTRUMENT, SI-114) before and after the addition of 10 mL samples. Two samples were taken from each reactor every 24 hours. The loaded pans were placed in a drying oven (Fisher Scientific, Model: 6917) overnight at 105 ^{o}C. Pans were removed from the oven the next day and left on the laboratory counter to cool for five minutes and then the mass was recorded. The mass difference between the empty and dried loaded pans was used in determination of microalgae biomass productivity, noting that any BBMs residue was not taken into account (i.e. 0.00055 g/mL). Figure 8 summarizes the analytical measurements for microalgae quantification and their outcomes.

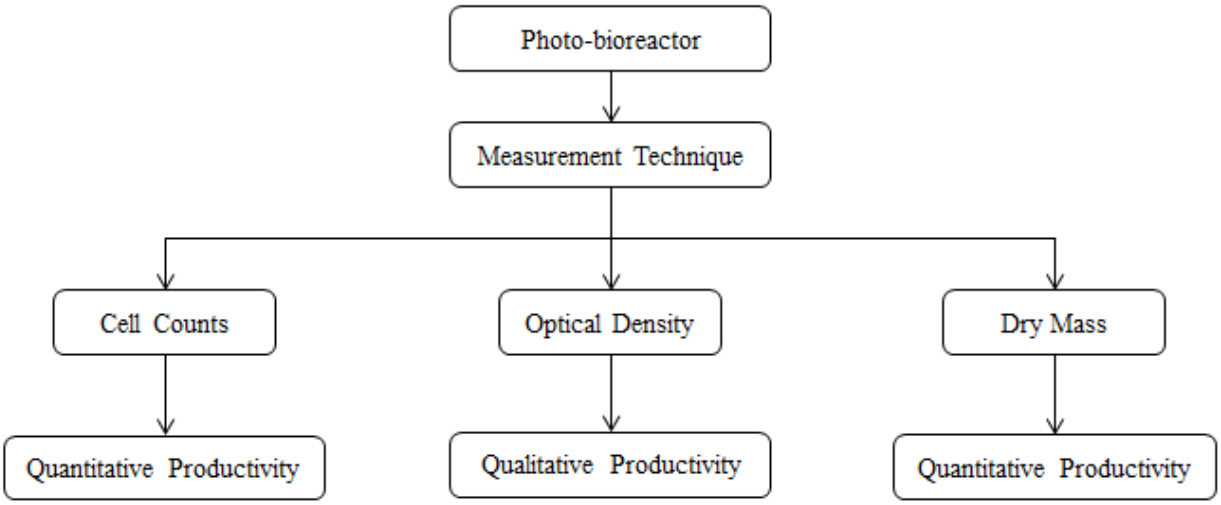

Figure 8: Summary Flowchart of Analytical Measurements for Microalgae.

3.5. Electrocoagulation Apparatus

The electrocoagulation reactor (see Figure 9) was made of PVC plastic with a working volume of 1.35 L (L: 20 cm, W: 5 cm, H: 15 cm). The unit operated in batch mode with a mono-polar electrode configuration. The electrodes were horizontally inserted through side supporters attached to the reactor walls; where a 4 cm gap between the electrodes was kept constant for all

experiments. The electrode was a flat sheet made of aluminum (Purity: 99%) and low carbon iron (purity: 98%), purchased from McMaster-Carr. All plates were cut identically with a submerged area of 200 cm^2. Both metals were used as anode and cathode, depending on the experiment. Current was supplied to the electrocoagulation unit from DC power source (GWINSTEK, SPS-3610) with a maximum current of 10 Amp. and maximum voltage of 36 Volt. A magnetic stirring plate was used to provide homogenous mixing during the operation of electrocoagulation. A pH meter (accumet® BASIC, AB15) was used to monitor the acidity of the solution being treated.

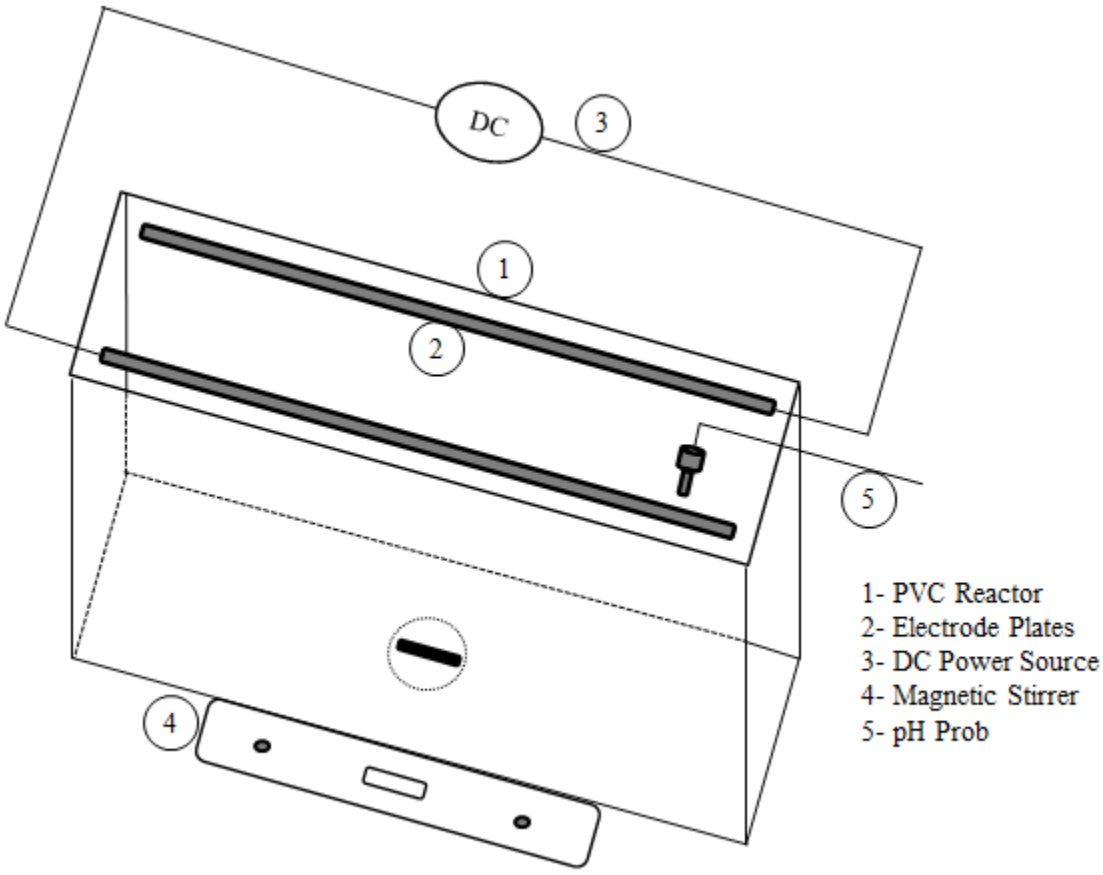

Figure 9: A Schematic Diagram of Electrocoagulation Unit Assembly.

An electrocoagulation experiment was run as follows. 1L of microalgae solution was taken from the photo-bioreactor and mixed with approximately 1g of electrolyte agent (sodium chloride) to reduce the potential resistance. The solution pH was measured before and after each experiment and adjusted by adding either a dilute sodium hydroxide or hydrochloric acid, depending on the desired pH. The flat plates (electrodes) were polished using sand paper, weighed, and placed in the reactor. Current was supplied for 60 min after the microalgae solution was poured into the reactor. Plates were removed from the reactor after the run was completed, rinsed with distilled water, dried and weighed to obtain metal dissolution measurement. Treated algal solution was then transferred to a clean graduated cylinder for the sedimentation experiment.

3.6. Analytical Measurements on Electrocoagulation

The destabilization of the microalgae suspension during electrocoagulation was measured by three methods, cell counts, optical density, and dry mass determination as described in section 3.4. Microalgae destabilization is defined as disturbing the solids suspension by either chemical or physical forces to enhance the downstream separation. A matrix of 26 samples was taken for each electrocoagulation experiment. A 1 mL sample was withdrawn by pipette every 5 minutes for dry mass analysis, totally 13 samples over the hour of operation. Similarly, a second 1 mL sample was withdrawn at the same time for cell count and optical density analysis. The sampling resulted in a 2.6% loss in the volume treated. The pH meter was calibrated regularly using buffer solution (i.e. pH levels of 4, 7, and 10). The recovery (destabilization) efficiency was determined by the following equations;

$$\eta_{CC} = \frac{CN_i - CN_f}{CN_i} \qquad \text{Eq(1)}$$

$$\eta_{OD} = \frac{(OD_i - OD_{blank}) - (OD_f - OD_{blank})}{(OD_i - OD_{blank})} \quad \text{Eq(2)}$$

$$\eta_{DM} = \frac{m_i - m_f}{m_i} \quad \text{Eq(3)}$$

Where η_{CC} is the recovery efficiency based on cell count, CN_i initial cell count, CN_f final cell count, η_{OD} is the recovery efficiency based on optical density, OD_i initial optical density of solution, OD_f final optical density of solution; noting that the optical density values were subtracted from blank solution (i.e. de-ionized water) to correct for the background reading, η_{DM} is the recovery efficiency based on dry mass, where m_i initial mass, and m_f is the final mass.

3.6.1. Calibration Curves for Microalgae Quantification

The quantification of microalgae cell density was done using various methods (i.e. cell count, optical density, and dry mass). The assessment process was done with the aid of ImageJ software. Figure 10 represents a regression fit that allows determining the cell density of microalgae suspension using spectrophotometry absorbance values. The absorbance values at 680 nm correlate well with the physical cell count (R^2=0.9687). Figure 11 and 12 represent regression fits between cell density and dry mass, as well as absorbance at 680 nm and dry mass respectively. The correlation is not well fitted, simply because measuring microalgae cell density based on dry mass was challenging due to contamination intervention of metals during the course of electrocoagulation.

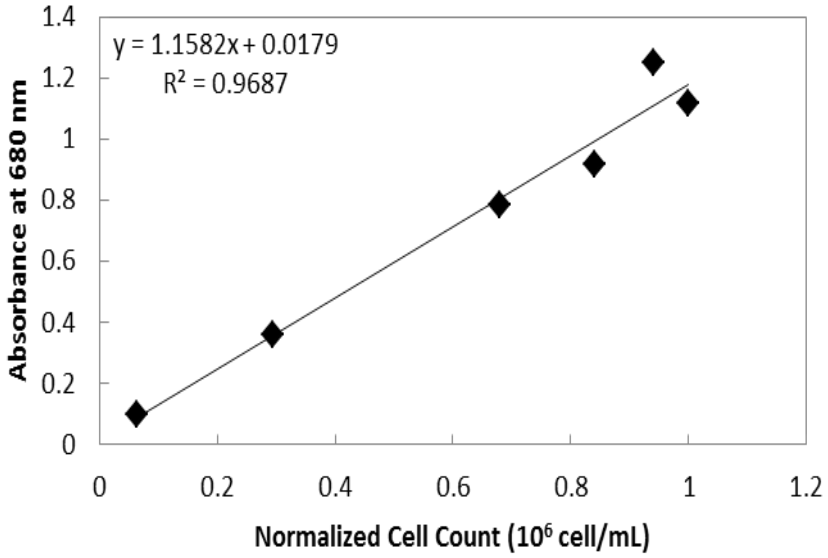

Figure 10: Regression Fit between Cell Density and Absorbance for Microalgae Quantification.

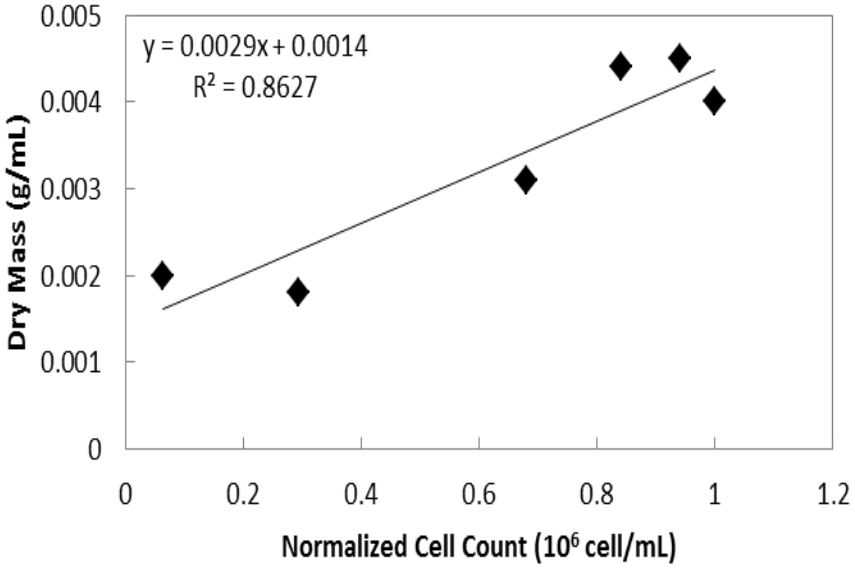

Figure 11: Regression Fit between Cell Density and Dry Mass for Microalgae Quantification.

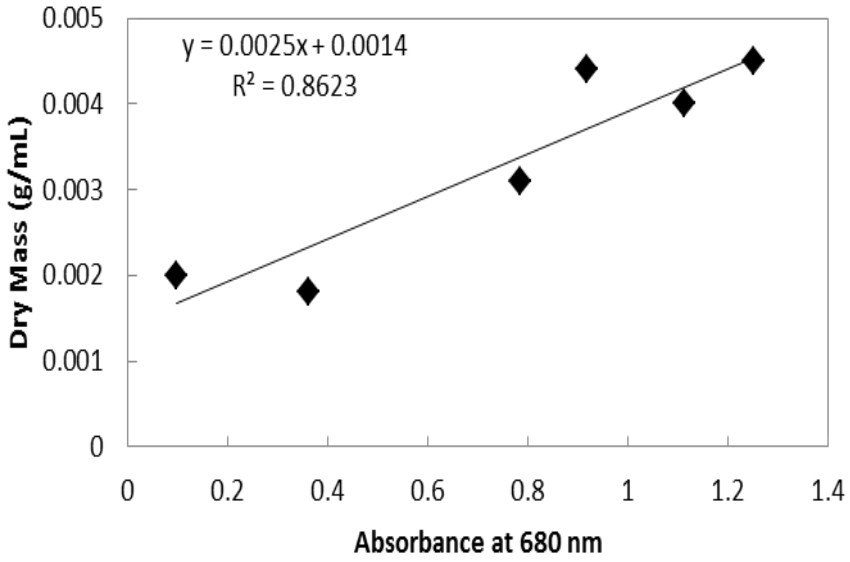

Figure 12: Regression Fit between Absorbance and Dry Mass for Microalgae Quantification.

3.7. Sedimentation Experiments

Sedimentation experiments were carried out in a graduated glass cylinder with a working volume of 1.25 L (43 cm in height and 6 cm diameter). After electrocoagulation, the solution of destabilized suspension was transferred from the electrocoagulation reactor to a beaker to determine the solution weight, using larger scale (OHAUS®, NVL2101/1), to be analysed. The coagulated solution was transferred to the graduated cylinder and allowed to settle for 60 min. The height of the interface between the biomass supernatant layer and clear water was visually recorded at different time intervals. The results were used to determine the settling velocity (cm/min) of microalgae after electrocoagulation and also to determine the amount of cultivation medium recycled.

After the sedimentation test was conducted, the clarified solution was separated by transferring it in a clean beaker leaving the pre-concentrated solution in the graduated cylinder. This separation was done visually by decanting the clarified (i.e. less dense) solution manually.

The mass of both solutions was compared to determine the concentration factor and the percentage of medium that can be returned to cultivation system. A 10 mL sample of clarified solution was retained for metal analysis. 50-90 mL of pre-concentrated algal solution was transferred to aluminum pans and oven dried for 24 hours to determine the water content. The dried biomass was then used to determine the accumulated metal via ICP-OES. The clarified solution was stored in glass jars to be reused for microalgae growth, whereas the pre-concentrated solution was retained for downstream treatment (i.e. limestone filtration).

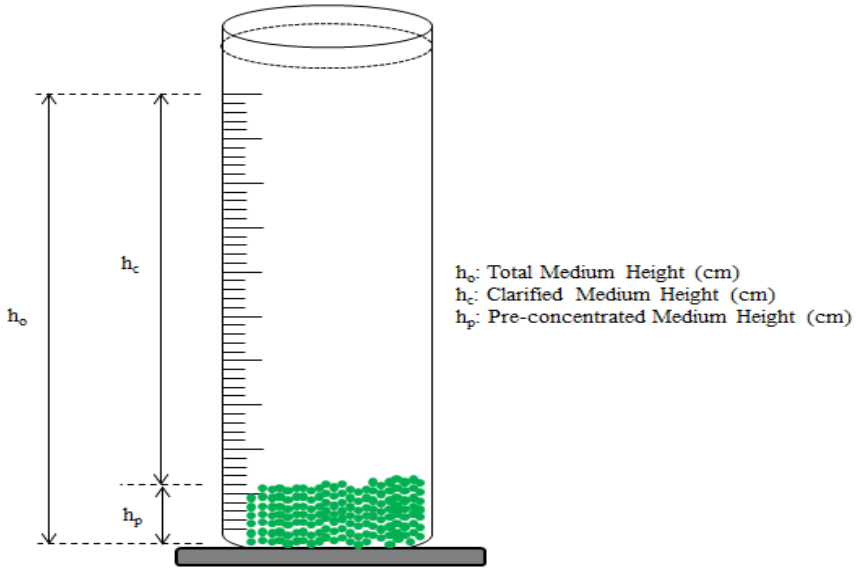

Figure 13: A Schematic Diagram of Microalgae Sedimentation.

3.8. Aluminum and Iron Analysis

The content of aluminum (Al) and iron (Fe) was analyzed in both coagulated algal biomass and process solution separated after electrocoagulation treatment. The concentration of metals in liquid and solid samples was determined using Inductively Coupled Plasma Optical Emission Spectrometry. Measurements of the liquid samples started with the addition of few drops of nitric acid to completely dissolve the trace amount of any organic biomass that may retain in the solution. All liquid samples were filtered using 0.45 µm membranes to ensure a

complete solids removal. The solid samples of microalgae biomass were digested in nitric acid using a microwave oven (MARS 230/60, Model No. 907501). The digestion procedure started with washing and cleaning the pressure vessels. The mass of empty vessels was recorded, 0.5-1 g of algal solids was added to the vessel. The loaded vessels with biomass were weighed before adding 10 mL of nitric acid to each one. The pressure vessels were left exposed to ambient air for a minute to allow any chemical reactions to take a place. The vessels were labeled, weighed, and returned to the microwave rotor. The prepared samples were heated at 180 ^{o}C for 10 minutes. The vessels were weighed after digestion to account for any mass loss, then moved to the fume-hood and opened with caution due to generated pressure. Duplicates of each digested sample were diluted in accordance to the dedication limit using rinse water. The diluted samples were sent for analysis at the Environmental Science Group Laboratory at RMCC.

3.9. Sand Filter Experiments

3.9.1. Bed Material

Limestone was an appropriate material as a filter medium for this study, since the scraped filter cake would contain algal biomass-Al/Fe hydroxides-limestone and all are suitable for use in clinker production. Limestone aggregates were obtained from LafargeHolcim Canada Inc, Bath, Ontario. The size reduction of aggregates was done in two stages at the Geological Engineering Laboratory at Queen's University. A medium-size jaw crusher was used in the first stage to produce medium aggregates; afterwards, a small-size jaw crusher was used to further grind the aggregates to fine particle (micron level). The ground limestone was sieved using mechanical shaker to separate the bulk into different size fractions. A stack of seven sieves was used in the particle-sized analysis (5 mm, 2.5 mm, 1.25 mm, 1 mm, 600 μm, 420 μm, and 250 μm). 1 kg of ground limestone was discharged into the sieves stack and placed in the mechanical

shaker located at the Civil Engineering Laboratory, RMCC. The shaker was turned on for 10 minutes. After the vibration was done, the mass of retained material in every sieve was recorded to plot the size distribution curve shown in Figure 14.

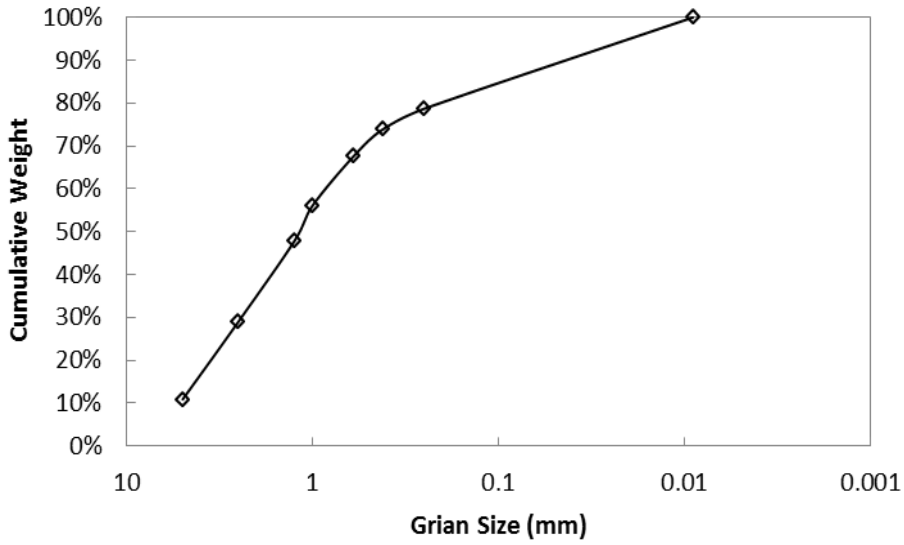

Figure 14: Size Distribution of Limestone Aggregates.

3.9.2. Filter Apparatus

As shown in Figure 15, the filtration apparatus consisted of five parts: movable plunger (3.1 cm inner dimeter, 3.5 cm outer diameter and 15.1 cm in height), graduated plunger sleeve (3.5 inner diameter, 4.0 cm outer diameter, 10.8 cm in height), backing screen (3.5 cm diameter and 1 cm in height), circular sheet of wire mesh and sampling adapter. The plastic backing screen was designed with larger perforations as a physical supporter for various sizes of wire mesh sheets (stand drain), which was placed on the top of the movable plunger. The pores size of the mesh sheet had to be smaller than the particles diameter of the filter medium; therefore, several mesh sheets were used for different grain sizes of limestone. The mesh sheet also acted as a drain channel for passing solution. The movable plunger and sampling adopter were placed

inside and on top of the graduated sleeve respectively. The following schematic shows the assembly of the limestone filter.

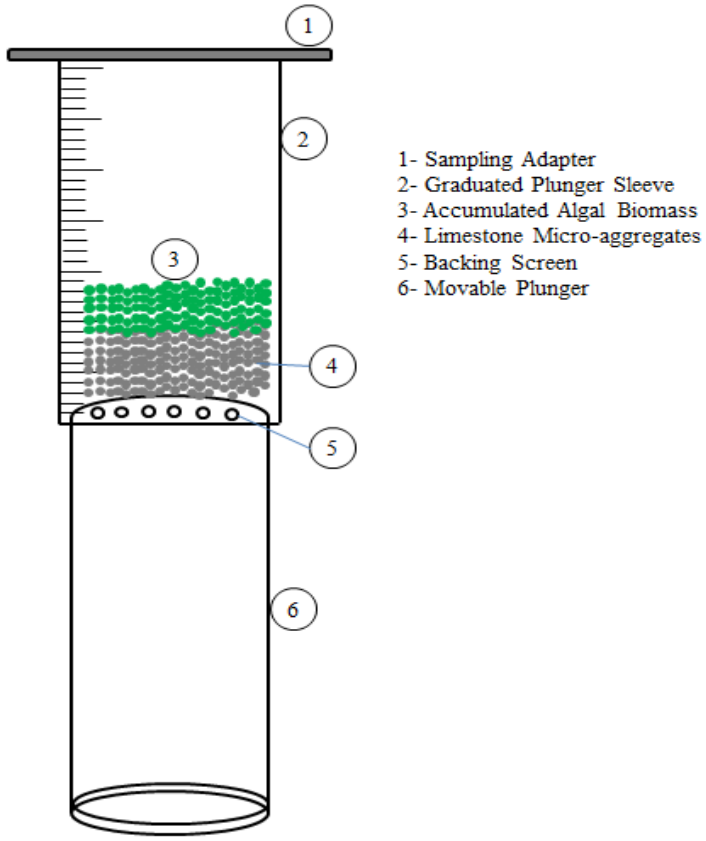

Figure 15: A Schematic Diagram of Sand Filter Assembly.

Filtration experiments began by placing the filter assembly over a beaker on a balance, which allowed the mass of captured solution to be measured. The material of the filter bed was weighed and placed into the plunger sleeve. The filter performance was tested by varying the grain sizes of the bed media.

The filter bed media was pre-wetted using 50 mL of distilled water before each test to reduce the adhesion effects of limestone. A 50 mL sample of pre-concentrated algal solution was poured into the filter and the mass of medium passing through was recorded for 60 minutes using digital camera. After the filtration experiment was done, the plunger was raised to release the

biomass cake and limestone bed. At the sampling adapter, the biomass cake and a portion of the filter bed were scraped to be used in downstream unit (i.e. briquetting). A sample of the filter cake was tested to determine the water content after filtration.

3.10. Passive Drying Tests

A mixture of microalgae biomass, metal hydroxides, and fine limestone were manually blended and transferred in aluminum pans to form cylindrical briquettes. Different ratios between microalgae and limestone were investigated to determine the heating value. The water content was determined before and after passive drying. The water reduction after the passive drying was compared to those obtained after filtration. The mixture was placed on a laboratory bench to be dried under ambient conditions. The water content of the solids was determined every 24 hours by measuring the mass loss. The measurements were halted when the mass was held constant. Then, the solids were placed in the oven at 105 ^{o}C for 24 hours to ensure a complete drying to calculate final water content.

3.11. Thermogravimetric Analysis (TGA) Tests

TGA was used to determine the material characteristics (i.e. approximate analysis and decomposition reactions) by continually recording the mass of a sample while the temperature was raised at a specific rate. All experiments were conducted using TA instruments Q50 model provided in Chemistry and Chemical Engineering Department at RMCC. Experiments were carried in an oxidative environment; where air was used as the oxygen (O_2) source, noting that gas flows included 40 mL/min air and 40 mL/min N_2 for balance. Before each TGA run, a platinum sample pan was cleaned and tared in a nitrogen (N_2) environment. A 10-15 mg sample was placed into the sample pan and then automatically hooked into the TGA furnace. The tests

were conducted up to a maximum temperature of 850 ^{o}C with heating rate of 10 ^{o}C/min. In this study, TGA tests were performed to characterize the following materials:

- Pure algal biomass (*Chlorella vulgaris*): to investigate the proximate analysis (i.e. percentage of volatile organic matter, fixed carbon, and ash).
- Coagulated algal biomass: to estimate the accumulation of metals (Al and Fe) in biomass. The mass difference between residues of untreated algal biomass and coagulated biomass is anticipated to dominate by metal contamination.
- Post-filtration residue: to investigate the amount of biomass passing through the filter.

3.12. Bomb Calorimetry Tests

A calorimeter was used to measure the calorific value of the pure microalgae biomass, coagulated microalgae biomass, and the multi-purpose briquettes. The calorimetry apparatus used in this study was Parr instrument, model 6200, located at Royal Military College of Canada. A 1 g pellet consisting of 50% sample powder and 50% benzoic acid was made with a press and a die. The pellet was placed in a sample pan after the mass was recorded. A cotton fuse was placed over the electrodes metal rod in which having both ends of the fuse in contact with the pellet. A 1mL distilled water aliquot was then added to the bomb to act as an absorbent for gases released during combustion. The bomb was sealed, pressurized with oxygen, placed in the calorimeter bucket, and then the electrodes were attached. A warm bath of 2L distilled water (25 ^{o}C ± 1 ^{o}C) was poured in the bucket then the bomb was activated. At the end of each run, heating value in J/kg was recorded.

Chapter 4 Results and Analysis

This chapter summarizes the collected data of each process and the relative analysis. The findings are used to comprehend the chemical and physical mechanisms to produce a value-added product via microalgae and its implication in cement plants.

4.1. Microalgae Cultivation

A microalgae culture was grown in a closed photo-bioreactor using a nutrient rich solution with a gas phase composition of 20% CO_2 and 80% air. The growth of microalgae was monitored for 105 hours (4.4 days); where the exponential phase started at ~ 48 hours and ended at ~ 90 hours as shown in Figure 16. The highest cell density attained after 105 hours (i.e. linear phase) was 78×10^6 cell/mL, equivalent to 1.13 g/L of biomass on dry basis, obtained from dry mass measurements. The water content after microalgae maturation was found to be 99.88%; meaning that 3.85 m^3 would be needed to produce 1 kg/day of biomass.

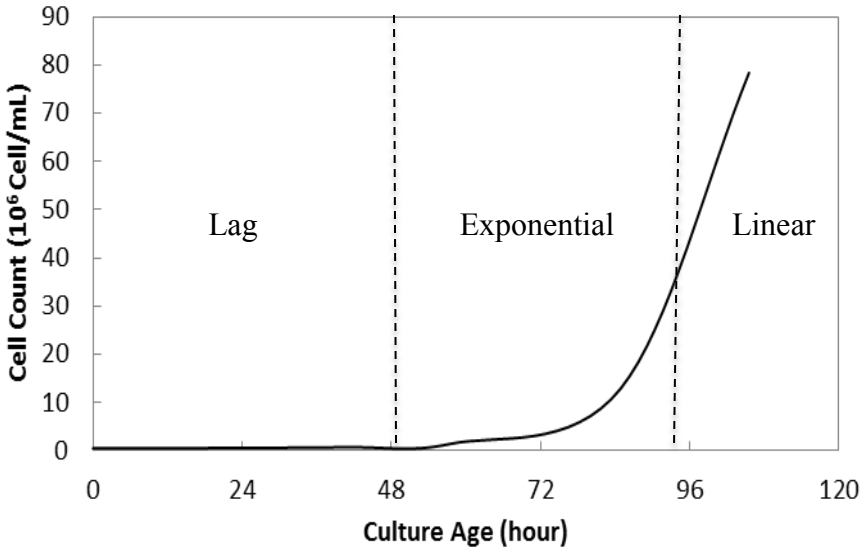

Figure 16: Growth Curve of *Chlorella vulgaris* in Photo-bioreactor.

4.2. Electrocoagulation Tests

Electrocoagulation was employed to produce metal ions in situ to disturb the algal suspension through charge neutralization. The effectiveness of electrocoagulation was evaluated under different operating conditions where the control parameters (i.e. current density, solution pH, and stirring speed) were varied. Testing was conducted at two scenarios below:

1. Aluminum plate as working anode and iron plate as cathode.
2. Iron plate as working anode and aluminum plate as cathode.

4.2.1. Process Performance Using Aluminum Anode

4.2.1.1. Effect of Stirring Speed

Stirring the microalgae solution during the experiment was a control parameter for the performance of electrocoagulation. Three stirring speeds were used in this study to evaluate the effect of mixing on the recovery efficiency of microalgae while holding current density and initial solution pH constant. Figure 17 shows the removal efficiency data at 0, 100, and 200 rpm. The three stirring speeds had little effect such that the removal efficiencies at 10 min and 45 min were found to be 15% and 93% respectively at all speeds. This lack of influence by stirring suggests the attachment between microalgae cells and aluminum hydroxide did not limited by physical mixing, but rather other mechanisms were involved. As observed, the movements of micro-bubbles produced at the surface of anode and cathode generated convective currents in the reactor and therefore enhanced the contact rate between microalgae cells and metal hydroxides. Additionally, the electrophoretic motion would be anticipated to induce the destabilization of microalgae suspension. Electrophoretic motion refers to the movement of objects due to the effect of an electrical field. The attachment between aluminum hydroxides and microalgae suspension could occur when the negatively charged algal cells were carried towards the anode

by the induced electrical field. Studies showed that system homogenization is adversely affected at high mixing speeds; the formed algae-metal flocs are degraded and continuously dispersed over the entire reactor, thus reducing removal efficiency [50, 81]. Noting that the error bars represent experimental variations; n=2.

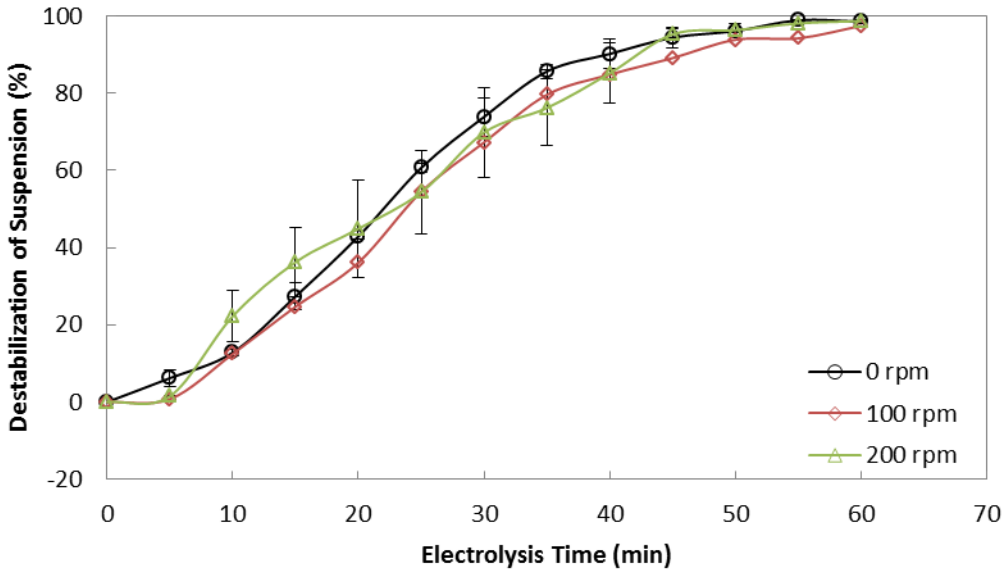

Figure 17: Microalgae Destabilization at Different Stirring Speeds, CD: 15 Amp/m^2, pH: 6, Al anode.

4.2.1.2. Effect of Current Density

Current density was another operating parameter that may affect the performance of electrocoagulation. The dosage of both metal ions (i.e. Al^{3+}, Fe^{2+}, and Fe^{3+}) and the generation of micro-bubbles were dependent on the current density. In this study, microalgae recovery was evaluated at four different current densities, 15 Amp/m^2, 30 Amp/m^2, 60 Amp/m^2, and 120 Amp/m^2. Noting that 15 Amp/m^2 was chosen as the lowest current density to provide the minimal energy required to drive the chemical reactions of metal dissolution. Figure 18 shows the destabilization of microalgae at those values. It was found that the destabilization time was inversely proportional to current density. After 10 min of electrocoagulation, 3% of microalgae

suspension was recovered at 15 Amp/m^2; whereas, 85% of microalgae suspension was recovered at 120 Amp/m^2.

The observations suggested that the higher microalgae recovery at 120 Amp/m^2 was not taking place solely due to the release of more metallic ions to the solution, but also due to the generation of micro-bubbles at the surface of electrodes. The release of metal ions was greater at higher current densities. Figure 18 clearly shows that microalgae destabilization was faster at higher current densities. The involvement of micro-bubbles generation raised the possibility that a portion of the microalgae kept their surface negative charge which is disadvantageous for downstream dewatering processes, i.e. sedimentation. It was observed that the microalgae recovery at lower current density was a function of both attachments of metal hydroxides and micro-bubble flotation but not at higher current density.

This finding can be verified by the pH change of the microalgae solution during the course of treatment. As it can be seen from Figure 19, at current density of 15 Amp/m^2, the medium pH has increased only from 6.00 to 7.12 after 1 hour of operation; whereas, the pH has increased to 8.96 at 120 Amp/m^2. The additional pH increase at higher current density suggested that the generation of hydrogen bubbles and hydroxide ions at the cathode was greater, leading to an excess of OH^- ions. This may be due to the fact that two oxidation reactions at the anode (i.e. water and metal) were competing with only one reduction reaction at the cathode (i.e. water). There is an energy trade-off between recovery efficiency and operation cost since the optimal current density suggested is ranged between 20-25 Amp/m^2 [54]. It can be understood that operating electrocoagulation at higher current density leads to a reduction in the destabilization time, but the energy consumption increases. Detailed energy consumption calculations are

described in section 4.2.6 (see table 8). Noting that the error bars represent experimental variations; n=2.

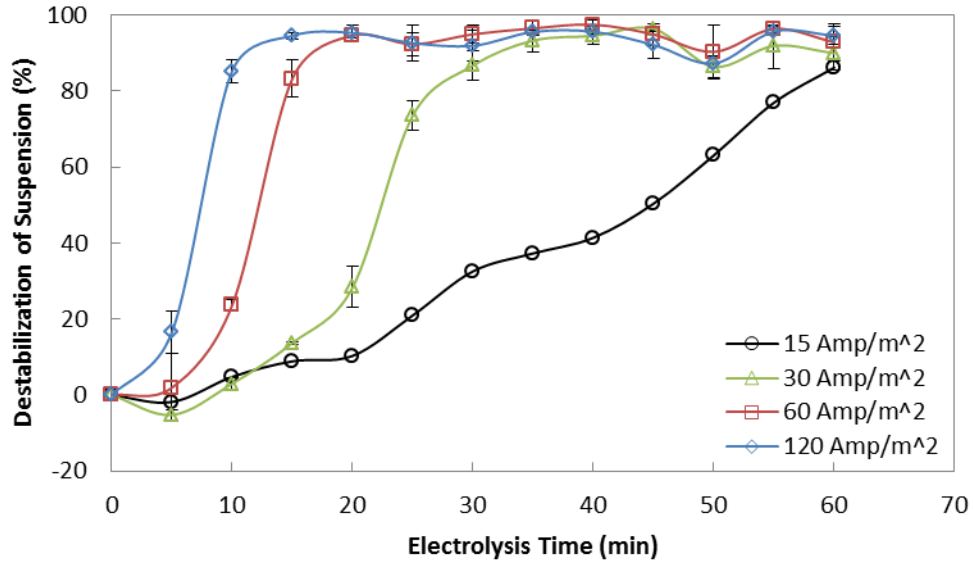

Figure 18: Microalgae Destabilization at Different Current Densities, SS: 100 rpm, pH: 6, Al Anode.

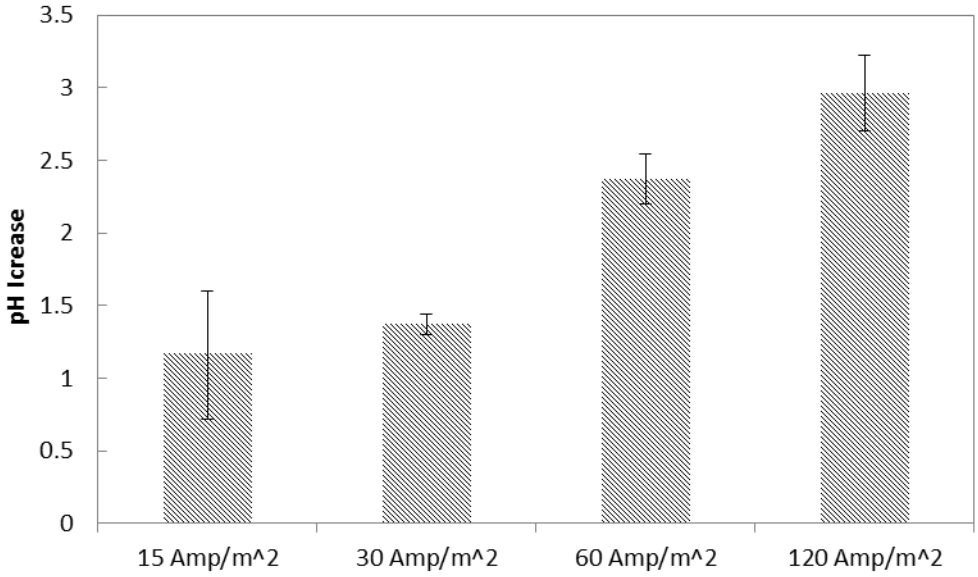

Figure 19: Solution pH Increase at Different Current Densities using Al Anode.

4.2.1.3. Effect of Solution pH

The pH of the microalgae solution being treated during electrocoagulation was another control parameter to consider, since it affects metal hydroxide speciation. The formation of metallic hydroxides varies significantly under acidic and alkaline environments. In this study, microalgae recovery was evaluated at three pH levels; 4, 6, and 8. As shown in Figure 20, the destabilization under acidic conditions followed a similar trend, 90% of microalgae suspension was destabilized after 30 min. This suggests that positively charged metallic hydroxides binded to the negative surface of microalgae cells. The recovery efficiency under slightly alkaline conditions (i.e. pH=8) may not have been as effective, given the excess of negatively charged hydroxide ions were promoted which may reduce the microalgae removal. The microalgae destabilization achieved a plateau for all three pH levels after 30 mins, indicating that enough soluble ions were provided for coagulation.

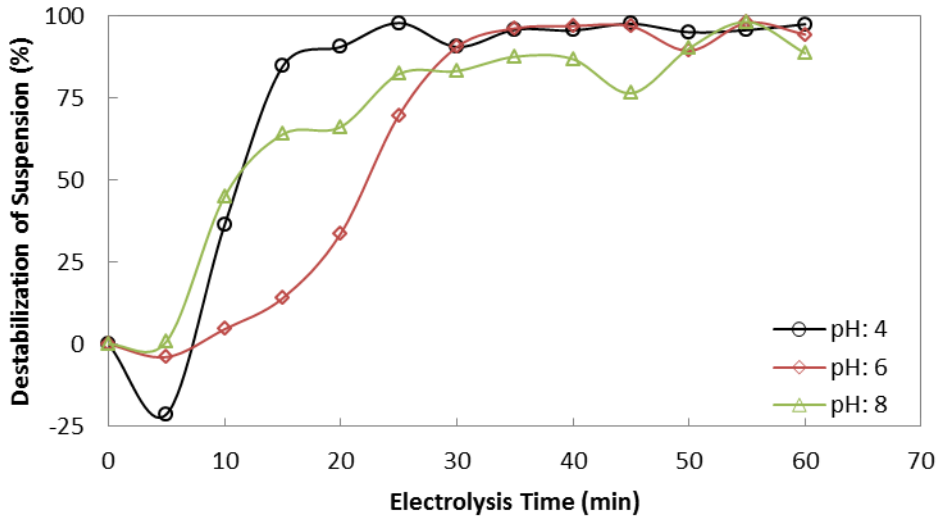

Figure 20: Microalgae Destabilization at Different pH, CD: 30 Amp/m^2, SS: 100 rpm, Al anode.

4.2.2. Process Performance Using Iron Anode

In this section, the effects of stirring speed and solution pH on the electrocoagulation performance using iron anode were not considered, since no significant effects have been noticed while aluminum anode used (results presented in section 4.2.1). The performance of the iron anode was only investigated at different current densities, leading to a better understanding of the ferric hydroxide effectiveness to disturb organic matter (i.e. microalgae biomass) and the results were compared to those using aluminum anode.

A set of experiments was performed using iron anode at current densities of 15, 30, 60, and 120 Amp/m^2. Results, presented in Figure 21, indicate that the degree of microalgae destabilization was lower at 15 and 30 Amp/m^2 compared to 60 and 120 Amp/m^2. At 15 Amp/m^2, the highest destabilization of 48% was attained after 60 min of electrolysis. At 120 Amp/m^2, about 84% of the microalgae suspension was destabilized within the first 10 min of electrolysis. Comparing the microalgae destabilization data of using iron and aluminum as anode material helps in understanding the suitability of electrocoagulation as a primary dewatering process. At lower current density (i.e. 15 Amp/m^2), the destabilization using the aluminum anode was 42% higher than using the iron anode. This suggests that iron is a less efficient material to remove organic matter. Additionally, the energy required to form iron hydroxide (i.e. ΔH_f^o= - 84 kJ/mol) is higher than aluminum hydroxide (i.e. ΔH_f^o= - 69.7 kJ/mol), suggesting that less iron hydroxides were produced compared to aluminum hydroxide when same current density is applied. The destabilization degree at high current density; in particular at 120 Amp/m^2, were in agreement for both anode materials, supporting the hypothesis made previously in which micro-bubbles flotation was the pre-dominant mechanism regardless of anode material used.

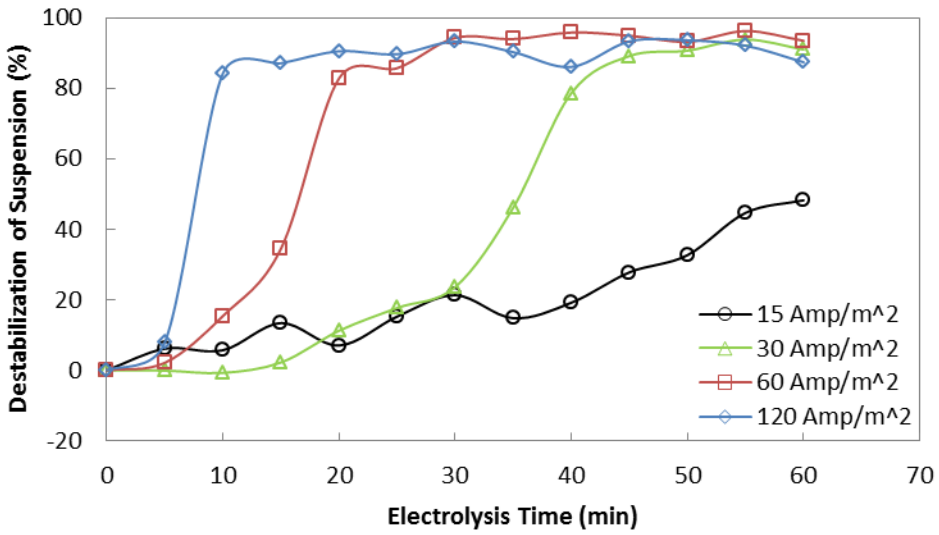

Figure 21: Microalgae Recovery at Different Current Densities, SS: 0 rpm, pH: 6, Fe Anode.

Figure 22 shows the increase of the solution pH during the electrocoagulation using iron anode. The increase of pH at 120 Amp/m^2 indicated the excess amount of unreacted hydroxide ions was generated at the cathode. However, the lack of pH change at current densities of 15, 30, and 60 Amp/m^2 may indicate a constant concentration of OH^- ions in the solution.

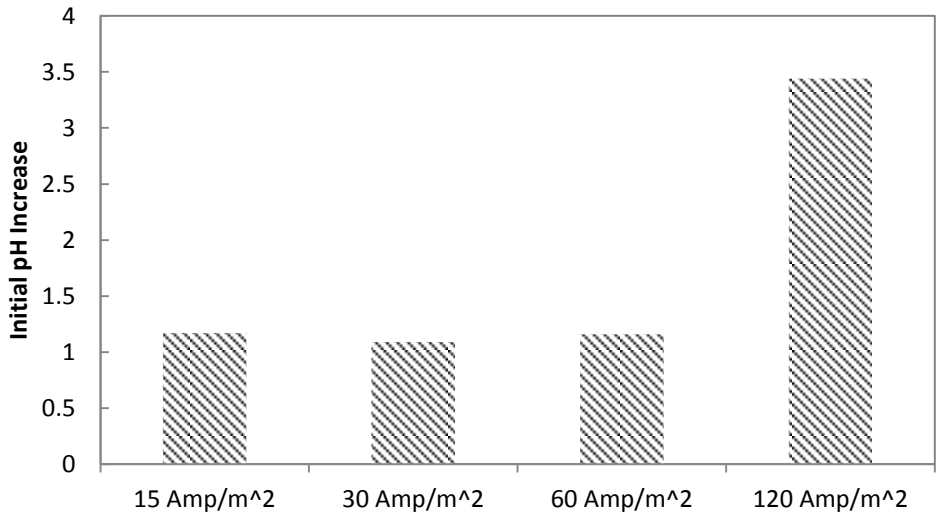

Figure 22: Solution pH Increase at Different Current Densities using Fe Anode.

In theory, the higher the current applied is, the more OH^- ions will present in solution; however, a portion of OH^- bind with the metallic cations released to forming metal hydroxides. Due to the metal solubility and the competition of water oxidation at the anode, it was challenging to back calculate the total amount of OH^- ions generated.

4.2.3. Metal Absorption Analysis

This section explains the accumulation of both metals, i.e. aluminum and iron, in both the algal biomass and the process water during electrocoagulation. As shown in Table 6, the aluminum contained in the algal biomass increased with the current density such that the aluminum exposed to the process as a whole at 120 Amp/m^2 was 8.5 times higher than at 15 Amp/m^2. Results showed the percentage of aluminum accumulated in algal biomass at 15 Amp/m^2 and 120 Amp/m^2 were found as 7% and 31% respectively, assuming a uniform distribution of metal ions in solution and solids. On the other hand, the aluminum content retained in the process water was found almost constant at all current densities, suggesting that the majority of metal accumulated with the algal biomass. Moreover, the total mass of aluminum released and the summation of aluminum mass absorbed by microalgae and that retained in process water did not balance. This can be due to an experimental error of measuring the weight of the metal plates. In addition to that, a portion of the metal may be lost during rinsing the plates before re-weighting; which was not done in this study.

Table 7 shows similar findings for iron accumulation with respect to various current densities. The dissolution of iron during electrocoagulation was greater than aluminum on a mass basis, thus, more metal exposure was achieved, leading to higher absorption. The accumulation of iron in the algal biomass at 15 Amp/m^2 and 120 Amp/m^2 were found as 12% and 41% respectively. The iron remaining in the process water after electrocoagulation was very low

compared to the total mass released. Based on the solubility of metal hydroxides in pure water, $Fe(OH)_2$ is found the most soluble complex follow by $Al(OH)_3$ and then $Fe(OH)_3$, suggesting that ferric hydroxides participation took place faster than aluminum hydroxide (see Appendix C-3). Despite the significant difference of aluminum and iron dissolution during electrocoagulation, it is reasonable to suggest that absorption capacity of algal biomass was limited to certain extent. For instance, the total mass of iron released at 120 Amp/m^2 was at least twice higher than aluminum, but only additional 10% of iron was accumulated in algal biomass compared to aluminum.

Table 6: Accumulation of Aluminum during the Operation of Electrocoagulation

Current Density	15 Amp/m^2	30 Amp/m^2	60 Amp/m^2	120 Amp/m^2
Al Conc. in biomass (g_{Al}/g_{Algae})	0.070	0.177	0.236	0.319
Al Conc. in solution (mol/L)	0.00015	0.00011	0.00018	0.00022
Biomass Conc. in solution (g_{Algae}/L)	3.300	3.000	2.600	2.200
Mass loss of Al Anode (g)	0.120	0.260	0.460	1.010
Mass of Al absorbed by biomass (g)	0.232	0.531	0.612	0.702

Table 7: Accumulation of Iron during the Operation of Electrocoagulation

Current Density	15 Amp/m^2	30 Amp/m^2	60 Amp/m^2	120 Amp/m^2
Fe Conc. in biomass (g_{Fe}/g_{Algae})	0.119	0.208	0.309	0.405
Fe Conc. in solution (mol/L)	0.00019	0.00030	0.000017	0.000017
Biomass Conc. in solution (g_{Algae}/L)	2.200	2.600	2.100	2.300
Mass loss of Fe anode (g)	0.280	0.580	1.180	2.310
Mass of Fe absorbed by biomass (g)	0.261	0.542	0.648	0.932

4.2.4. TGA Tests on Coagulated Algal Bio-solids

A set of TGA experiments was conducted to characterize the behaviour of coagulated microalgae biomass in a combustion system. The TGA results of five samples coagulated under different current densities using an aluminum anode are presented in Figure 23-(a). The sample mass of untreated algal bio-solids experienced a rapid decrease between 275 ^oC and 450 ^oC. However, the mass drop after 500 ^oC slowed down and plateau was obtained of which 80% of the initial sample mass had oxidized by 850 ^oC. Similarly, the mass loss of algal bio-solids that

coagulated at 15, 30, 60, and 120 Amp/m^2 begins at 275 ^oC and levelled off between 550 ^oC and 850 ^oC, but the mass fraction of residues after combustion differed significantly from untreated algal bio-solids. For example, 70.1% of initial mass was burned out at 15 Amp/m^2; whereas, only 50.3% was burned when the sample was coagulated at 120 Amp/m^2. This is an indication of the aluminum content level accumulated during electrocoagulation.

To have an estimate of the metal content, the leftover residue of untreated bio-solids was subtracted from the leftover residues of the treated bio-solids. The calculated mass fractions of aluminum accumulated in the algal bio-solids at 15 Amp/m^2 and 120 Amp/m^2 are 9.5% and 29.5% respectively. This is comparable to the findings obtained using ICP-OES. The aluminum content accumulated to algal bio-solids at 15, 30, and 60 Amp/m^2 was also linearly correlated with the theoretical amount estimated using Faraday's Law of Electrolysis and the amount of hydroxides ions remained in the solution (see Figure 23-b). This indicates that the formation of aluminum hydroxides was not solubility limited, as the concentration of hydroxide ions increased with current density.

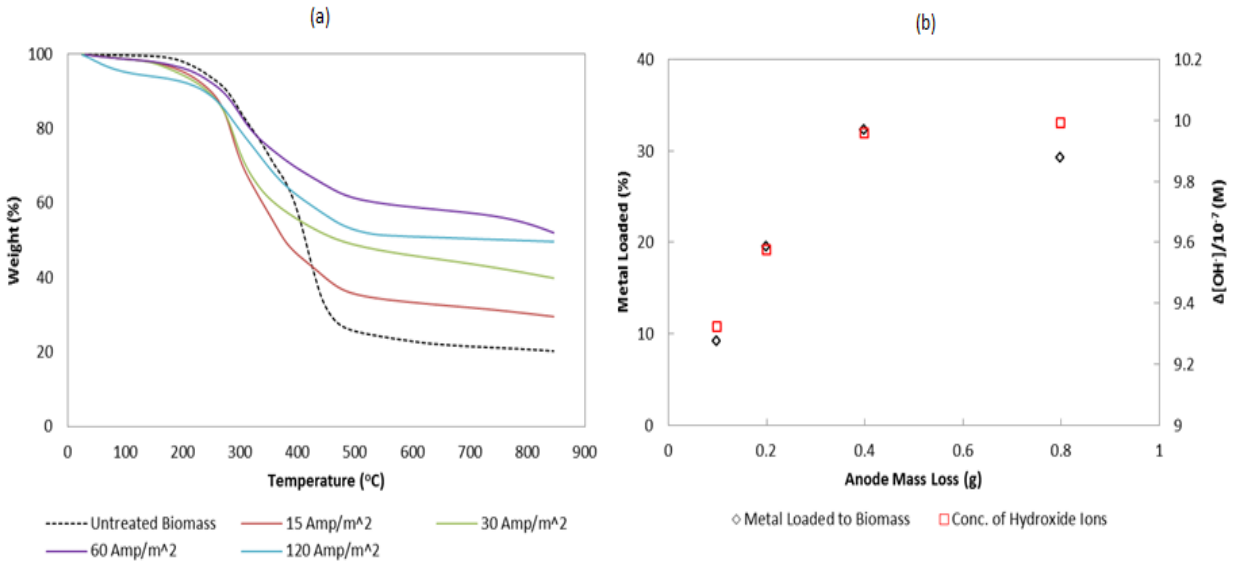

Figure 23: Characterization of Coagulated Biomass Using Al Anode, (a) Weight Change from 0-850 ^{o}C, (b) Correlation between Anode Mass Loss based on Faraday's Law and Metal Contamination in Biomass.

Figure 24 shows the rate of mass change with time. The degradation stages of coagulated biomass is explained by the overlapping peaks from 275 ^{o}C to 550 ^{o}C. This behaviour suggests that the reactions occurring over that range were de-volatilization of organic matter and oxidation of fixed carbon. The mass of aluminum metal accumulated in the coagulated bio-solids was taken as the difference between the ash contents of untreated bio-solids and the mass of leftover residues of treated bio-solids (Figure 23-(a)). The aluminum hydroxides decompose to aluminum oxide and water at temperatures between 300 ^{o}C and 500 ^{o}C; however, it is challenging to distinguish the decomposition peaks of aluminum hydroxides since it falls under the same thermal regime of biomass de-volatilization.

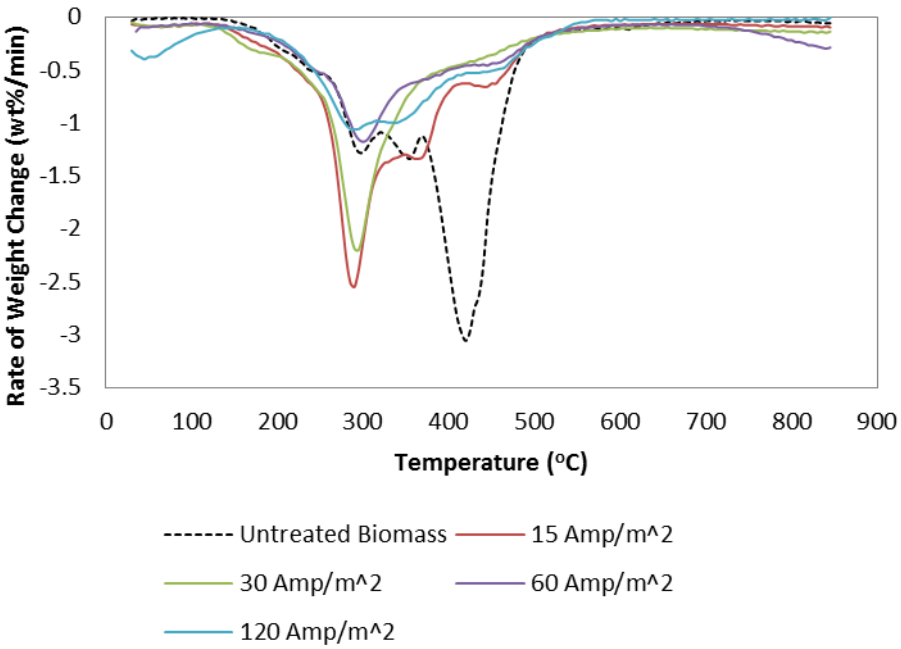

Figure 24: Rate of Weight Change vs. Temperature Characterization of Coagulated Biomass Using Al Anode.

Another set of TGA tests was conducted on coagulated bio-solids using an iron anode under the same conditions. Figure 25-(a) indicates the amount of iron content attached to the algal bio-solids after electrocoagulation at different current densities. It was assumed that the mass difference between untreated and treated bio-solids at 850 ^{o}C to be iron compounds. For example, at 15 Amp/m^2, the mass of metal in the bio-solids was 10.2%, while it was 33.2% at 120 Amp/m^2. As shown in Figure 25-(b), a linear correlation between the iron content taken by the bio-solids and the theoretical content of iron dissolved was found at all current densities. The concentration of hydroxides was near constant at 15, 30, and 60 Amp/m^2, suggesting the formation of ferric hydroxides was solubility limited. The mass of residues using iron and aluminum anodes (see Figure 23-(a) and Figure 25-(a)) was very similar, indicating that the capacity of microalgae bio-sorption was limited to a certain extent. Figure 26 indicates that both volatile content and fixed carbon of the coagulated biomass decomposed between 200 ^{o}C and 500 ^{o}C. No mass drop was noticed between 500 ^{o}C and 650 ^{o}C, but a decrease was observed

above 700 ^{o}C, suggesting the presence of iron carbonate. Noting that there was no such behaviour was observed with aluminum anode.

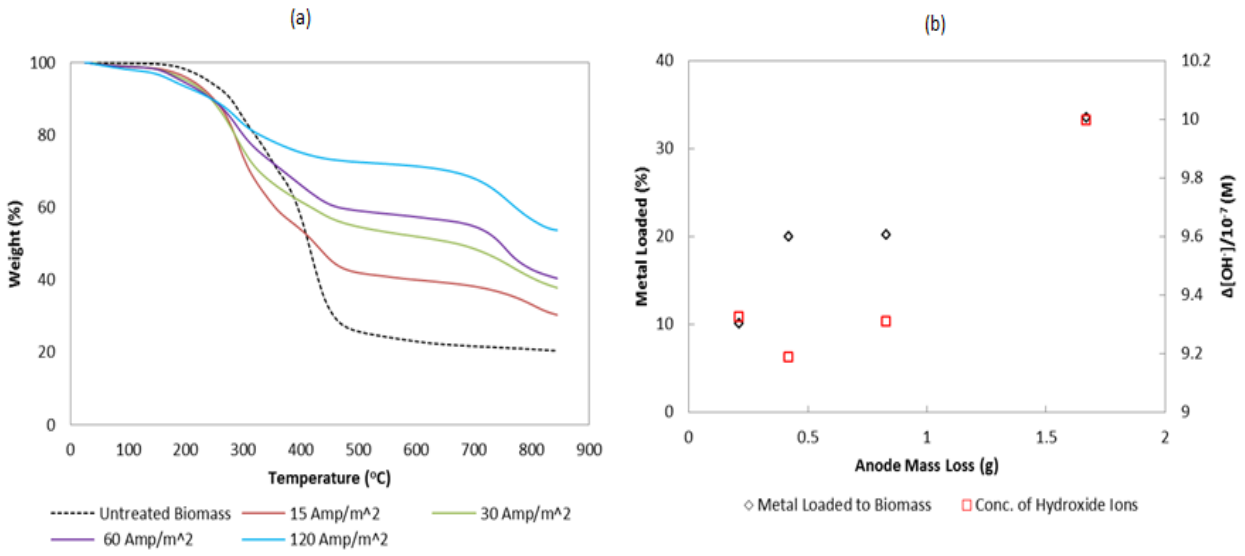

Figure 25: Characterization of Coagulated Biomass Using Fe Anode, (a) Weight Change from 0-850 ^{o}C, (b) Correlation between Anode Mass Loss based on Faraday's Law and Metal Contamination in Biomass

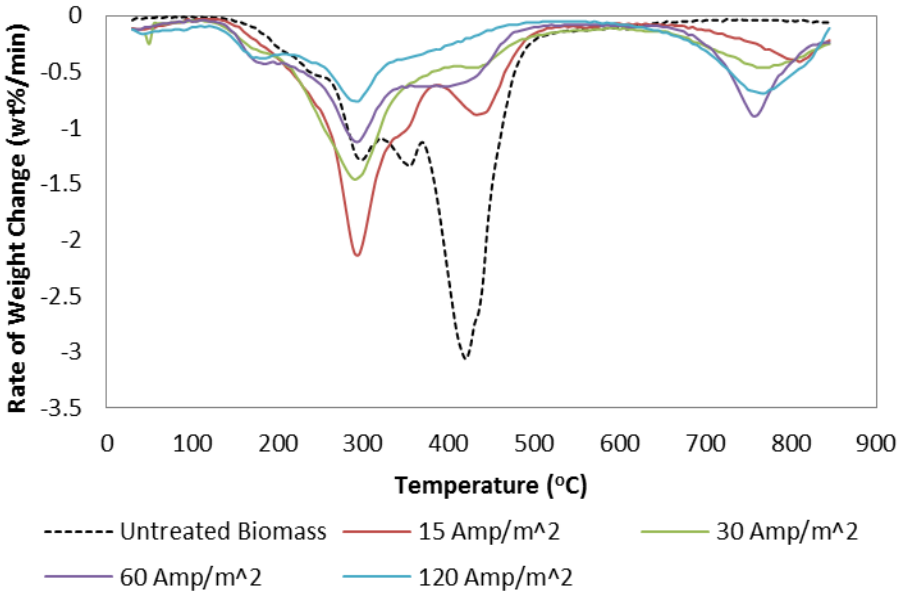

Figure 26: Rate of Weight Change vs. Temperature Characterization of Coagulated Biomass Using Fe Anode.

4.2.5. Calorific Value of Coagulated Algal Bio-solids

Energy content is a key parameter for evaluating microalgae as an alternative solid fuel. In this section, the energy content of microalgae biomass before and after electrocoagulation was investigated to understand the effects of metal hydroxide on the thermal conversion. The water content of all samples used in this study was approximately zero since the samples were thermally dried prior to testing. Figure 27 shows the heating values, expressed in MJ/kg, of coagulated biomass using aluminum and iron anodes. The heating value of microalgae before the treatment was found as 28.1 $MJ/kg_{drybiomass}$, which is higher than the expected value for algal biomass presented in section 2.5.

The energy content of the coagulated biomass declined as the metal loading increased during electrocoagulation. The biomass coagulated at 15 Amp/m^2 with iron anode had a heating value of 18 MJ/kg while at 120 Amp/m^2, it was reduced to 4.4 MJ/kg. Additionally, the relation between the energy content and the mass of leftover residues obtained from TGA was correlated. This suggests that the coagulated biomass was loaded with metals and the heat released during the combustion was absorbed by to the hydroxide decomposition endothermic reactions. The absorption rate of aluminum and iron hydroxides by microalgae biomass was comparable at all current densities except for 120 Amp/m^2, since the heat of combustion was significantly different. According to the data obtained from ICP-OES, TGA, and Bomb Calorimeter, the amount of iron released at higher current density was greater than aluminum; therefore, the tendency of iron hydroxide accumulation on biomass was higher, leading to a greater energy reduction. In addition, the content of iron oxides is 3 times lower than aluminum oxides in cement raw meal therefore the duration of microalgae destabilization using iron anode will be lower.

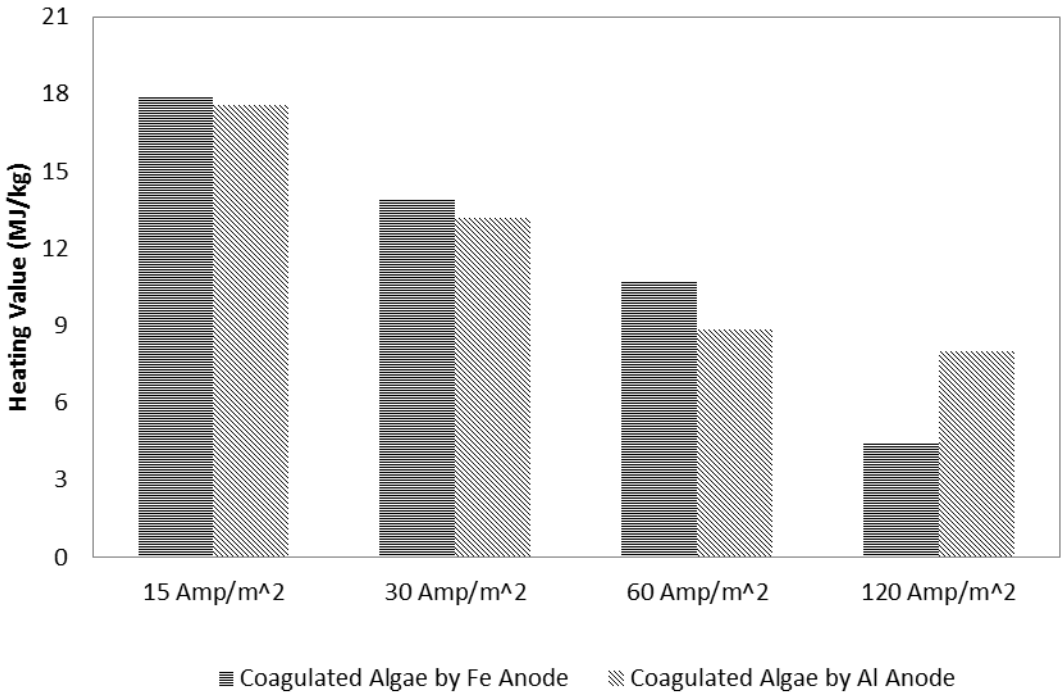

Figure 27: Energy Content of Coagulated Algal Bio-solids.

4.2.6. Power Consumption

Power consumption analysis helps in determining the economic feasibility of electrocoagulation process. The minimum amount of electricity consumed per mass unit of dry microalgae recovered (E, kWh/$kg_{drybiomass}$) was calculated using the following equation [50];

$$E = \frac{UIt}{1000V\eta_a c_i} \qquad \text{Eq(4)}$$

Where U is the voltage (V), I is the applied current (Amp.), t is the time in (hr), V is the reactor volume (m^3), $\eta_a$is the removal (destabilization) efficiency, and c_i is the initial density of microalgae (kg/m^3). As stated in Table 8, the minimal energy consumption using the aluminum anode was reached at longer electrolysis time when lower current density was applied due to the fact that the highest microalgae recovery was not achieved till the end of the operation.

Table 8: Power Consumption (kWh/kg$_{dry\ biomass}$) at Different Current Densities, SS: 100 rpm, pH: 6 and Al Anode.

CD (Amp/m^2) \ ECT (min)	10	20	30	40	50	60
15	0.849	-	0.518	0.449	0.265	0.240*
30	4.361	1.186	0.663	0.826*	1.120	1.273
60	2.408	1.271*	1.868	2.455	3.115	3.722
120	3.408	5.766*	8.757	11.631	16.039	18.218

ECT: Electrocoagulation Time; CD: Current Density
*: Power Consumption at Highest Destabilization (> 90%)

Applying moderate to higher current densities led to shortening the electrolysis time with higher recovery efficiency, but an energy penalty was imposed. The highest microalgae recovery at 15 Amp/m^2 was achieved after 60 min of electrolysis after 0.240 kWh/kg$_{dry\ biomass}$ was consumed. At 30 Amp/m^2, the electrolysis time was shortened by 20 min and the power consumption increased to 0.826 kWh/kg$_{drybiomass}$. Similarly, rapid microalgae recovery was observed while electrocoagulation was operating at 120 Amp/m^2, i.e. 95% recovery was achieved after only 20 min consuming 5.77 kWh/kg$_{dry\ biomass}$.

Comparing the iron anode to aluminum anode, it can be seen that more energy was consumed, due to the poorer microalgae destabilization by iron hydroxides. Table 9 indicates that the highest recovery efficiencies were, in most cases, reached near the end of electrocoagulation cycle, which imposed an extra energy penalty. For example, 90% of microalgae suspension was destabilized after 50 min at 30 Amp/m^2, with energy demand of 1.40 kWh/kg$_{dry\ biomass}$. The lowest energy requirement at the same operating condition was as 1.29 kWh/kg$_{dry\ biomass}$, where 79% of the suspension destabilized after 40 min. Energy can be wasted if electrocoagulation proceeds beyond the saturation point of microalgae recovery. From an energy

point of view, the power consumption after 40 min at current density of 30 Amp/m^2 may be inefficient, because the removal efficiency improved only by 14%. Energy-wise, there is also trade-off between the power consumption and operating time, especially at industrial scale.

Table 9: Power Consumption (kWh/$kg_{dry\ biomass}$) at Different Current Densities, SS: 0 rpm, pH: 6 and Fe Anode.

CD (Amp/m^2) \ ECT (min)	10	20	30	40	50	60
15	2.560	4.148	2.053	3.042	2.232	1.184*
30	-	4.532	3.233	1.295*	1.403	1.678
60	6.430	2.394*	3.155	4.140	5.320	6.364
120	3.310*	6.088	8.954	12.939	14.804	19.104

ECT: Electrocoagulation Time; CD: Current Density
*: Power Consumption at Highest Destabilization (48-84%)

Operating at lower current densities lead to longer retention times and thus larger reactors. There were other parameters that may alter the power consumption during electrocoagulation, the distance between electrodes and solution conductivity. For consistency, both of the aforementioned parameters were kept constant throughout all experiments.

4.3. Settling Characteristics of Microalgae

The objective of electrocoagulation was to improve the settling behaviour of a microalgae suspension by neutralizing the negative charge and increasing the microalgae density. The settling velocity of microalgae cells was a function of the metal dosage and the contact time during electrocoagulation. In theory, the higher the metal dosage, the faster the suspension will settle. Results presented in Figure 28-29, suggest the opposite, meaning the settling velocity of destablized suspension at 15 Amp/m^2 were faster than those at 120 Amp/m^2.

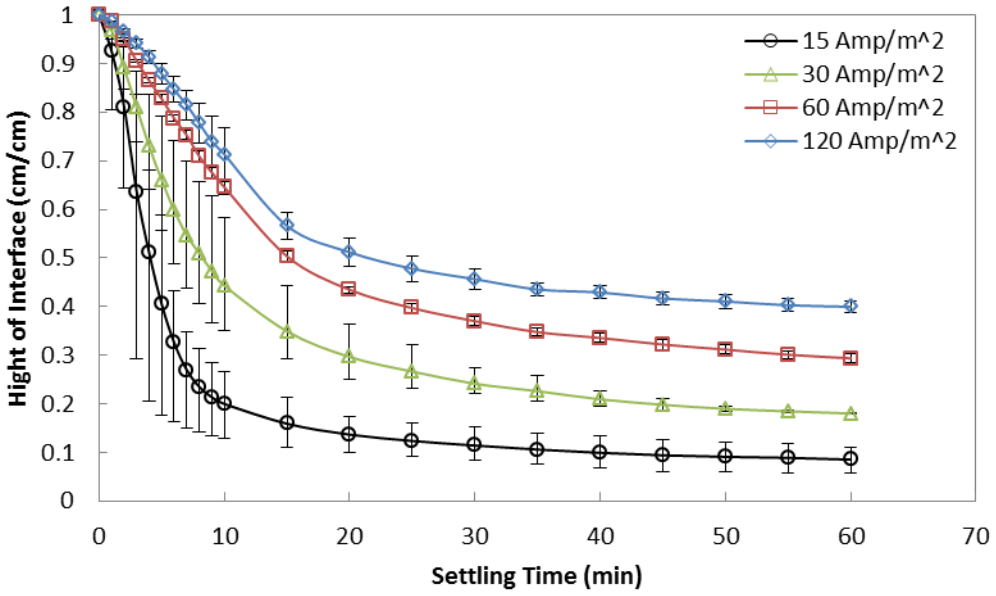

Figure 28: Sedimentation Tests of Coagulated Microalgae, SS: 100 rpm, pH: 6, and Al Anode.

The dissolution of aluminum ions after 60 min at 15 Amp/m^2 and 120 Amp/m^2 were estimated as 0.097 g and 0.776 g respectively. Despite the higher dosgae of aluminum ions at higher current density, the settling characteristic was found to be poorer. The settling velocity of coagulated biomass at 15 Amp/m^2 and 120 Amp/m^2 after 5 min of sedimentation were found as 4.04 cm/min and 0.79 cm/min respectively (see table 10). The higher the settling velocity is, the higher the removal and recycling of process water would be.

Table 10: Settling Velocities of Coagulated Biomass Using Al Anode.

	CD (Amp/m^2)	Settling Velocity (cm/min)
EC-Sed	15	4.04
	30	2.33
	60	1.21
	120	0.79

Despite the high recovery of process water at 15 Amp/m^2 (i.e. 82-90%), the water content of the algae decreased by less than 1% (see table 11). It is clear that the contact time between microalgae suspension and aluminum ions at the lowest current density was longer than at

highest current density. Although, the electrocoagulation time was fixed for all experiments, but the vast majority of microalgae suspension floated to the top of the reactor during the first 20 min of electrocoagulation at 120 Amp/m^2.

Table 11: Water Content Reduction after Electrocoagulation and Sedimentation Treatment Using Al Anode.

	CD (Amp/m^2)	ρ (g/L)	WC_i (%)	WC_f (%)	PMR (%)
EC-Sed	15	1.20	99.89	99.22	82.88
	30	0.90	99.91	99.36	75.26
	60	1.28	99.87	99.30	60.98
	120	1.18	99.88	99.35	57.74

This observation was attributed to micro-bubble generation. Settling at higher current density suggests that only a small portion of counter mettalic ions were absorped by microalgae suspension, meaning the negative charge of the microalgae cells were not fully neutralized. Also, it may be due to the presence of micro-bubbles in solution that prevents spontaneous sedimentation. Noting the error bars represent experimental variations; n=6 for 15 Amp/m^2, n=3 for 30 Amp/m^2, n=2 for 60 and 120 Amp/m^2. Figure 29 shows the settling behaviour of microalgae suspension destabilized using iron anode.

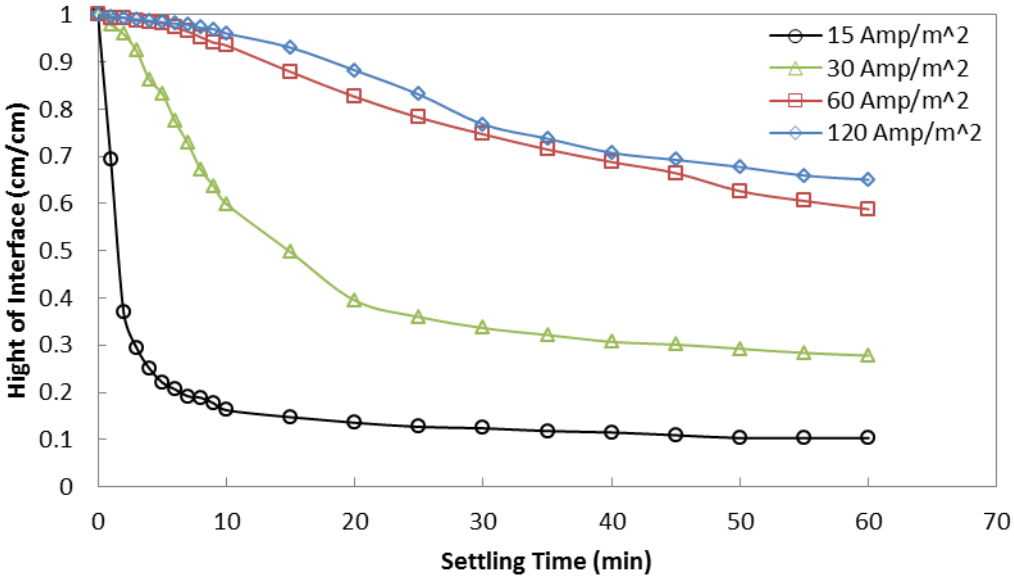

Figure 29: Sedimentation Tests of Coagulated Microalgae, SS: 0 rpm, pH: 6, and Fe Anode.

The results presented in Table 12 show the settling velocities of microalgae coagulated using iron hydroxides followed a similar trend as those coagulated using aluminum anode. For example, the biomass coagulated at 15 Amp/m^2 settled at a velocity of 5.13 cm/min while that coagulated at 120 Amp/m^2 settled at 0.10 cm/min.

Table 12: Settling Velocities of Coagulated Biomass Using Fe Anode.

	CD (Amp/m^2)	Settling Velocity (cm/min)
EC-Sed	15	5.13
	30	1.19
	60	0.12
	120	0.10

The water content reduction attained at 15 Amp/m^2 was found to be 0.6% and process water recovered was found to be 86% (see table 13). These findings suggest that gravity sedimentation was not only a function of metal dosage but it also be affected by the contact time between hydroxides and negative suspension during the course of electrocoagulation. In other

words, the microalgae suspension treated at higher current densities did not reach the highest degree of charge neutralization, which justifies the disturbance role of micro-bubbles generation; where the destabilization by flotation was the predominant over charge neutralization.

Table 13: Water Content Reduction after Electrocoagulation and Sedimentation Treatment Using Fe Anode.

	CD (Amp/m^2)	ρ (g/L)	WC_i (%)	WC_f (%)	PMR (%)
EC-Sed	15	1.20	99.89	99.34	86.18

4.4. Filtration Tests

In this section, the performance of the sand filter was investigated using limestone with grain sizes of limestone, 250, 420, and 600 μm. The limestone filter was evaluated based on four parameters including the volume of solution removed, fouling time, filtration rate, and the quality of filtrate. Figure 30 represents the experimental results of the filtrate volume passed through a pre-wetted bed at different grain sizes. As it can be seen, the filtrate volume passed after 60 min of operation time at all grain sizes ranged between 81% and 86%. Despite the small differences of filtrate volume passed, the filter performance was affected by the accumulation of a microalgae cake. For example, the solution retention at 250 μm reached a plateau after 30 min while a continuous decrease of the solution was observed at 420 μm and 600 μm. This suggests that filter fouling would be faster at smaller particle sizes due smaller pores size. It can also be observed that the amount of water retained in the biomass was a function of fouling rate. For example, the filter bed at 250 μm was completely clogged after 30 min with 16% of the initial solution volume remained in the filter cake and bed. Contrary, the filter bed at 420 μm and 600 μm experienced a partial fouling after 40 mins, where the filtrate volume kept passing at a rate of 0.1%. Table 14 indicates that the water content of the concentrated algal solution using limestone

grains size of 250 µm was reduced from 99.24% to 93.45%. Noting that the error bars represent experimental variations; n=3 for 250 µm, n=2 for 420 µm and 600 µm.

Table 14: Water Content Reduction after Limestone Filter Treatment Using Three grains Sizes.

	Size(µm)	ρ (g/L)	WC_i (%)	WC_f (%)	PMR (%)
Filtration	250	7.80	99.24	93.45	84
	420	11.30	98.89	94.22	81
	600	10.14	98.96	95.21	86

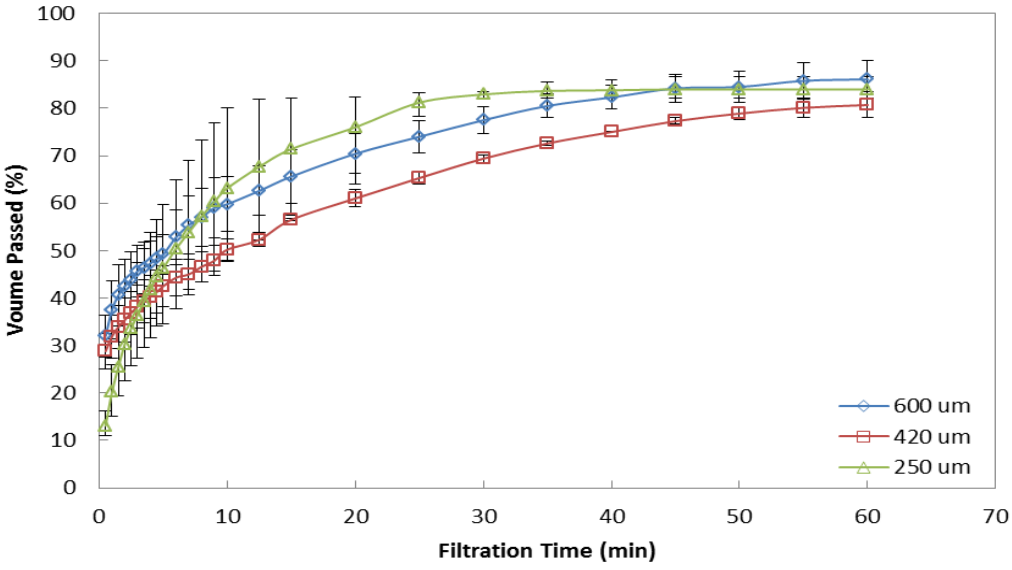

Figure 30: Performance of Sand Filter Using Three Grain Sizes of Limestone.

Figure 31 shows that the filtration rate at the beginning of each test was influenced by pores size of the filter bed. After 0.5 min of filtration, a higher filtration rate of 32 mL/min was achieved using 600 µm particles while only 13 mL/min was achieved with 250 µm. The filtration rate declined to 4.5 mL/min at all grain sizes after 5 min due to the build up of filter cake. Despite the solubility of limestone, a little portion of the bed dissolved during filtration and precipitated in the collected filtrate. TGA tests were performed on the residues passing the filter

to investigate the degree of microalgae penetration. Noting that error bars represent experimental variations; n=3 for 250 µm, n=2 for 420 µm and 600 µm.

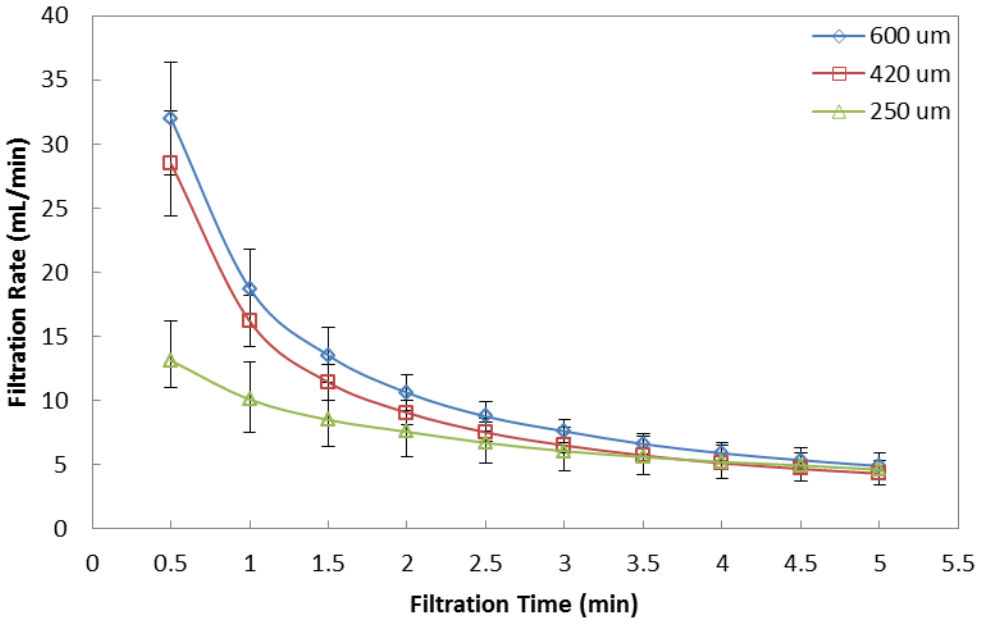

Figure 31: Filtration Rate vs. Filtration Time for Various Grain Sizes.

Figure 32 shows that microalgae penetration was indicated during filtration using aggregate sizes of 420 µm and 600 µm as bed media. The residues were a mix of limestone and penetrated biomass; the results were compared to pure limestone to aid evaluation. The mass difference between pure limestone and residues obtained at 420 µm and 600 µm were found as 8% and 16% respectively. The mass differences were anticipated to be the amount of microalgae penetrated with the filtrate. In short, there is a trade-off between the filtrate quality, water removal and the filtration time. Larger bed grains size reduces the filtration time, fouling issues, and the volume of the filter head tank, but a portion of microalgae biomass may penetrate through the bed which can adversely affect the effluent quality.

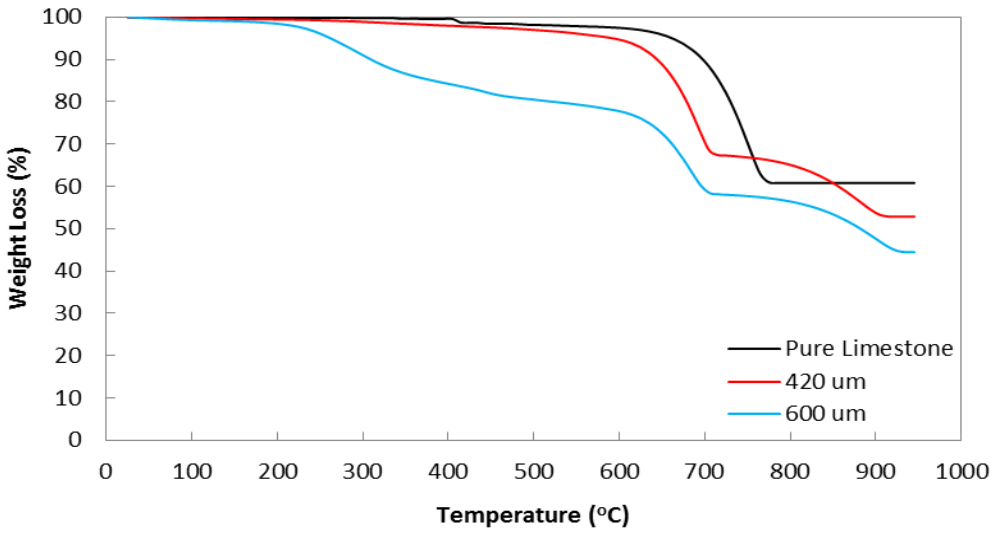

Figure 32: Characterization of Filtration Leftover Residues for Microalgae Penetration.

4.5. Briquetting and Drying Tests

Upon the completion of biomass filtration, the water content of the biomass cake was higher than alternative fuel specifications. The water content was further reduced by briquetting where a portion of the filter bed and the algae filter cake were mixed to form a stable solid. The solid fuel was then exposed to the atmosphere to allow passive drying for further moisture content reduction. Table 15 shows the proportions of algae and limestone of three briquettes before and after the passive drying phase. The water content of microalgae cake was reduced from 93.45% to somewhere between 55-65% after limestone blending. The mass of limestone was held constant to evaluate the water reduction as varying masses of algal biomass. The percentages of algal biomass in mix 1, mix 2, and mix 3 on wet basis (before drying) were 72%, 57%, and 39% respectively. Despite the variations of algal biomass in the mixes, similar drying trends were observed with water content reduction ranging between 3-25% within the first 24 hours (see Figure 33). This is can be due to the use of similar sized briquettes.

Table 15: Briquettes Proportions and their Associated Water Content before and after Drying.

Briquettes	Before Drying				After Drying			
	Mass (g)	Algal Biomass (%)	Limestone (%)	WC (%)	Mass (g)	Algal Biomass (%)	Limestone (%)	WC (%)
Mix 1	16.15	72.32	27.68	57.75	4.38	18.03	81.97	3.21
Mix 2	10.45	57.13	42.87	62.70	4.00	10.00	90.00	8.91
Mix 3	7.46	39.01	60.99	65.91	3.85	4.93	95.07	24.83

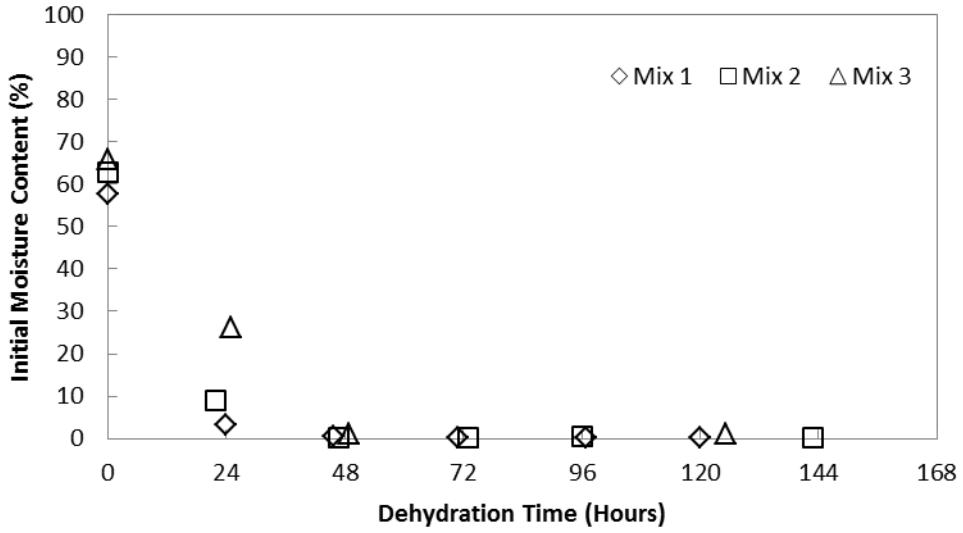

Figure 33: Passive Drying of Multi-purpose Briquettes.

Summary of Dewatering Results

Figure 34 represents the data summary of the water content reduction of microalgae solution using the novel multi-process approach with energy avoided with respect to thermal drying. Starting with 1000 g of microalgae solution consisting of 998.80 g water and 1.20 g algal bio-solids; resulting in water content of 99.88%. The initial water content of microalgae solution has reduced by 0.64% after a combined treatment of electrocoagulation and sedimentation, equivalent to 842.1 g of the process water. Evaporating that water would consume 2055 kJ of energy. The water content of pre-concentrated microalgae solution has decreased by an additional 5.79% using limestone filter. The energy that could be avoided to evaporate the water removed by the filter is 340 kJ. Only 17.12 g of water remained in the algal biomass out of

998.80g after the dewatering treatment including electrocoagulation, sedimentation, and limestone filtration. 99.82% of the remained water was removed by briquetting and passive drying; where 40.93 kJ of water evaporation energy was avoided.

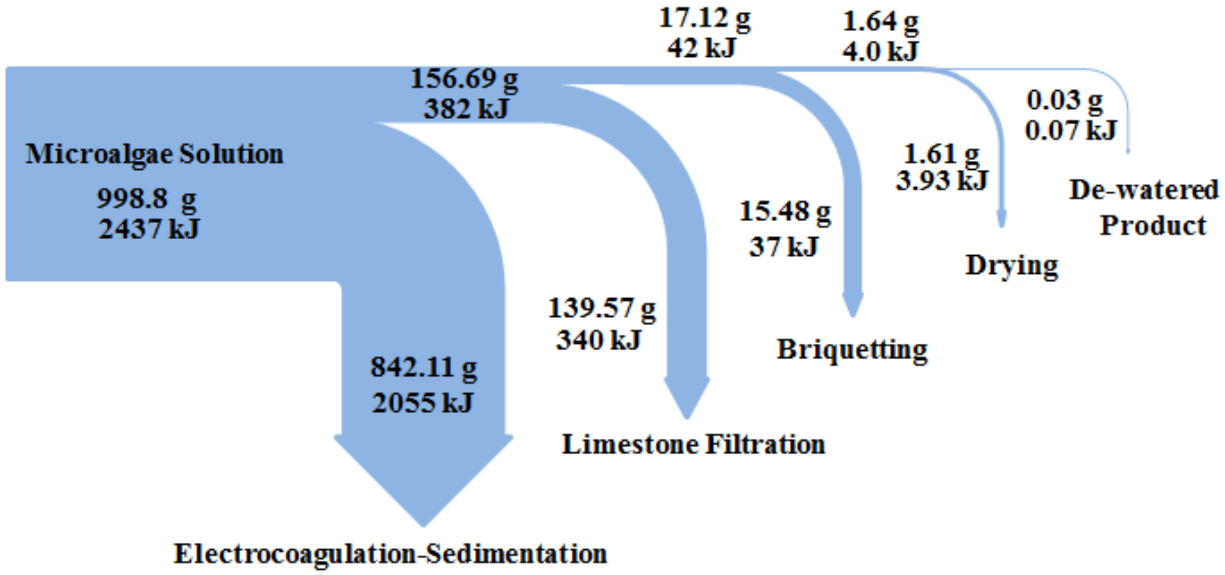

Figure 34: Water Reduction of Each Stage within the Proposed Dewatering Approach.

4.6. Discussion and Implication

Microalgae solution cannot be directly used as a fuel; thus, the use of multi-processes technique for harvesting (separation and dewatering) provided the means to understand the reliability and effectiveness in terms of technical and economic point of view. This section focuses on some of the engineering aspects of process optimizing for multiple scenarios of microalgae dewatering (see Table 16). The discussion includes the operational time and the associated energy consumption of microalgae destabilization during electrocoagulation with respect to the four current densities as well as the energy required to pump the solution to sedimentation vessels, the total volume of electrocoagulation and sedimentation reactors, the area of filter and the amount of water loss. Secondly, to briefly consider the potential change of

emissions of fuel switching using the end-product (i.e. algal bio-solids of the multi-purpose feed stock) compared to a reference fuel (i.e. coal).

Table 16: The Outcomes of Several Process Design Configurations.

Scenario No.	Current Density (Amp/m^2)	Energy Consumption (J)		Total Volume of Rectors (L)		Filter Area (m^2)	Water Loss (%)
		EC.	Pumping	EC.	Sed.		
1	15	4140	13.72	4	4	0.0064	1.25
2	30	11404	14.52	2	2.5	0.0090	5.25
3	60	21945	21.70	1	2.5	0.0098	7.75
4	120	79315	16.40	1	2.5	0.0071	12.5

The analysis was based on the results presented in sections (4.2.1.2), (4.2.6), (4.3), and (4.4). The first scenario was electro-coagulating 4 L of microalgae culture at 15 Amp/m^2. 90% destabilization was reached after 60 min of electrolysis time using four electrocoagulation reactors with a volume of 1 L each. The energy consumed to electro-coagulate the microalgae suspension was 4140 J. Four primary settlers with a volume of 1 L each were employed to densify the algal solution; where 13.72 J were consumed for pumping. To process the pre-concentrated algal solution, four filtration units were put in place with a bed surface area of 0.0016 m^2 each. The total volume collected after sedimentation and filtration was 3.95 L, meaning 1.25% of the culturing solution was lost to evaporation during passive drying. For the sake of comparison, scenario 1 is considered as a reference case. In the second scenario, 87% destabilization was reached after 30 min of electrocoagulation at 30 Amp/m^2, reducing the number of reactors to only 2 and the total reactor volume by 50%. There was a trade-off between the capital cost and the energy consumed such that the total energy consumption was 2.7x higher at 30 Amp/m^2. Using three secondary settlers resulted in reducing the total reactor volume by 37.5%. The volume of pre-concentrated algal solution was higher, leading to increase the total

filter area of the filters by 41%; although the unit number was reduced to half. The following schematics show the process configurations for scenario 1 and scenario 2.

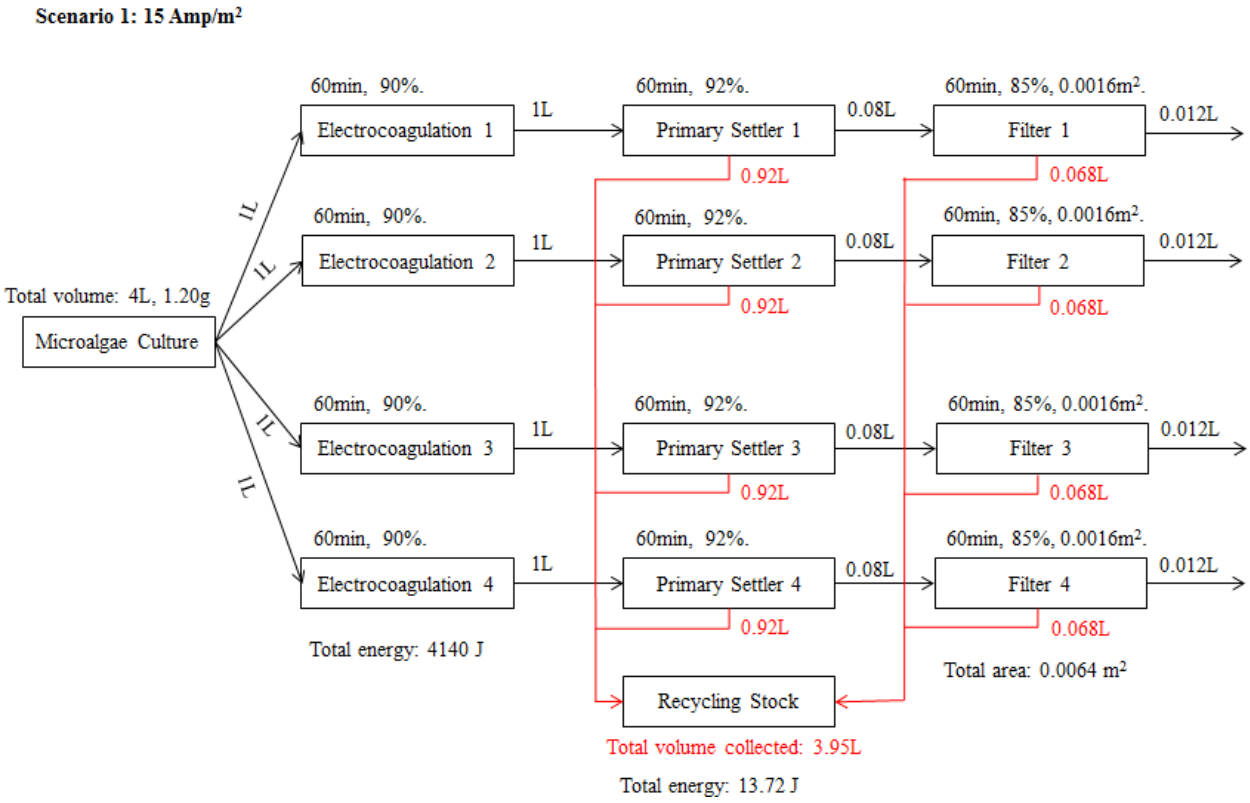

Scenario 2: 30 Amp/m²

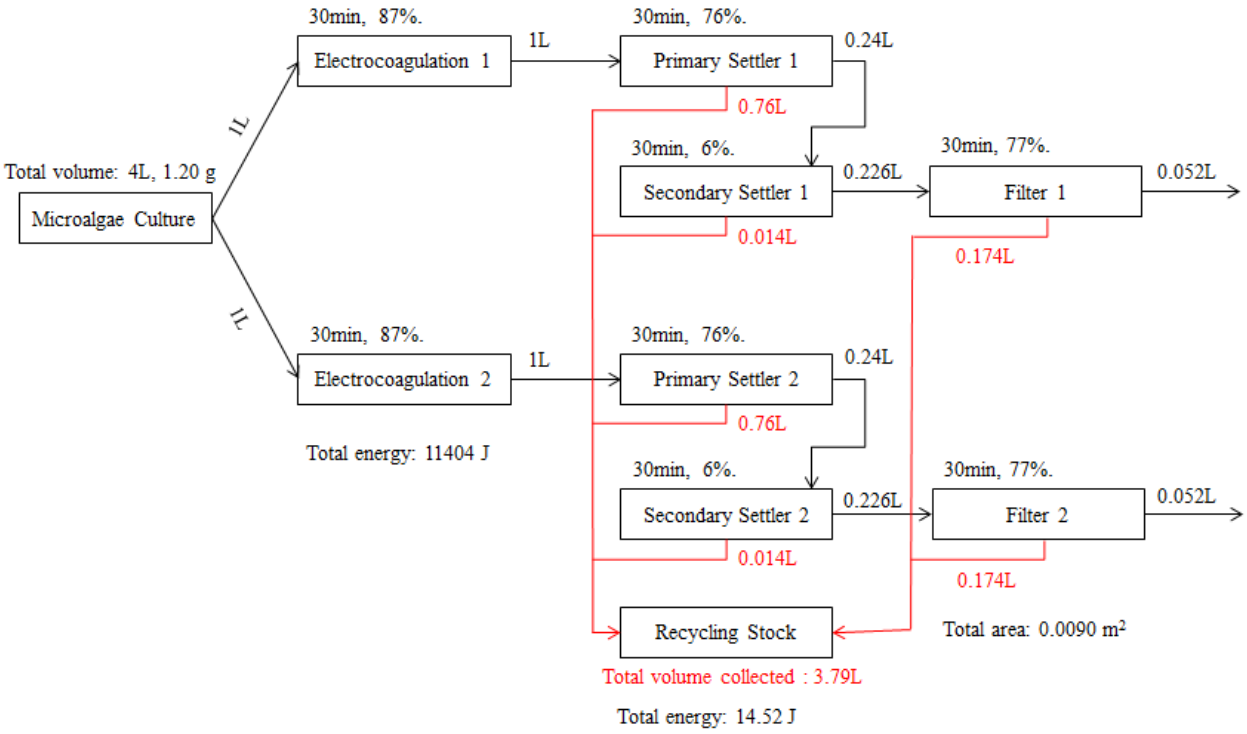

Applying 60 Amp/m^2, the total volume of electrocoagulation reactors has reduced by 77% with one unit operating for 20 min attaining 95% destabilization. Due to the high voltage, the energy consumed to process 4 L of microalgae culture was 21,945 J, noting that it is 5.3x higher than 15 Amp/m^2. A single primary settler and two secondary settlers were considered to thicken the solution where 63% of the process water was removed. Only one filter was employed to further process the pre-concentrated solution every 20 min with a bed surface area of 0.0098 m^2, which was 1.5x higher than the area of the four filters combined used to treat the solution processed at 15 Amp/m^2. Despite reducing the number of filters, the highest water removal after 20 min was 69%, leading to an increase in the water loss (i.e. 7.75%).

Scenario 3: 60 Amp/m^2

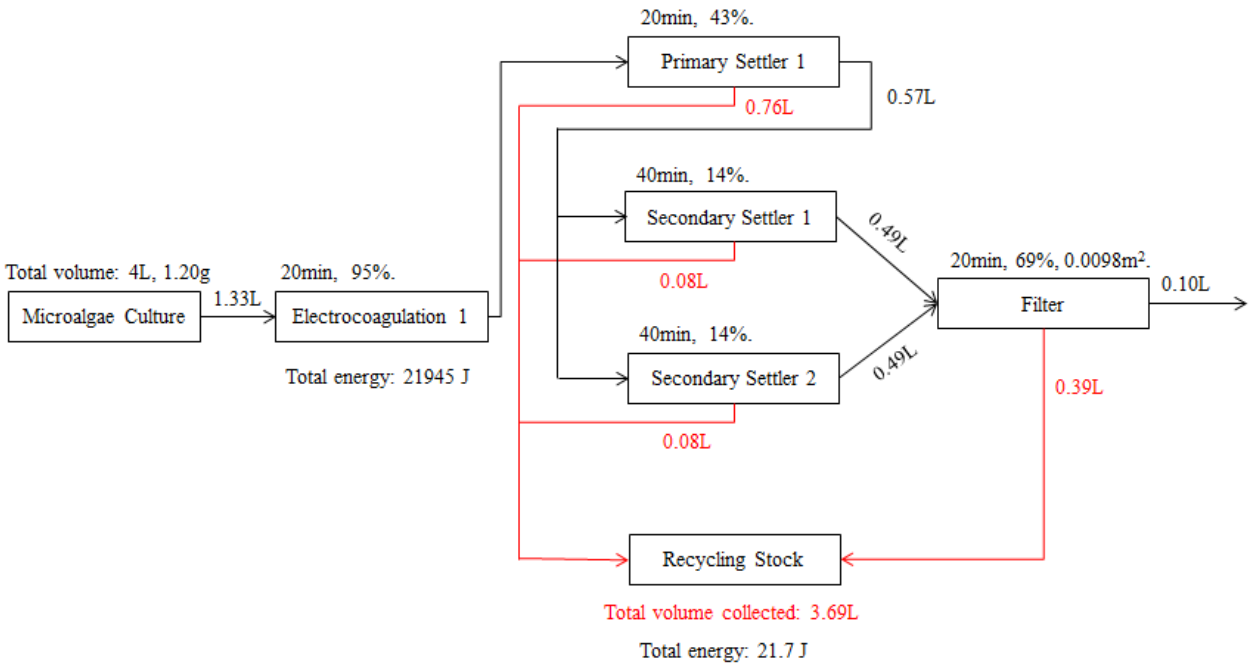

In the fourth scenario, 1L of algal solution was electro-coagulated in a single reactor at 120 Amp/m^2 every 15 min with 95% destabilization. The volume of electrocoagulation reactor was reduced by 75% but the total energy input increased to 79,315 J. To pre-concentrate the solution processed in one hour, four settlers were put in place in which one was primary and three were secondary with a total volume of 2.5 L. A single filter was employed to bring the water content of the pre-concentrated solution down, noting that the length of each batch is 15 min such that a 65% of the process water was removed. The required surface area of the filter bed to handle the pre-concentrated solution coming from the settler was 0.0071m^2, which was 11% larger than for 15 Amp/m^2. Due to the short filtration time, 12.5% of the culturing medium was retained either in the filter cake or bed. The following schematic lays out the processes used in dewatering 4 L of microalgae per hour at 120 Amp/m^2.

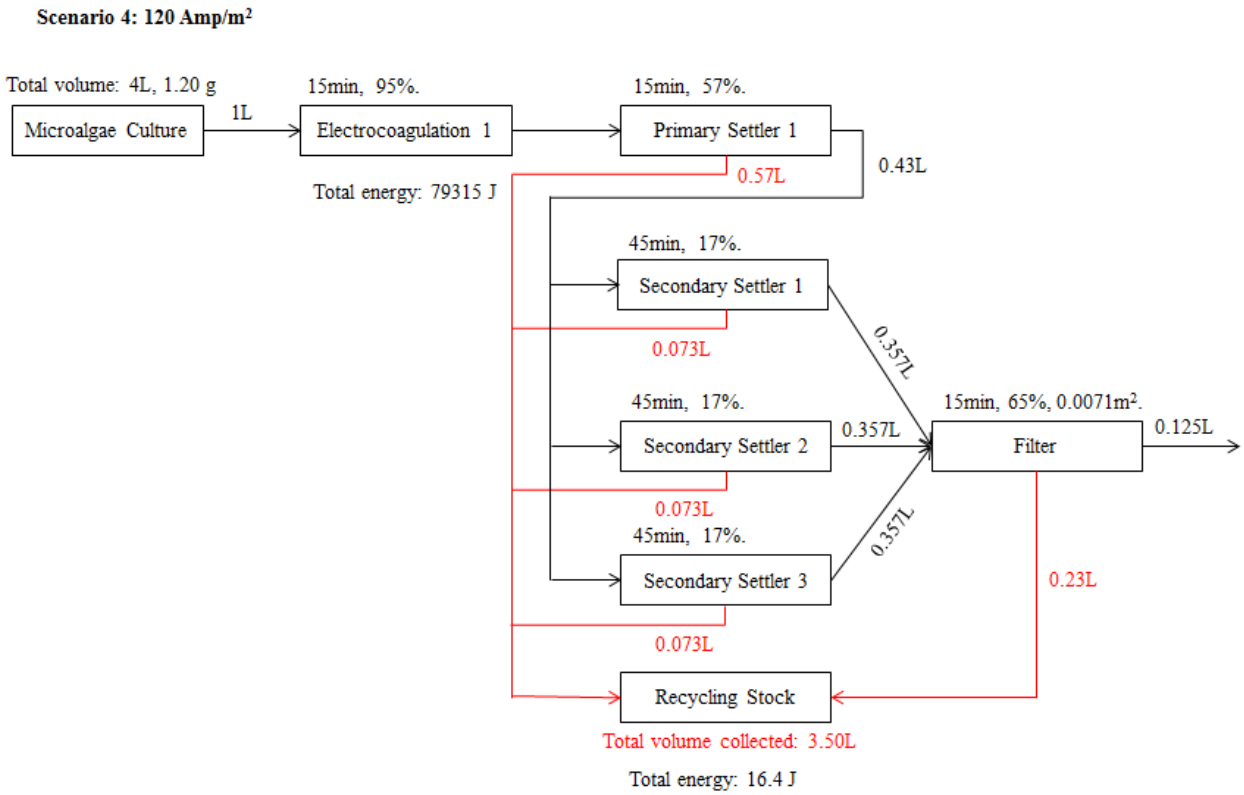

The change of combustion products was evaluated using two types of fuels (i.e. coal "reference fuel" and algal bio-solids "alternative fuel"). As indicated in Table 17, the total emissions volume generated of fuel combustion in 20% excess air to produce 1 kg of clinker was found to be very similar, i.e. 0.73 m^3/kg_{cil} for coal and 0.70 m^3/kg_{cil} for algal bio-solids. The emissions consist of four components, CO_2, H_2O, SO_2, and N_2. The amount of CO_2 in the calciner exhaust was found to be 12.5% using algal bio-solids and 15% using coal. The water vapour was found to be 15% using algal bio-solids and only 5% using coal. The CO_2 volume using algal bio-solids was reduced by 0.0197 m^3/kg_{cli} (or 0.0354 kg CO_2/kg_{cli}). Full fuel substitution in the calciner led to 4% reduction of the total CO_2 emissions (i.e. calcination and fuel combustion CO_2). The CO_2 reduction level was not significant from an industrial perspective, but the advantage of fuel substitution was that 18% of the total CO_2 emissions would be biogenic. The energy requirement to produce 1 kg of clinker in the calciner is 1.905

MJ; thus, the fuel mass required to meet the energy demand using coal, with a heating value of 29.7MJ, was 0.064 kg. On the other hand, the multi-purpose feed stock was prepared in a briquette form. The alternative fuel standards required by the cement industry were 14 MJ and 15 wt% H_2O; therefore, the ideal mix consisted of 80% algal bio-solids, 5% limestone, and 15% water. The briquette mass required to provide the energy demand to produce 1 kg clinker was 0.136 kg in which 0.108 kg was algal bio-solids. The feed rate of alternative fuel was 1.68x higher than coal as per 1 kg clinker basis. The amount of CO_2 released from a typical cement plant, producing 3290410 kg_{cil} a day, is 2912012 kg. The emissions were estimated using CO_2 emission factor and bio-fixation factor which are 0.885 kg CO_2/kg_{cil} and 1.83 kg $CO2/kg_{algalbiomass}$ respectively. If 10% of CO_2 would be captured via microalgae cultivation, 159126 kg algal biomass will be produced. The size of the reactor that would accommodate the algal solution to produce the aforementioned biomass is 0.61 million m^3. The biomass productivity value found in this study (i.e. 0.26 kg/m^3.day) was used to maintain the calculations.

Table 17: Combustion Emissions of Two Fuel Types (Coal and Algal Bio-solids).

Emissions	Coal	Algal Bio-solids
	Volume (m^3/kg_{cil})	Volume (m^3/kg_{cil})
CO_2	0.1078	0.0881
H_2O	0.0391	0.1058
SO_2	0.0001	-
N_2	0.0021	0.0132
Total volume at 20% access air (m^3/kg_{cil})	0.7300	0.7000
Total volume + Kiln exhaust (m^3/kg_{cil})	1.0900	1.0600

Chapter 5 Conclusions and Future Directions

The contribution of this research study was the development of a novel dewatering approach for densification of algal bio-solids to be used as an alternative fuel at cement plants. The dewatering approach investigated in this study advances the concept to avoid thermal drying for producing a solid biofuel using microalgae. It has been shown that the metal additives (i.e. aluminum and iron) used in cement raw meal can be introduced with the dewatering process; particularly via electrocoagulation. This study also shows the environmental co-benefits of utilizing algae-based fuel in cement calciner such that emissions of fossil CO_2 may be reduced, and biogenic CO_2 is enhanced.

In Chapter 2, the author has been reviewed the relevant literature which helped in comprehending the cement manufacturing route, including the preparation of cement raw meal, sources of CO_2 generation in pyro-process, and the potential mitigation technologies. The role of microalgae utilization as biofuel has been discussed; most importantly, the challenges of common dewatering technologies have been compared in terms of concentration level and energy demand. Lastly, direct combustion of algal biomass was reviewed; although, there was no such industrial application of that kind published in the literature to the knowledge of the author.

In Chapter 3, the materials and methodologies of the experiment have been established. Starting with preparing the culturing medium for microalgae cultivation, and then followed by designing the electrocoagulation apparatus. Analytical measurements for microalgae recovery have conducted using three different methods, i.e. cell count, optical density, and dry mass; however, regression models between each one have been developed. The coagulated algal

biomass was digested based on well-established procedure for quantification of metal accumulation. The apparatus and tests of sedimentation, limestone filtration, briquetting, and passive drying have been laid out, designed, and examined. Characterization instruments; i.e. ICP-OES, TGA, and Bomb Calorimetry, were used to study the behaviour of the products.

In Chapter 4, the results and analysis of a series of experiments are presented. The effectiveness of multiple chemical and physical processes for water content reduction under optimal conditions, bio-sorption of metals, ideal blending mix, and characterization of end-products was evaluated and therefore the following conclusions were drawn:

C4.1. The tests showed that electrocoagulation performance was not affected by varying stirring speed and solution pH. The parameter that had a significant impact was current density. The optimal current density, pH, and stirring speed were found as 15 Amp/m^2, 6 and 0 rpm respectively. The optimal conditions were determined based on the highest destabilization achieved, minimal metal dissolution, minimal power consumption, and no pH adjustment of solution prior the treatment.

C4.2. Using aluminum as anode at 15 Amp/m^2 was found to be more efficient compared to iron. With the aluminum anode, the recovery efficiency was found to be 42% higher, the metal dissolution was 2.33x lower, and the power consumption was 5x lower after 60 min of treatment. Additionally, the resultant contamination from excessive iron dissolution may complicate the direct recycling of the post-electrocoagulation solution for microalgae re-cultivation.

C4.3. ICP-OES results showed that higher metal exposure correlates with greater bio-sorption. For example, the aluminum accumulation in biomass at 15 Amp/m^2 was 7% while 32% at 120 Amp/m^2. Similarly, TGA results also showed that the mass of coagulated biomass at

lower current density (i.e. 15 Amp/m^2) was 9.5% while it was 29.5% at higher current density (i.e. 120 Amp/m^2).

C4.4. The calorimetry tests showed that the energy content of coagulated biomass decreased as the metal accumulation increased, in part because the hydroxide decomposition reactions are endothermic. For instance, the heating value of biomass coagulated using aluminum anode at 15 Amp/m^2 was 18 MJ/$kg_{drybiomass}$; whereas, the heating value of biomass coagulated at 120 Amp/m^2 was 4.4 MJ/kg. The energy content is inversely proportional to the metal accumulation to the algal bio-solids. For instance, the energy content of algal bio-solids coagulated at 120 Amp/m^2 was reduced 4x compared to 15 Amp/m^2; whereas, the metal accumulation was increased 4.5x.

C4.5. Sedimentation tests showed that the settling behaviour of microalgae was a function of destabilisation mechanism during the course of electrocoagulation. At lower current density (i.e. 15 Amp/m^2) two destabilization mechanisms were involved; charge neutralization and micro-bubble flotation; where 92% of the process water was recycled. Contrary, at higher current density (i.e. 120 Amp/m^2), the predominant destabilisation mechanism was micro-bubble flotation; where only 60% of the process water was recycled which indicates that the microalgae suspension kept its negative charge and destabilisation occurred by another mechanism than charge neutralization. The pH increase during the course of electrocoagulation was another indicator for the amount of micro-bubble generated. At higher current density, the increase of pH was almost 3x higher due to the excess of hydroxide ions generated at the cathode.

C4.6. Filtration tests showed that limestone micro-aggregates were an appropriate material to be used as a filter bed. The filtrate volume passed was not significantly affected by

the increase of the bed grains size. The tendency of filter fouling would be higher at smaller bed grains due to smaller pores size. Higher filtration rate was obtained using grains size of 600 μm, because of wider pores channels provided, leading to shorten filtration time, reducing fouling, and volume of the filter head tank.

C4.7. Scraping and mixing the algal biomass cake with a portion of the filter bed overcame the conventional backwashing technique in microalgae filtration technology to eliminate fouling issues and provide structure to the briquette.

C4.8. The water content of microalgae solution was reduced from 99.88% to less than 15% with minimal power consumption under optimal conditions.

C4.9. Theoretical calculations showed that full substitution of the multi-purpose feedstock as alternative fuel in the cement calciner would lead to a 4% reduction of total CO_2 emissions of which biogenic CO_2 accounted for 18% of the CO_2 emissions generated.

The following are the suggested future directions that rose from experimental observations and analysis.

FD4.1. After each electrocoagulation-sedimentation experiment, the clear medium was recycled and stored in sealed glass jars. Re-growing microalgae in the recycled medium to investigate for the toxicological effects of metals on the productivity. This step leads to a better understanding of the growth behaviour in metal-contaminated medium of which clean water utilization and salt addition to the microalgae cultivation can be minimized.

FD4.2. Aluminum and iron anodes were used one on a time to perform electrocoagulation experiments. To accumulate both aluminum and iron hydroxides in algal biomass at the same experiment, to meet metal additives requirements by cement plant, electrocoagulation should operate at a reversible mode such that flapping the direction of current during operation course allows the dissolution of both electrodes (see Figure 35). Additionally, switching the current direction should be studied and checked whether or not it has an effect on the minimization of the biofilm formation on the electrodes surface.

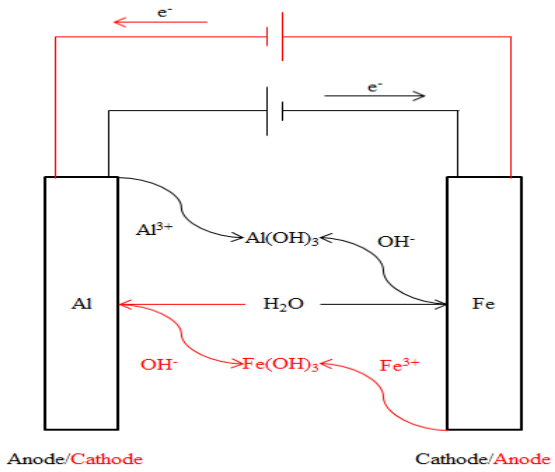

Figure 35: Schematic Diagram of the Reversible Mode of Electrocoagulation Operation.

FD4.3. During electrocoagulation experiments, the total mass of aluminum released and the summation of aluminum mass absorbed by microalgae and that retained in process water did not balance. Additionally, the effects of atomic weight of sacrificial anode materials (i.e. aluminum and iron) has not been considered. To have a better control of metal dissolution and accumulation in algal biomass, inert electrodes "graphite" should be used to mimic the functional nature of sacrificial electrodes in terms of micro-bubbles generation. However, aqueous solution of metal ions should be added accordingly to enhance agglomeration.

FD4.4. All filtration experiments were run as batch therefore design improvements of the proposed filter should be considered, where the process performance shall be evaluated under continuous and pressurized flow. Additionally, the design configuration of the filter should be expanded; for example, a membrane-based filter made of limestone and silica.

FD4.5. Most of the multi-purpose briquettes were made of similar sizes and shapes. However, varying the briquettes' shapes and geometries as well as the additives may have an impact on drying time; therefore, conducting future experiments in this regard worth trying.

FD4.5. The knowledge extracted from this study will be used in scaling up every unit operation to meet the real world demand.

References

[1] "The Keeling Curve," Scripps Institution of Oceanography, UC San Diego , 22 January 2017. [Online]. Available: https://scripps.ucsd.edu/programs/keelingcurve/. [Accessed 24 January 2017].

[2] Government-of-Canada, "Canada's Second Biennial Report on Climate Change|Report," The Minister of Environment and Climate Change, 2016.

[3] R. Lyman, "Climate Change Targets for Canada Examining the Implications | Report," Calgary, 2015.

[4] L. Barcelo, J. Kline, G. Walenta and E. Gartner, "Cement and Carbon Emissions," *Materials and Structures ,* vol. 47, pp. 1055-1065, 2014.

[5] B. Metz, O. Davidson, H. d. Coninck, M. Loos and L. Meyer, "IPCC Special Report on Carbon Dioxide Capture and Storage," Cambridge University Press, New York, 2005.

[6] The-Pembina-Institute-and-Environmental-Defence, "Alternative Fuel Use in Cement Manufacturing, Implications, opportunities, and barriers in Ontario," Cement Association of Canada and Holcim (Canada Inc) | Report , 2014.

[7] L. G., "Mathematische Modelle Zum Prozess Des Brennes Von Zementklinker," *Zkg International ,* vol. 55, 2002.

[8] S. N. Ghosh, Advances in Cement Technology: Chemistry, Manufacturing, and Testing, New Delhi: Tech Books International , 2002.

[9] D. O'Connor, "St. Marys Cement Tests Burning Alternative Fuel," 11 05 2011. [Online]. Available: http://www.stratfordbeaconherald.com/2011/05/18/st-marys-cement-tests-burning-alternative-fuel. [Accessed 24 01 2017].

[10] "The Use of Alternative Materials in the European Cement Industry," Ecra, 1 2016. [Online]. Available: https://www.ecra-online.org/uploads/media/ECRA_Newsletter_1-2016.pdf. [Accessed 24 01 2017].

[11] T. Hills, D. Leeson, N. Florin and P. Fennell, "Carbon Capture in the Cement Industry: Technologies, Progress, and Retrofitting," *Environmental Science and Technology ,* vol. 50, pp. 368-377, 2015.

[12] S. P. Cuellar-Bermudeza, J. S. Garcia-Perez, B. E. Rittmann and R. Parra-Saldivar, "Photosynthetic bioenergy utilizing CO2: an approach on flue gases utilization for third generation biofuels," *Cleaner Production,* vol. 98, pp. 53-65, 2015.

[13] Pond-Biofuels, "Canadian Cement Plant Becomes First to Capture CO2 in Algae | Earth and

Industry," [Online]. Available: http://www.pondbiofuels.com/Company/News/assets/earthandindustry_com.pdf. [Accessed 05 01 2017].

[14] M. Boot-Handford, J. Abanades, E. Anthony, M. Blunt, S. Brandani, N. M. Dowell, J. Fern´andez, M. Ferrari, R. Gross, J. Hallett, R. Haszeldine, P. Heptonstall, A. Lyngfelt, Z. Makuch, E. Mangano, R. Porter and e. al., "Carbon Capture and Storage Update," *Energy and Environmental Science,* vol. 7, pp. 130-189, 2014.

[15] M. C. Romano, M. Spinelli, S. Campanari, S. Consonni, M. Marchi, N. Pimpinelli and G. Cinti, "The Calcium Looping Process for Low CO2 Emission Cement Plants," *Energy Procedia,* vol. 61, pp. 500-503, 2014.

[16] D. Barker, S. Turner, P. Napier-Moore, M. Clark and J. Davison, "CO2 Capture in the Cement Industry," *Energy Procedia,* vol. 1, pp. 87-94, 2009.

[17] S. Grönkvist, M. Bryngelsson and M. Westermark, "Oxygen Efficiency with Regard to Carbon Capture," *Energy,* vol. 31, no. 15, pp. 3220-3226, 2006.

[18] F. Zeman, "Oxygen Combusion in Cement Production," *Energy Procedia,* vol. 1, pp. 187-194, 2009.

[19] W. Klinthong, Y.-H. Yang, C.-H. Huang and C.-S. Tan, "A Review: Microalgae and Their Applications in CO2 Capture and Renewable Energy," *Aerosol and Air Quality Research ,* vol. 15, pp. 712-742, 2015.

[20] M. S. A. R. ,. S. R. S. A. ,. Z. M. Noor Shazleen Sharfadeen, "Comparative Carbon Dioxide Capture from Air between Chlorella Vulgaris and Chlorella Sorokiniana," *Indian Journal of Science and Technology,* vol. 9(21), pp. 1-7, 2016.

[21] S. Cong, "Algae Based Carbon Capture and Utilizaiton Feasibility Study-Initial Analysis of Carbon Capture Effect Based on Zhoushan Case Pre-study in China," Industrial Ecology, Royal Institute of Technology | Report , 2012.

[22] "Algae-based Biofuels: Applications and Co-products," FAO Aquatic Biofuels Working Group, Rome, 2010.

[23] K. Sudhakar, M. Premalatha and K.Sudharshan, "Energy Balance and Exergy Analysis of Large Scale Algal Biomass Production," *The 2nd Korea - Indonesia Workshop & International Symposium on Bioenergy from Biomass,* pp. 66-69, 2012.

[24] "Cement Maker First In World to Capture CO2 with Algae," Clean|Break, 18 March 2010. [Online]. Available: http://www.cleanbreak.ca/2010/03/18/cement-maker-first-in-world-to-capture-co2-with-algae/. [Accessed 06 01 2017].

[25] A. Talec, M. Philistin, F. Ferey, G. Walenta, J.-O. Irisson, O. Bernard and A. Sciandra, "Effect of Gaseous Cement Industry Effluents on Four Species of Microalgae," *Bioresource Technology,* vol. 143, pp. 353-359, 2013.

[26] M. L. Gerardo, S. V. D. Hende, H. Vervaeren, T. Coward and S. C. Skill, "Harvesting of Microalgae within a Biorefinery Approach: A Review of the Developments and Case studies from pilot-plants," *Algal Research,* vol. 11, pp. 248-262, 2015.

[27] F. McDonough, "Energy from Waste Webinar," 8 February 2016. [Online]. Available: https://wise.uwaterloo.ca/rrp_webinar2017. [Accessed 28 March 2017].

[28] D. Xu, Y. Cui, H. Li, K. Yang, W. Xu and Y. Chen, "On the Future of Chinese Cement Industry," *Cement and Concrete Research,* vol. 78, pp. 2-13, 2015.

[29] Kema, "Industrial Case Study: The Cement Industry," San Francisco, California | Report , 2005.

[30] M. L. Bill Neuffer, "Alternative Control Techniques Document Update - NOx Emissions from New Cement Kilns," EPA, 2007.

[31] P. Alsop, H. Chen and H. Tseng, "Raw Materials," in *The Cement Plant Operations Handbook*, Surrey, UK, 2007, pp. 23-30.

[32] E. Benhelal, G. Zahedi, E. Shamsaei and A. Bahadori, "Global Strategies and Potentials to Curb CO2 Emissions," *Journal of Cleaner Production,* vol. 51, pp. 142-161, 2013.

[33] S. Mishra and N. A. Siddiqui, "A Review On Environmental and Health Impacts of Cement Manufacturing Emissions," *International Journal of Geology, Agriculture and Environmental Sciences ,* vol. 2, pp. 26-31, 2014.

[34] K. S. Mujumdar, K. Ganesh, S. B. Kulkarni and V. V. Ranade, "Rotary Cement Kiln Simulator (RoCKS): Integrated Modeling of Pre-heater, Calciner, Kiln and Clinker Cooler," *Chemical Engineering Science,* vol. 62, pp. 2590-2607, 2007.

[35] N. Chatziaras and C. S. Psomopoulos, "Use of Waste Derived Fuels in Cement Industry: A Review," *Managment of Environmental Quality,* vol. 27, pp. 178-193, 2016.

[36] Y. Li, M. Horsman, N. Wu, C. Q. Lan and N. Dubois-Calero, "Biofuels from Microalgae," *Biotechnology Progress ,* vol. 24, no. 4, pp. 815-820, 2008.

[37] M. S. Orosz and D. Forney, "A Comparision of Algae to Biofuel Conversion Pathways for Energy Storage Off-Grid | Report," 2008.

[38] C. Safi, B. Zebib, O. Merah, P.-Y. Pontalier and C. Vaca-Garcia, "Morphology, Composition,

Production, Processing and Applications of Chlorella Vulgaris: A Review," *Renewable and Sustainable Energy Reviews,* vol. 35, pp. 265-278, 2014.

[39] S. Awaluddin, S. Thiruvenkadam, S. Izhar, Y. Hiroyuki, M. K. Danquah and R. Harun, "Subcritical Water Technology for Enhanced Extraction of Biochemical Compounds from Chlorella vulgaris," *Hindawi Publishing Corporation, BioMed Research International,* pp. 1-10, 2016.

[40] A. S. Mirón, M.-C. C. Garcia, F. G. Camacho, E. M. Grima and Y. Chisti, "Growth and Biochemical Characterization of Microalgal Biomass Produced in Bubble Column and Airlift Photobioreactors: Studies in Fed-batch Culture," *Enzyme and Microbial Technology,* vol. 31, pp. 1015-1023, 2002.

[41] R. Narala, S. Garg, K. Sharma, S. Thomas-Hall and M. D. a. Y. Li, "Comparison of Microalgae Cultivation in Photobioreactor, Open Raceway Pond, and a Two-Stage Hybrid System," *Frontiers in Energy Research,* vol. 4, pp. 1-10, 2016.

[42] Y. Chisti, "Large-Scale Production of Algal Biomass: Raceway Ponds," *Springer International Publishing Switzerland ,* pp. 21-40, 2016.

[43] D. R.Poirier, E. Michaux and M. S. Fulleringer, "Design of a Small Scale Algae Cultivation System to Produce Biodiesel | Report," Department of Bioresource Engineering, McGill University, 2008.

[44] C. F. Murphy and D. T. Allen, "Energy-Water Nexus for Mass Cultivation of Algae," *Environmental Science and Technology ,* vol. 45, pp. 5861-5868, 2011.

[45] A. Juneja, R. M. Ceballos and G. S. Murthy, "Effects of Environmental Factors and Nutrient Availability on the Biochemical Composition of Algae for Biofuels Production: A Review," *Energies,* vol. 6, pp. 4607-4638, 2013.

[46] G. Chen and Y.-T. Hung, "Electrochemical Wastewater Treatment Processes," in *Handbook of Environmental Engineering*, Totowa, NJ, The Humana Press Inc, 2007, p. 57.

[47] G. Sharma, "Electrocoagulation and Microfiltration Hybrid System for Water Treatment," University of Technology (UTS) | Master of Engineering Thesis , Sydney, 2011.

[48] C. Ucar, "Arsenic Removal From Drinking Waters by Electrocoagulation and Filtration," Dokuz Eylul University | Master of Science Thesis , 2011.

[49] R. Davis, J. Markham, C. Kinchin, N. Grundl, E. C. Tan and D. Humbird, "Process Design and Economics for the Production of Algal Biomass: Algal Biomass Proudction in Open Pond Systems and Processing Through Dewatering for Downstream Conversion," National Renewable Energy Laboratory | Report , Golden, 2016.

[50] D. Vandamme, S. C. V. Pontes, K. Goiris, I. Foubert, L. J. J. Pinoy and K. Muylaert, "Evaluation of

Electro-Coagulation–Flocculation for Harvesting Marine and Freshwater Microalgae," *Biotechnology and Bioengineering ,* vol. 108, no. 10, pp. 2320-2329, 2011.

[51] V. Kuokkanen, T. Kuokkanen, J. Rämö and U. Lassi, "Recent Applications of Electrocoagulation in Treatment of Water and Wastewater—A Review," *Green and Sustainable Chemistry,* vol. 3, pp. 89-121, 2013.

[52] A. E. Yilmaz, R. Boncukcuoğlu and M. M. Kocakerim, "A Quantitative Comparison Between Electrocoagulation and Chemical Coagulation for Boron Removal from Boron-Containing Solution," *Journal of Hazardous Materials,* vol. 149, pp. 475-481, 2007.

[53] M. Y. Mollah, P. Morkovsky, J. A. Gomes, M. Kesmez, J. Parga and D. L. Cocke, "Fundamentals, Present and Future Perspectives of Electrocoagulation," *Journal of Hazardous Materials,* vol. 114, no. 1-3, pp. 199-210, 2004.

[54] C. Comninellis and G. Chen, Electrochemisty for the Environment, New York: Springer Science and Nusiness Media , 2010.

[55] D. Zhang, Y. Yu, C. Li, C. Chai, L. Liu, J. Liu and Y. Feng, "Factors Affecting Microalgae Harvesting Efficiencies Using Electrocoagulation-Flotation for Lipid Extraction," *RSC Advances,* vol. 5, pp. 5795-5800, 2015.

[56] C. Brebbia, WIT Transactions on Ecology and the Enviroment, Water Pollution XIII, WIT Press , 2016.

[57] Y. Shen, "Carbon Dioxide Bio-Fixation and Wastewater Treatment via Algae Photochemical Synthesis for Biofuel Production," *Royal Society of Chemisty,* vol. 4, pp. 49672-49722, 2014.

[58] Y.-R. Hu, F. Wanga, S.-K. Wang, C.-Z. Liu and C. Guo, "Efficient Harvesting of Marine Microalgae Nannochloropsis Maritima Using Magnetic Nanoparticles," *Bioresource Technology,* vol. 138, pp. 387-390, 2013.

[59] D. T. Frost, "Bioflocculatin for Control of Wasterwater Pond," California Polytechnic State University | Master of Science Thesis , 2008.

[60] J. Liu, Y. Zhu, Y. Tao, Y. Zhang, A. Li, T. Li, M. Sang and C. Zhang, "Freshwater Microalgae Harvested via Flocculation Induced by pH Decrease," *Biotechnology for Biofuels,* vol. 6:98, pp. 1-11, 2013.

[61] A. J. Dassey, "Designing a Cost Effective Microalgae Harvesting Strategy for Biodiesel Production with Electrocoagulation and Dissolved Air Flotation," Louisiana State University | Doctor of Philosophy Thesis , 2013.

[62] N. Uduman, Y. Qi, M. K. Danquah, G. M. Forde and A. Hoadley, "Dewatering of Microalgal Cultures: A Major Bottleneck to Algae-Based Fuels," *Journal of Renewable and Sustainable Energy,* vol. 2, pp.

012701-0127015, 2010.

[63] D. H. Liu, "Sedimentation," in *Wastewater Treatment* , CRC Press LLC, 1999.

[64] S. O. Gultom and B. Hu, "Review of Microalgae Harvesting via Co-Pelletization with Filamentous Fungus," *Energies ,* vol. 6, pp. 5921-5939, 2013.

[65] B. Naghavi and R. Malone, "Algae Removal by Fine Sand/Silt Filtration," *Pergamon Press Ltd,* vol. 20, pp. 377-383, 1986.

[66] L. Huisman and W. Wood, "Slow Sand Filtration," World Health Organization | Report , Geneva, 1974.

[67] P. Le-Clech, V. Chen and T. A. Fane, "Fouling in Membrane Bioreactors Used in Wastewater Treatment," *Journal of Membrane Science,* vol. 284, no. 1-2, pp. 17-53, 2006.

[68] C.-L. Chen, J.-S. Chang and D.-J. Lee, "Dewatering and Drying Methods for Microalgae," *Drying Technology ,* pp. 443-454, 2015.

[69] P. Valdivia-Lefort, "An Optimal Harvesting and Dewatering System Mechanism for Microalgae," *Journal of Agricultural Machinery Science ,* vol. 7(2), pp. 211-215, 2011.

[70] A. Barros, A. Gonçalves, M. Simões and J. Pires, "Harvesting Techniques Applied to Microalgae: A Review," *Renewable and Sustainable Energy Reviews,* vol. 41, pp. 1489-1500, 2015.

[71] R. R. Soomro, T. Ndikubwimana, X. Zeng, Y. Lu, L. Lin and M. K. Danquah, "Development of a Two-Stage Microalgae Dewatering Process – A Life Cycle Assessment Approach," *Frontiers in Plant Science,* vol. 7, pp. 1-12, 2016.

[72] Z. Wang, J. Hou, D. Bowden and J. M. Belovich, "Evaluation of an Inclined Gravity Settler for Microalgae Harvesting," *Society of Chemical Industry,* vol. 89, pp. 714-720, 2013.

[73] K. Danis and Y.-H. Huang, "Comparision of Chemical Coagulation and Electrocoagulation for Boron Removal from Synthetic Wastewater Using Aluminium," *International Journal of Chemical, Molecular, Nuclear, Materials and Metallurgical Engineering ,* vol. 9, pp. 944-948, 2015.

[74] G. C. Mrema, L. O. Gumbe, H. J. Chepete and J. O. Agullo, "Grain Crop Drying, Handling and Storage," in *Rural Structures in the Topics: Design and Development* , Rome, FAO, 2011, pp. 364-367.

[75] Shelef, Sukenik and Green, "Microalgae Harvesting and Processing: A Literature Review," U.S. Department of Energy | Report , 1984.

[76] A. S. B. Bujang, "Properties and Bulk Drying of Biomass," Iowa State University, Master of Science Thesis , Ames, Iowa, 2011.

[77] D. R. Lide, Handbook of Chemistry and Physics, CRC Press LLC, 2004.

[78] O. M. S. and D. Forney, "A comparison of algae to biofuel conversion pathways for energy stroage off-grid," Massachusetts Institute of Technology , 2008.

[79] Y. Xu, P. Hellier, S. Purton, F. Baganz and N. Ladommatos, "Algal Biomass and Diesel Emulsions: An Alternative Approach for Utilizing the Energy Content of Microalgae Biomass in Diesel Engines.," *Applied Energy,* vol. 172, pp. 80-95, 2016.

[80] A. Yahia, G. Edris and G. Yasser, "Performance Evalution of a Bubble Column Photobioreactor for Carbon Dioxide Sequestration by Chlorella vulgaris," *Springer,* vol. 39, pp. 8453-8463, 2014.

[81] S. Bayar, Y. S. Yildiz, A. E. Yilmaz and S. Irdemez, "The Effect of Stirring Speed and Current Density on Removal Efficiency of Poultry Slaughterhouse Wastewater by Electrocoagulation Mehtod," *Desalination ,* vol. 280, pp. 103-107, 2011.

[82] A. Burns, "Photobioreactor Design for Improved Energy Efficiency of Microalgae Production," California Polytechnic State University, Master of Science Thesis , 2014.

[83] S. S. S. Vanderzee, "Carbon Sequestration Through the Production of Precipitated Calcium Carbonate from Waste Concrete," Queen's University | Master of Science Thesis , Kingston, Ontario, 2016.

[84]

Appendices

Appendix A: Theoretical

1. Comparison of Cultivation Systems

Table 18: Cultivation Systems Comparison, adopted from [82].

Open Ponds	Parameter	Photo-bioreactor
Very high due to open environment	**Cross-contamination**	Low due to closed and controlled environment
Weather dependent, high at hot seasons	**Evaporation of Culturing Medium**	Low at room temperature
High due to open environment	**Carbon Dioxide Losses**	Low due to gas circulation
High, multiple organisms grow due to microbial contamination	**Diversity of Cultivable Species**	Low, contamination risks are minimal
Easy to maintain due to the simplicity of cleaning the pond	**Production Flexibility**	Complicated to maintain due to the time and cost implications of cleaning the bioreactor
Environment dependent Low	**pH, Temperature, DO Conc.** **Process Control**	Operator dependent High
Depends on weather and strain Low (0.1-0.2 g/L)	**Production Time** **Biomass Production Rate**	Depends on Strain High (2-8 g/L)
Low	**Capital Cost**	High
Easy	**Process Scaling-up**	Complicated
Readily available	**Technology Availability**	Not demonstrated on a large scale
Many due to lower density culture	**Downstream Processes**	Few due to higher density culture
High	**Area to Volume Ratio**	Small
Poor	**Efficiency of Light Usage**	Exceptional
Mixing	**Expensive Parameters**	Temperature and oxygen control
Surface area of the pond	**Implications of Biomass Productivity**	Volume of the bioreactor

Appendix B: Experimental

1. Graphical Presentation of the Experiment

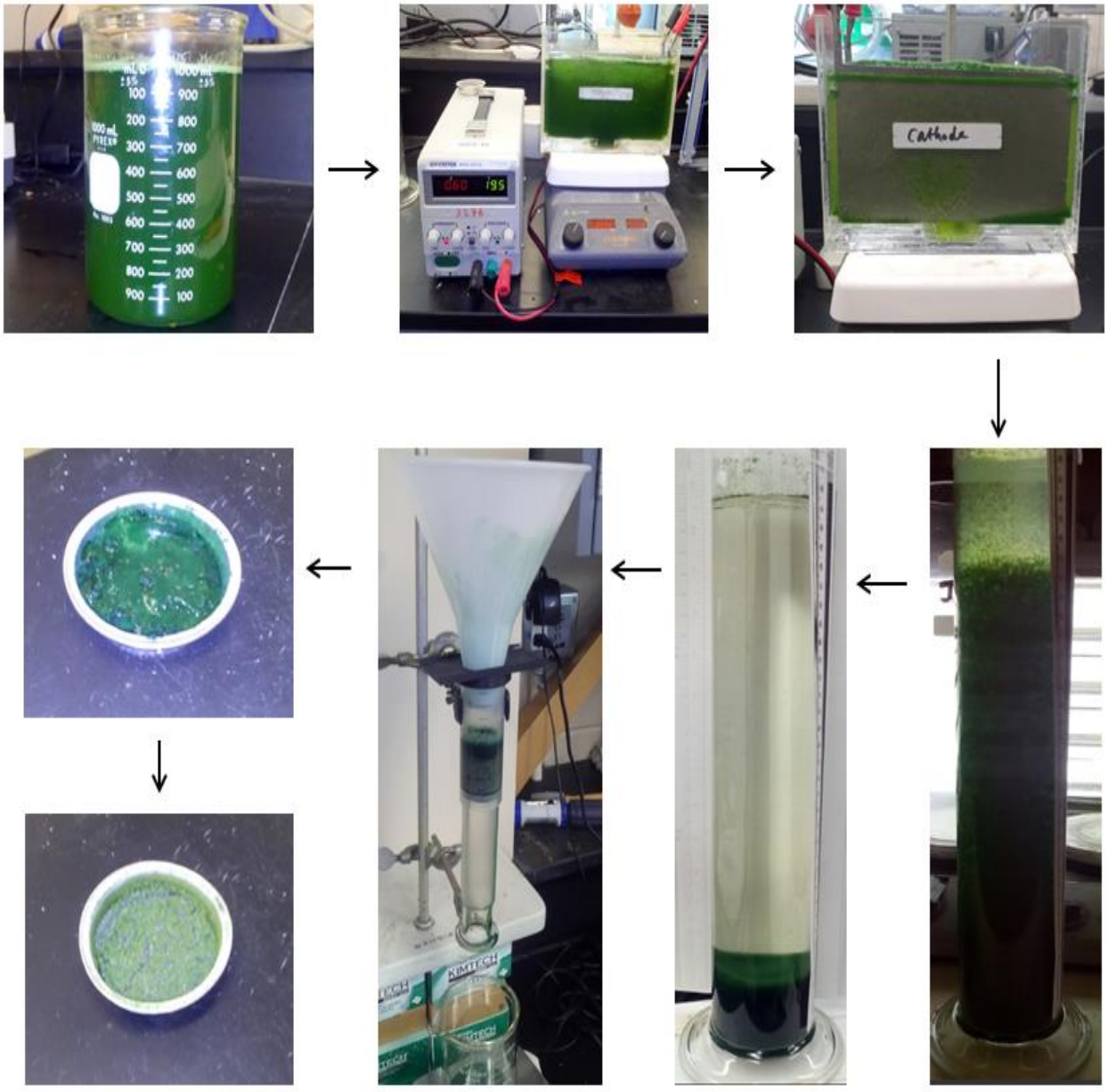

Figure 36: Experimental Stages of Multi-purpose Feedstock Production via Microalgae.

2. Electrocoagulation Reactor Assembly

Note: SOLIDWORKS drawing done by Mr. Clarence.

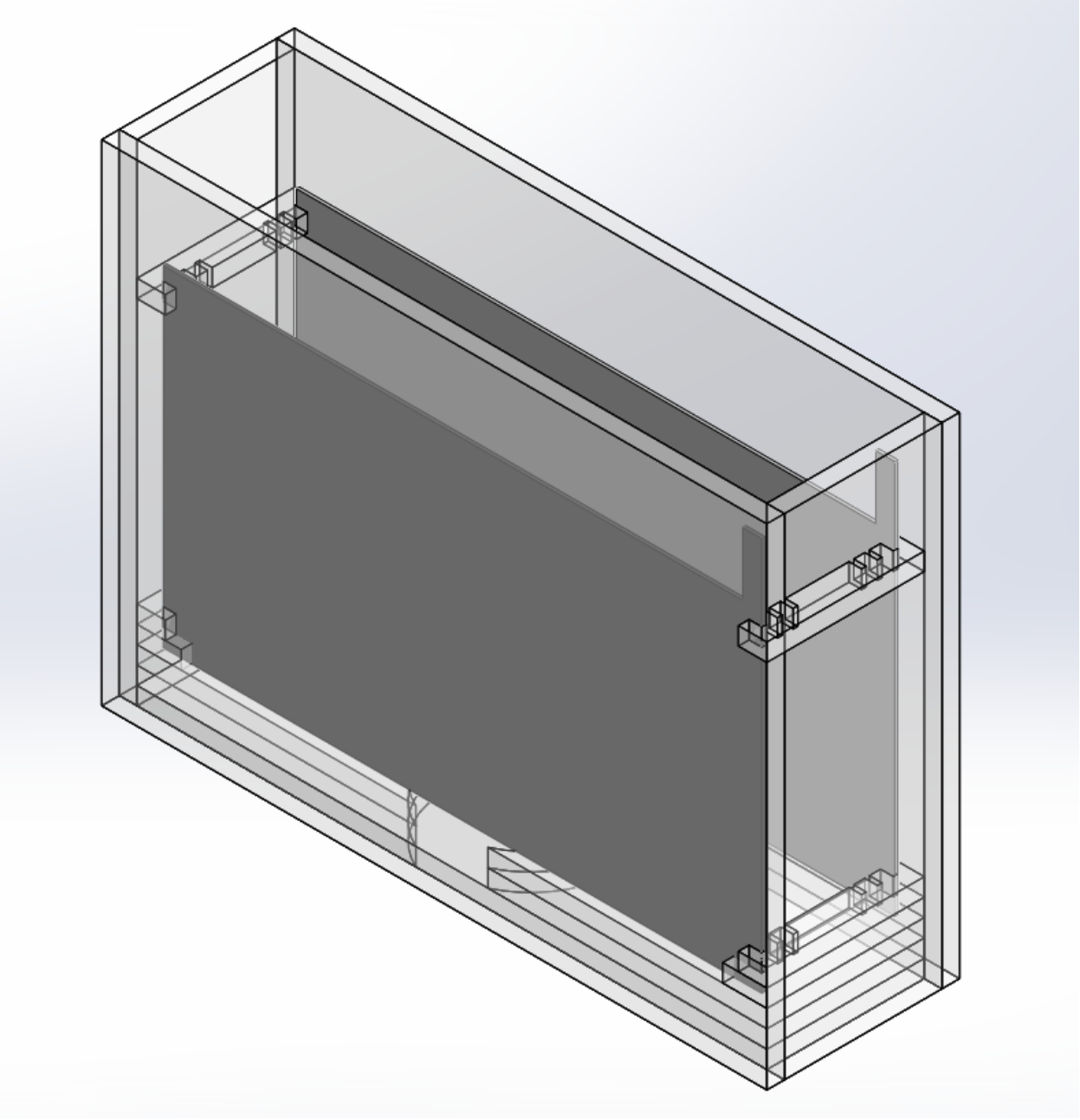

Figure 37: A Schematic Diagram of Electrocoagulation Reactor Assembly.

3. Limestone Filter Assembly

Note: SOLIDWORKS drawing done by Mr. Clarence.

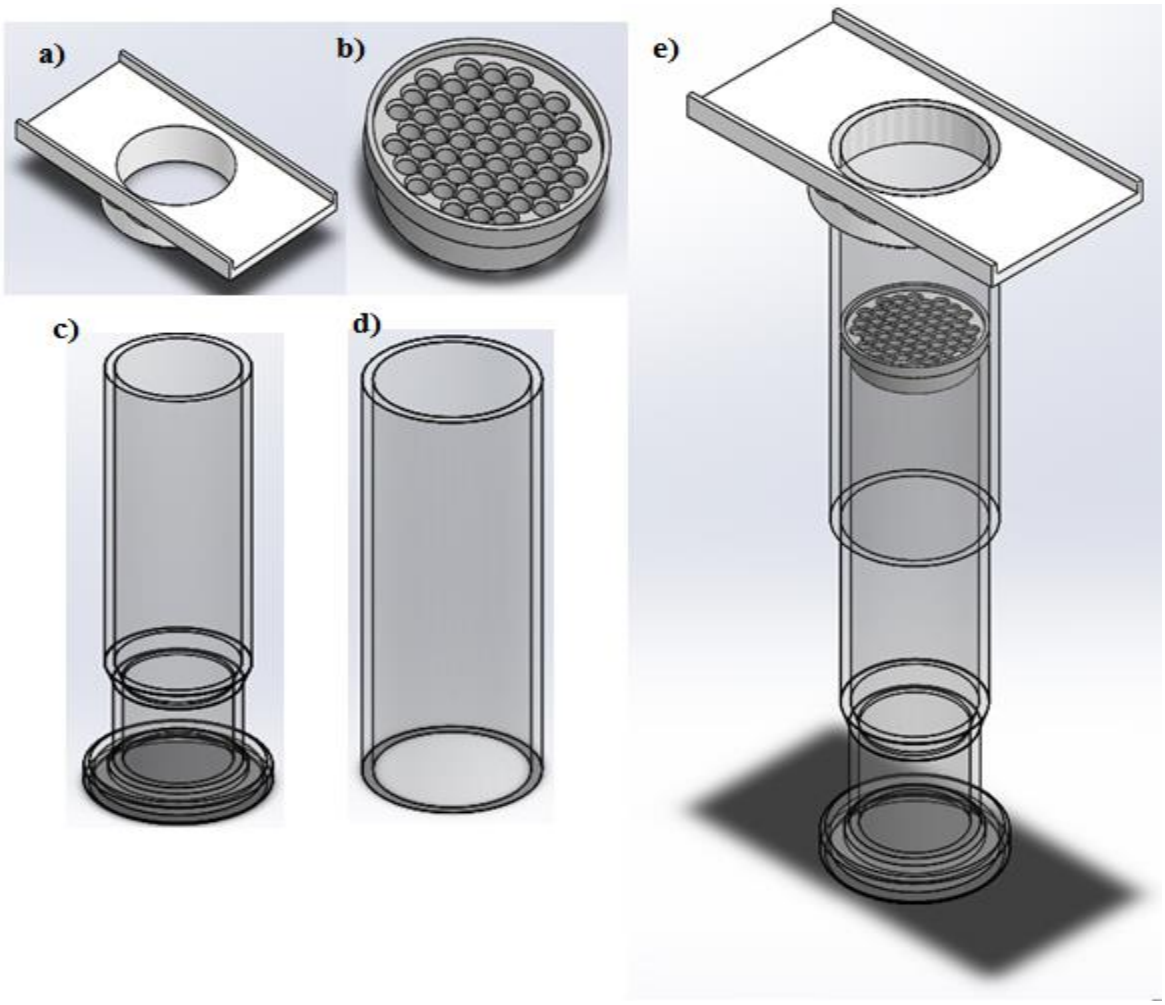

Figure 38: A Schematic Diagram of a) Sampling Adopter; b) Backing Screen; c) Movable Planger; d) Graduated Planger Sleeve; e) Limestone Filter Assembly.

Appendix C: Analysis

1. **<u>Automated Cell Counting for Microalgae</u>**

- An image of hemacytometer was taken by digital camera attached to microscope.

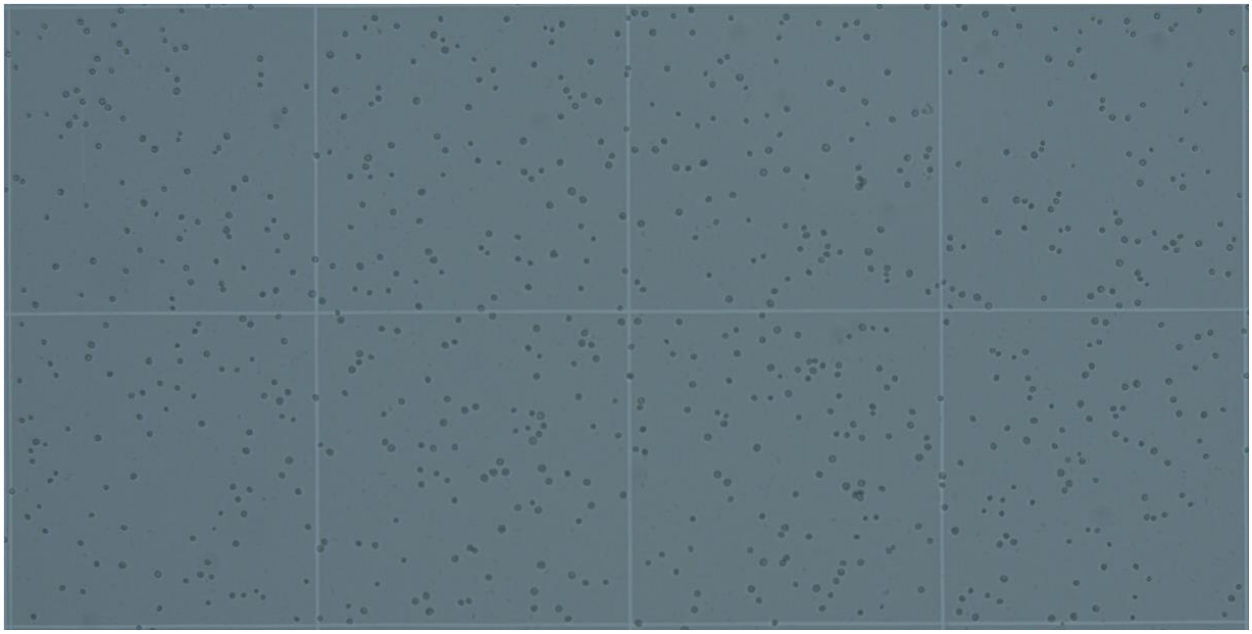

- The image was processed using ImageJ.

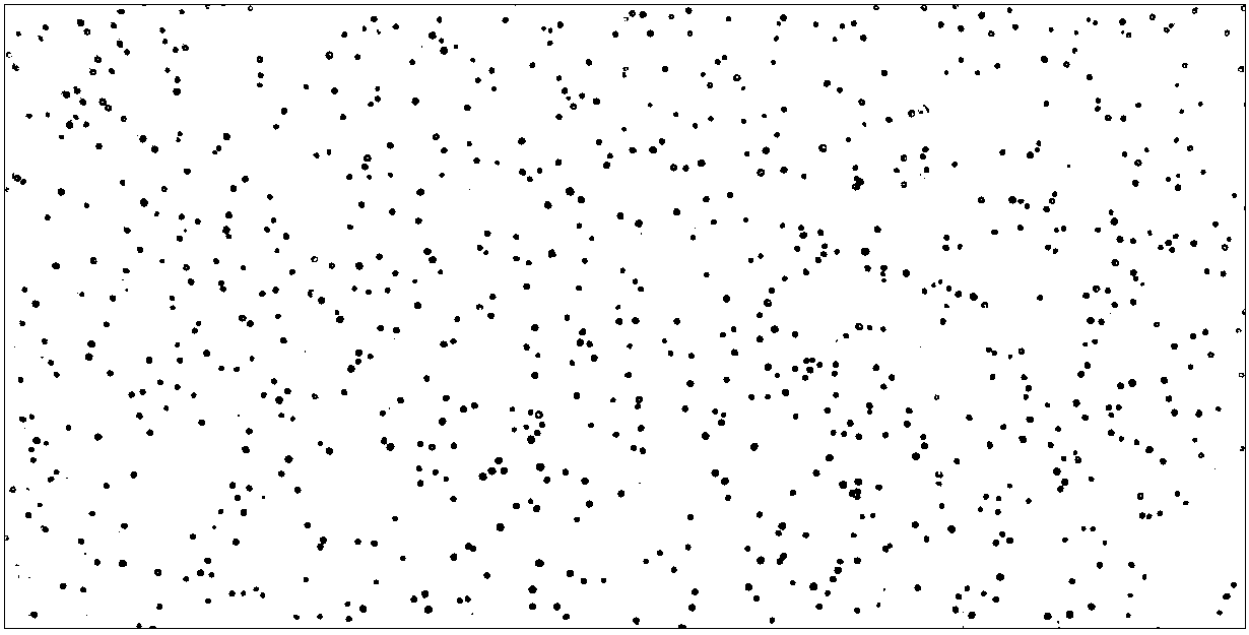

- The processed image is then analyzed to count cells that range from 10 pixel to infinity in size and from 0 to 1 in circularity.

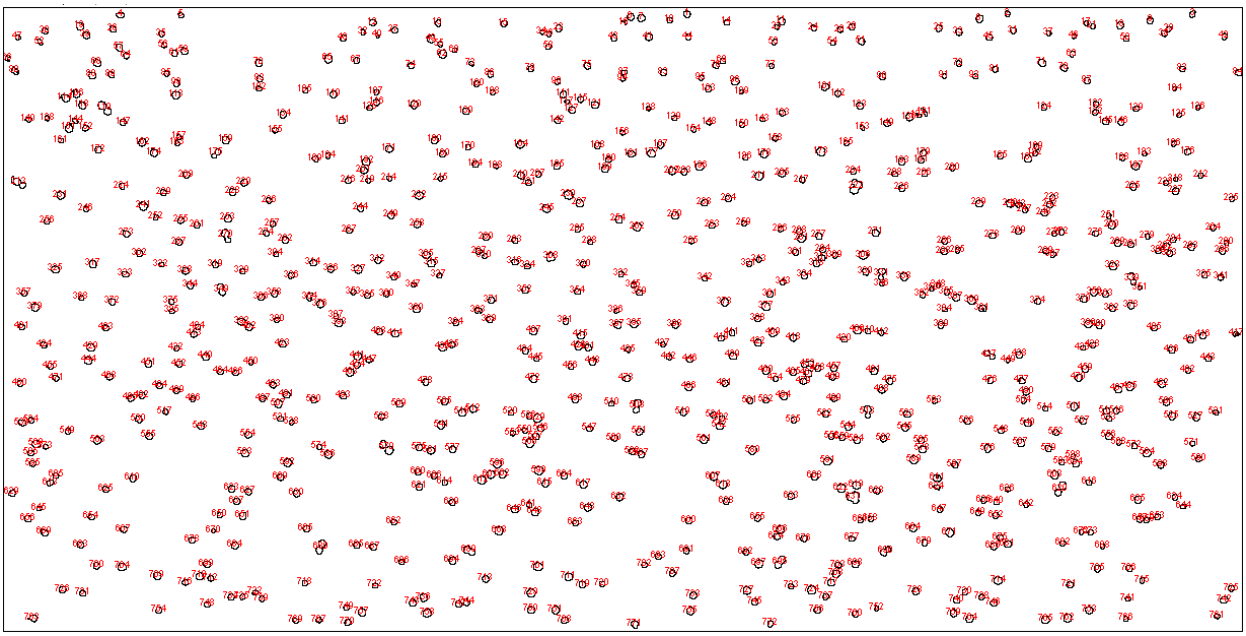

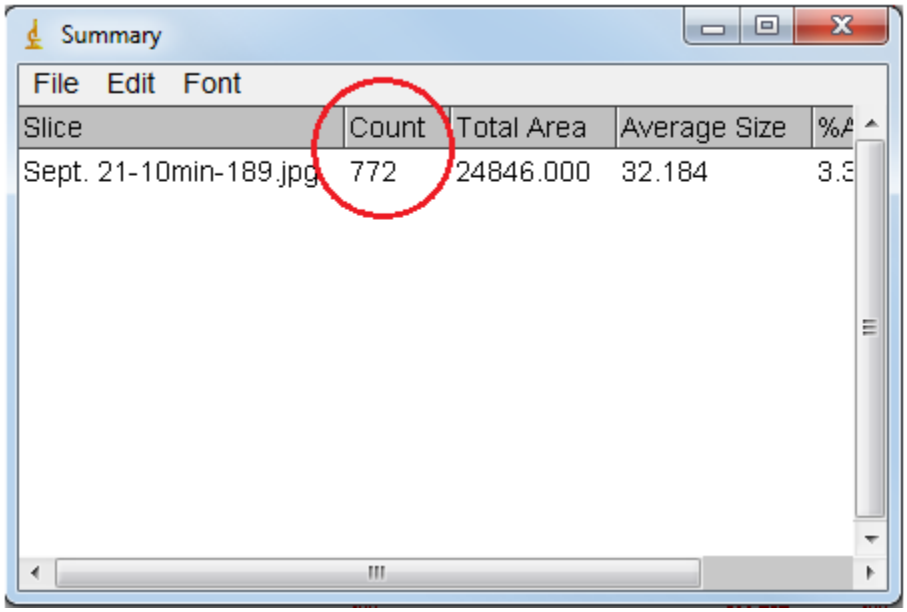

2. Optical Density Measurement

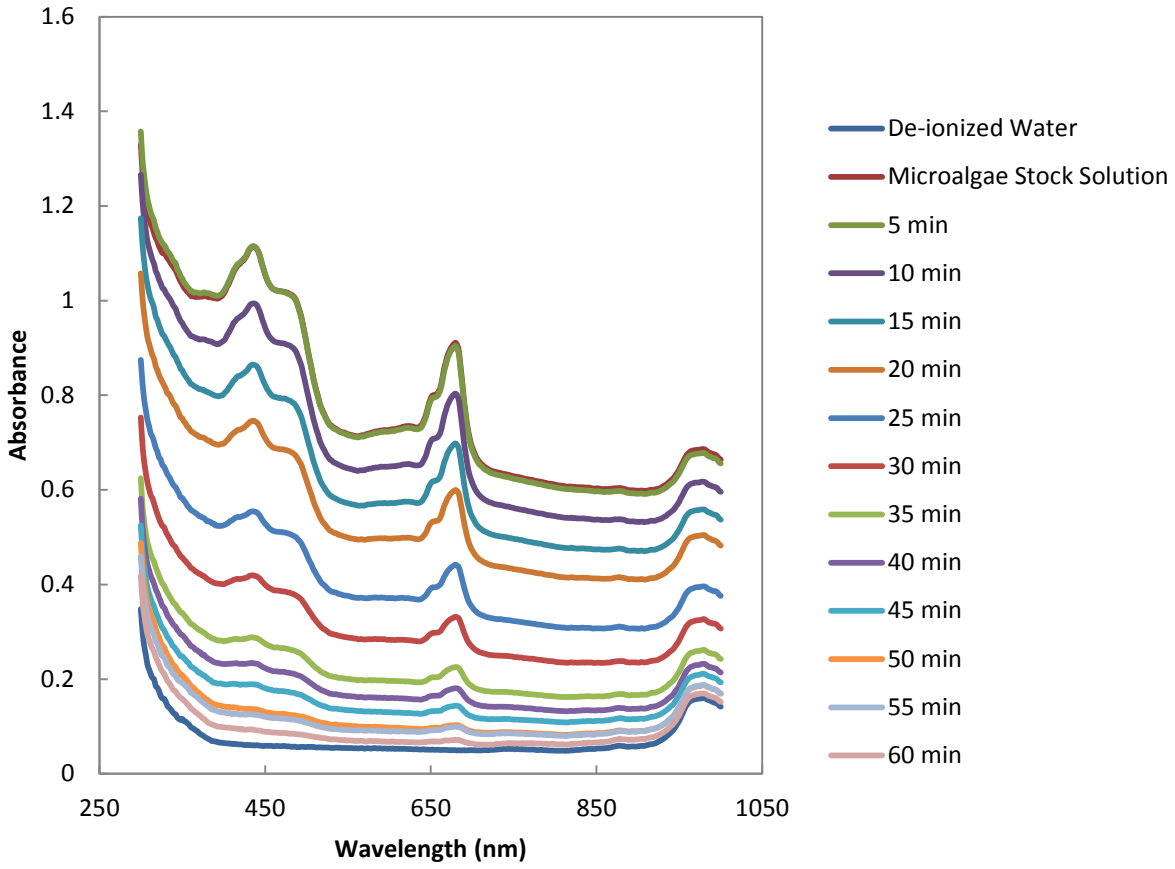

Figure 39: Optical Density Decrease during Electrocoagulation, CD: 15 Amp./m2, pH:6, Stirring Speed: 100 rpm, and Anode: Aluminum.

3. Determination of Metal Accumulation

- The following is the procedure used to determine the metal absorption in the algal biomass during the course of electrocoagulation

$$\text{Mass of metal}\left(\frac{\text{g}}{\text{g}_{\text{Algae}}}\right)=\left(\frac{\text{conc. in ppm}}{10^{6}}\right)\times \text{DF}$$

$$\times\left(\frac{\text{post digestion mass of bomb, algal biomass, HNO}_3-\text{mass of bomb, algal biomass}}{\text{mass of bomb, algal biomass}-\text{mass of empty bomb}}\right)$$

- The total mass of metal dissolved during electrocoagulation is determined using the following equation

$$\Delta m\ (g) = m_{pi} - m_{pf}$$

Where Δm is the total mass of metal dissolved (g), m_{pi} is the mass of anode plate before electrocoagulation (g), and m_{pf} is the mass of anode plate after electrocoagulation (g)

Sample Calculation

Mass of empty bomb (g)	129.72
Mass of bomb + algal biomass (g)	130.24
Post digestion mass of bomb + algal biomass + HNO_3 (g)	142.07
Dilution factor	100.00
Concentration of Al at 15 Amp/m^2 (ppm)	32.63
Mass of Al plate before electrocoagulation (g)	21.43
Mass of Al plate after electrocoagulation (g)	21.31

$$\text{Mass of Al}\left(\frac{\text{g}}{\text{g}_{\text{Algae}}}\right) = \left(\frac{32.63}{10^6}\right) \times 100 \times \left(\frac{142.07 - 130.24}{130.24 - 129.72}\right) = 0.070$$

$$\Delta m\ (g) = 21.43 - 21.31 = 0.12$$

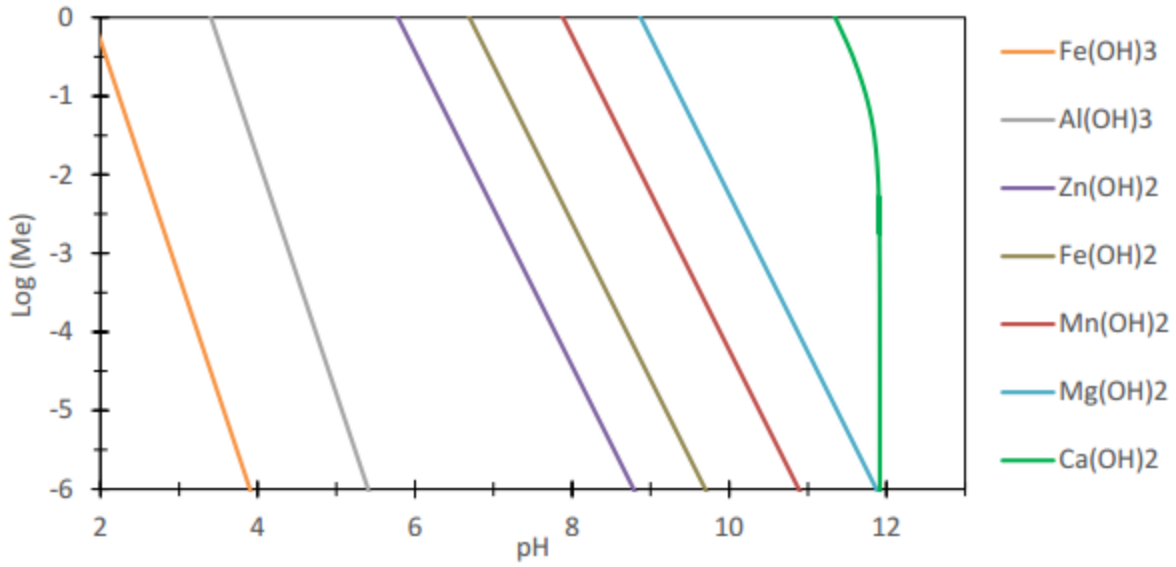

Figure 40: The Solubility of Metal Hydroxides in Pure Water [83].

The solubility order of metal hydroxides is as follows:

$$Ca(OH)_2 > Mg(OH)_2 > Mn(OH)_2 > Fe(OH)_2 > Zn(OH)_2 > Al(OH)_3 > Fe(OH)_3.$$

4. Determination of Hydroxide Ions Concentration

$$pHf + pOHf = 14$$

$$pHi + pOHi = 14$$

$$(pHf - pHi) + (pOHf - pOHi) = 0$$

$$\Delta pH - \Delta pOH = 0$$

$$\Delta pOH = pHi - pHf$$

$$\Delta[OH^-](M) = 10^{-pHi} - 10^{-pHf}$$

5. Determination of Combustion Emissions

Basis: 1 kg coal.

Element	%	Mass (kg)	No. of moles (kmol)	O_2 required (kmol)	Products (kmol)	Products (m^3)
C	82.7	0.827	0.0689	0.0689	0.0689	1.6850
H	5	0.050	0.0500	0.0125	0.0250	0.6112
S	0.3	0.003	0.0001	0.0001	0.0001	0.0023
O	10.1	0.101	0.0064	-0.0032	-	-
N	1.9	0.019	0.0014	-	0.0014	0.0332
Actual air required at 20% access (kmol)				0.448		
Total volume (m^3)				11.36		

Basis: 1 kg clinker using coal as fuel.

Element	%	Mass (kg)	No. of moles (kmol)	O_2 required (kmol)	Products (kmol)	Products (m^3)
C	82.7	0.0529	0.0044	0.0044	0.0044	0.1078
H	5	0.0032	0.0032	0.0008	0.0016	0.0391
S	0.3	0.0002	6E-6	6E-6	6E-6	0.0001
O	10.1	0.0064	0.0004	-0.0002	-	-
N	1.9	0.0012	8.6E-5	-	8.6E-5	0.0021
Actual air required at 20% access (kmol)				0.0238		
Total volume (m^3)				0.73		

Basis: 1 kg Algal Bio-solids.

Element	%	Mass (kg)	No. of moles (kmol)	O_2 required (kmol)	Products (kmol)	Products (m^3)
C	40.04	0.4004	0.0334	0.0334	0.0334	0.8158
H	6.35	0.0635	0.0635	0.0158	0.0317	0.7762
O	31.59	0.3159	0.0197	-0.0098	-	-
N	7.02	0.0702	0.0050	-	0.0050	0.1226
H_2O	15.00	0.1500	0.0083	-	0.0083	0.2037
Actual air required at 20% access (kmol)				0.2249		
Total volume (m^3)				6.45		

Basis: 1 kg clinker using algal bio-solids as fuel.

Element	%	Mass (kg)	No. of moles (kmol)	O_2 required (kmol)	Products (kmol)	Products (m^3)
C	40.04	0.0432	0.0036	0.0036	0.0036	0.0881
H	6.35	0.0068	0.0068	0.0017	0.0034	0.0838
O	31.59	0.0341	0.0021	-0.0010	-	-
N	7.02	0.0075	0.0005	-	0.0005	0.0132
H_2O	15.00	0.0162	0.0009	-	0.0009	0.0220
Actual air required at 20% access (kmol)				0.0243		
Total volume (m^3)				0.70		

6. Determination of Microalgae Settling Velocities

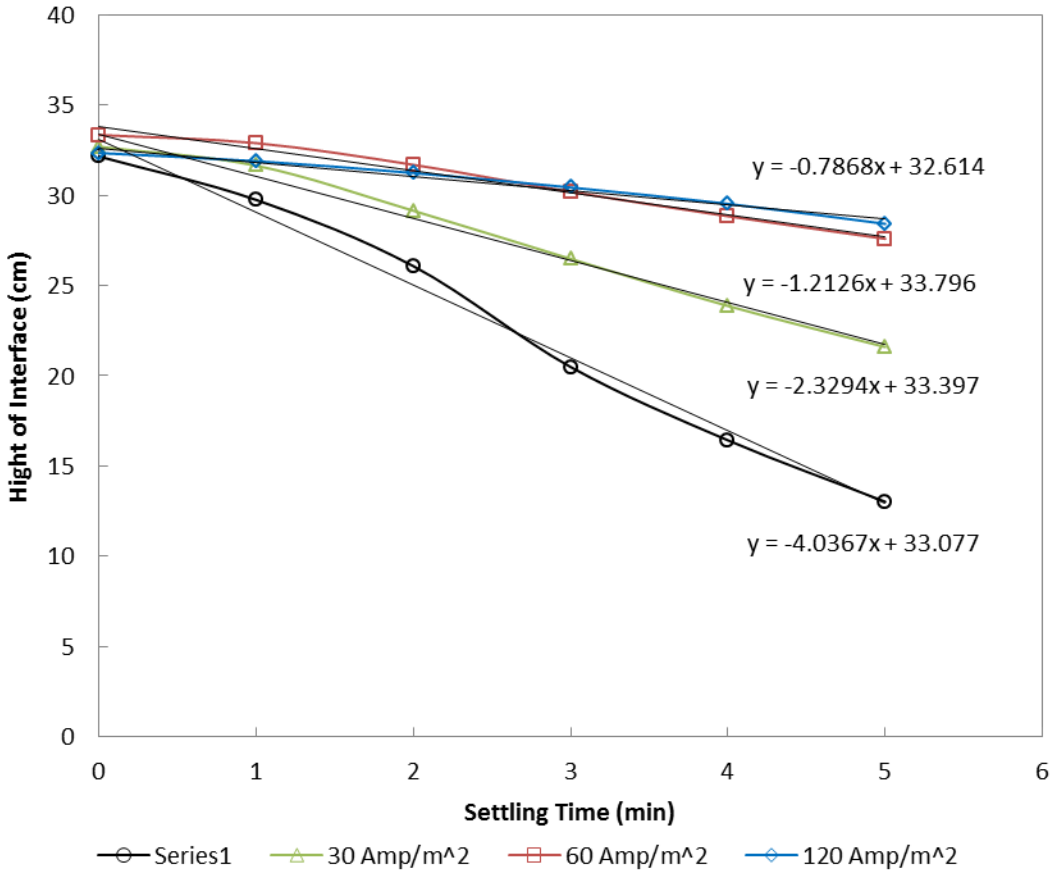

Figure 41: Settling Velocities of Coagulated Bio-solids using Alumium Anode.

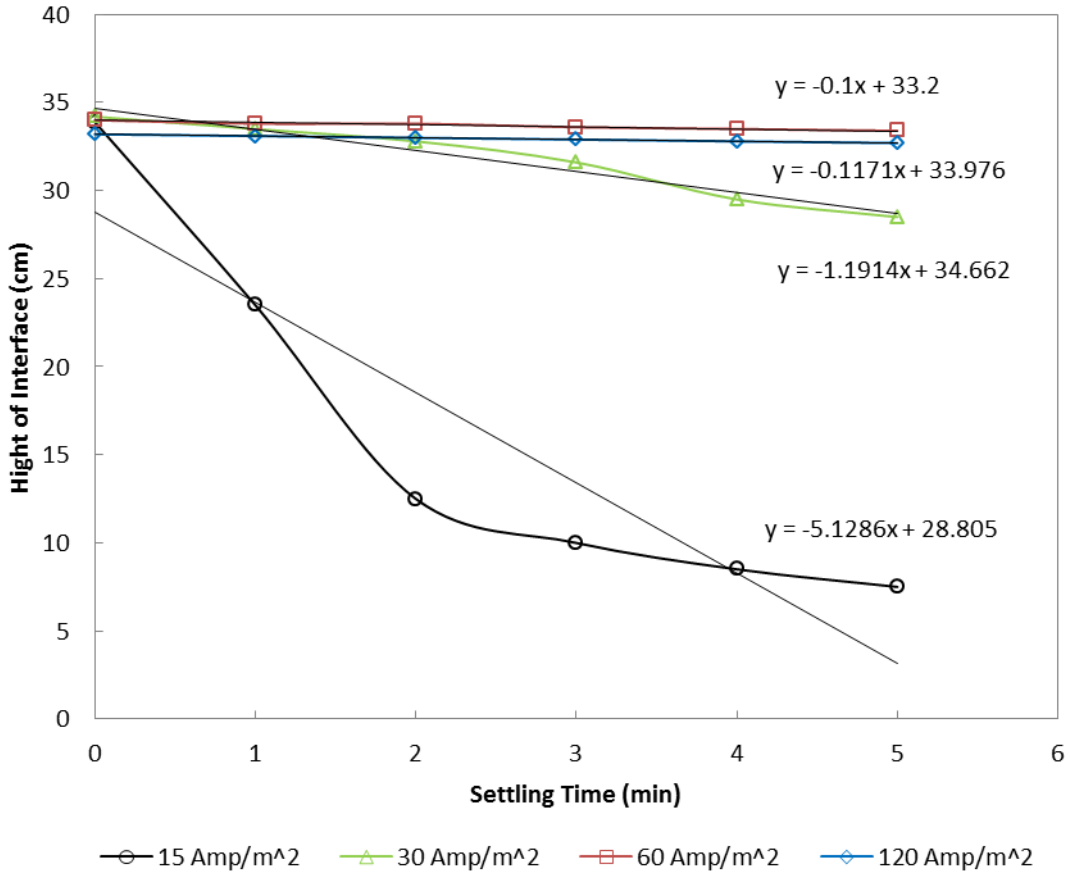

Figure 42: Settling Velocities of Coagulated Bio-solids using Iron Anode.

7. Determination of Briquettes Proportions

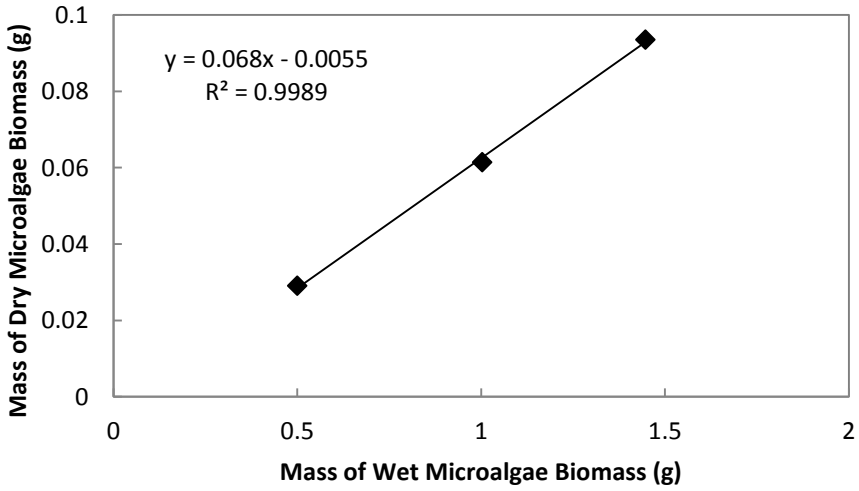

Figure 43: Regression Model between Wet and Dry Microalgae Biomass.

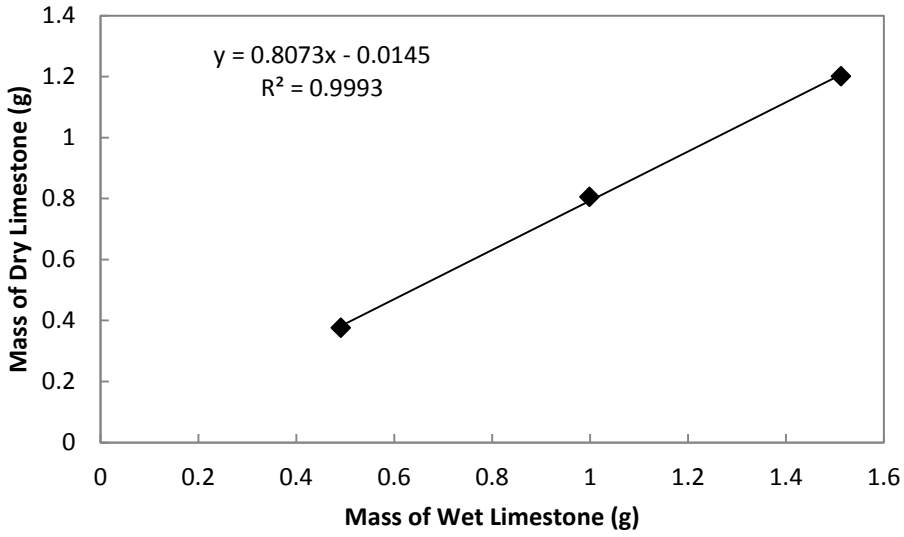

Figure 44: Regression Model between Wet and Dry Limestone.

Sample Calculation

Dry mass of briquette (g)	Algal biomass (%)	Limestone (%)
4.3838	18	82

$$Mass\ of\ dry\ algal\ biomass\ (g) = 4.3838 \times 0.18 = 0.7890\ g$$

$$Mass\ of\ dry\ limestone\ (g) = 4.3838 - 0.7890 = 3.5947\ g$$

$$Mass\ of\ wet\ algal\ biomass\ (g) = \frac{mass\ of\ dry\ algal\ biomass\ + 0.0055}{0.068}$$

$$= \frac{0.7890\ + 0.0055}{0.068} = 11.6838\ g$$

$$Mass\ of\ wet\ limestone\ (g) = \frac{mass\ of\ dry\ limestone\ + 0.0145}{0.8073}$$

$$= \frac{3.5947\ + 0.0145}{0.8073} = 4.4707\ g$$